PLOS ONE

Shell density of planktonic foraminifera and pteropod species Limacina helicina in the Barents Sea: assessment of relationship to environment conditions

--Manuscript Draft--

Manuscript Number:	PONE-D-20-18293R2
Article Type:	Research Article
Full Title:	Shell density of planktonic foraminifera and pteropod species Limacina helicina in the Barents Sea: assessment of relationship to environment conditions
Short Title:	Shell density of planktonic foraminifera and Limacina helicina
Corresponding Author:	Siri Ofstad UiT Norges arktiske universitet Tromsø, Troms NORWAY
Keywords:	ocean acidification; aragonite; calcite; calcification; FORAMINIFERA; pteropod; Barents Sea; Dissolution; computed tomography; marine ecology
Abstract:	Planktonic calcifiers, the foraminiferal species Neogloboquadrina pachyderma and Turborotalita quinqueloba , and the thecosome pteropod Limacina helicina from plankton tows and surface sediments from the northern Barents Sea were studied to assess how shell density varies with depth habitat and ontogenetic processes. The shells were measured using X-ray microcomputed tomography (XMCT) scanning and compared to the physical and chemical properties of the water column and to the carbonate chemistry including calcium carbonate saturation of calcite and aragonite. Both living L. helicina and N. pachyderma increased in shell density from the surface to 300 m water depth. Turborotalita quinqueloba increased in shell density to 150–200 m water depth. Deeper than 150 m, T. quinqueloba experienced a loss of density due to internal dissolution, possibly related to gametogenesis. The shell density of recently settled (dead) specimens of planktonic foraminifera from surface sediment samples was compared to the living fauna and showed a large range of dissolution states. This dissolution was not apparent from shell-surface texture, especially for N. pachyderma , which tended to be both thicker and denser than T. quinqueloba . Limacina helicina also increase in shell size with water depth and thicken the shell apex with growth. This study demonstrates that the living fauna in this specific area from the Barents Sea did not suffer from dissolution effects. Dissolution occurred after death and after settling on the sea floor. The study also shows that biomonitoring is important for the understanding of the natural variability in shell density of calcifying zooplankton.
Order of Authors:	Siri Ofstad
	Katarzyna Zamelczyk
	Katsunori Kimoto
	Melissa Chierici
	Agneta Fransson
	Tine Lander Rasmussen
Opposed Reviewers:	
Response to Reviewers:	Dear Academic Editor, We thank both reviewers for their constructive comments and feedback. Both anonymous reviewer #1 and anonymous reviewer #3 suggest minor revisions. We have corrected our manuscript following the reviewer's suggestions and address each comment below. Yours sincerely, Siri Ofstad, Katarzyna Zamelczyk, Katsunori Kimoto, Melissa Chierici, Agneta Fransson and Tine L. Rasmussen

Powered by Editorial Manager® and ProduXion Manager® from Aries Systems Corporation

Reviewer #1

I do not have time to scrutinise the manuscript in detail, but have read through you responses to reviewers' comments.
While most issues seem to have been acted on I must raise issue with the response to may final point regarding the shell thickness of L. helicina/Figure 8.
My observation that the only part of the shell to exhibit any variability in shell thickens was the spine was not a recommendation to measure shell thickness here! This would be the LAST place you should measure shell thickness for any environmental interpretation. The spine is structural and MUST increase in thickness as the diameter of the whorl it needs to support increases (in the same way that a tree trunk thickens are the tree gets taller). The outer wall is the area you should target and I maintain that these is no increase in thickness of the shell wall with increasing whorl number. This is worthy of note, but the spine thickness metrics and associated discussion is misguided and should be removed before this manuscript could be considered suitable for publication.

Reply: We are glad our responses and actions regarding your previous comments are satisfactory. We attempted to make the discussion points on the thickening of the spine speculative but understand that it is controversial. Therefore, Figure 8 has been edited, all whorl thickness measurements at the spine have been removed along with all mentions of it in the manuscript including the methods, supplementary tables and Figure S3.

Reviewer #3

Major comments

1. First, authors discussed about the vertical distribution of shell physical condition of living calcareous organisms against the background of the issue of ocean acidification. However, what they have done is the observation under the single environmental condition. Therefore, this study mainly reveals the growth process or ordinary life cycle of calcareous organisms that is ontogenetic process in other word. On the other hand, they did not compare the shell physical feature under the different acidification condition at different place or time. This means that it cannot discuss the impact of ocean acidification to calcification intensity of calcareous organisms from the sample set in this study. I suppose that author should clearly explain the importance for investigating the ontogenetic and growth process of these organisms. In my understanding, it would be like fine to add few sentences in Introduction that explain "what kind of knowledge is lacking in Ocean Acidification research" and "Why understanding ontogenetic and growth process of calcareous organism is necessary for Ocean Acidification research in the future".

Reply: Thank you for your in-depth comment on the overall objectives of the paper. We have now edited the introduction to make the research purposes clearer for the reader. As you suggested, we added a few sentences on why this research is relevant for ocean acidification research.

2. Second, I have something to worry about the shell samples from the surface sediments. In this study, authors also discuss about the shell samples from the surface sediment samples. However, I feel that this discussion is different from main theme of this study. I could not understand well why authors had to measure the shells in sediment sample. If they are definitely necessary in this study, authors should explain why it is necessary and what is the purpose of it. Furthermore, because some basic information of sediment samples is lack from this manuscript and figures, it is difficult to understand. The detail of samples can be quoted from other papers, but at least sediment samples location, water depth and super/under saturated to carbonate should be represented in the manuscript and/or figure of Map.

Reply: We see the surface sediment samples as a continuation of the water column story which focuses on the ontogenetic processes. The ontogenetic processes will affect how well the foraminifera will be preserved in the surface sediments. This further demonstrates the importance in studying ontogenetic and growth process of calcareous organisms. Planktonic foraminifera from surface sediments are primarily

Powered by Editorial Manager® and ProduXion Manager® from Aries Systems Corporation

	used in paleostudies, and the shell condition influences geochemical measurements. The surface sediments samples show that not all planktonic foraminifera develop a crust after gametogenesis, and experience differing degrees of dissolution of the internal chambers. The differences in these ontogenetic processes not only has the potential to effect water column ocean acidification studies, but also paleo-studies. The purpose of the surface sediment samples to the manuscript has been made clearer in the introduction, and more information on the samples has been added to the Material and Methods chapter (see reply below). Other comments Material and Methods Line 128- 2.2 Sampling of marine calcifiers, and/or Figure 1 (Map) I suggest to add more information about surface sediment sample (e.g., location, depth, etc). Reply: The coordinates, water depth and calcite saturation at the two box-core stations has been added to section 2.2.. The location is in the same area as the plankton tows, therefore no additional information has been added to the map in Figure 1. Results Line 236: The water column can be divided into two…… What is reason for separating the water column at 75 m? Is this same with thermocline? It is unclear for me how does this work in the following Results and Discussion. Reply: No actual separation of the water column has been done during for instance, statistical analysis. The word “divided” has been removed in order to avoid confusion. You are correct, the thermocline is indeed located at 75 m water depth. This is mentioned in the results section for the water chemistry because in addition to the warmer water temperature in the 0-75 m layer, the Ω saturation is elevated. This detail is relevant when we discuss the specimens sampled in the 0-50 m layer. Line 251-252: The outer shell walls are thick and dense, while….. This is just a comment. This is very interesting result. To me, it seems to be caused by inorganic dissolution of juvenile shell after shell calcification. But I have no idea why the shell can be dissolved in the water column such quickly. If this is due to the process of gamtogenesis, it must be very energy consuming ontogenetic process for foraminifera, because it is time consuming process to dissolve the calcified shell in the nature condition. Reply: Thank you for your comment. Yes, this is a very interesting observation which could suggest that the internal environment is extremely corrosive following gametogenesis. Line 314-339: 3.3.2 Planktonic Foraminifera from the surface sediments As describe in major comments, it is better to explain why measurement of shell samples from the surface sediment is necessary. Reply: The recently settled PF were primarily included to demonstrate the large range in calcite preservation in the 0-1 cm layer. We believe this will be of interest to the paleo-community. The preservation of the internal chambers will affect geochemical measurements, and the internal conditions were not apparent from the outer shell wall. Furthermore, by including the surface sediment samples we show an additional and promising use of the XMCT technology. As mentioned in the reply to your previous comment the reasoning for including the surface sediment samples has been made clearer in the introduction. Line 360-361: The way that L. helicina is distribution in the water relationship…..

Powered by Editorial Manager® and ProduXion Manager® from Aries Systems Corporation

	Is it possible that thinner shell wall is scanned as lower CT number due to the resolution of CT scanning? I don't mind this in the case of planktic foraminifera, because they are enough thick, but I'm wondering what about the case of pteropod with very thin shell wall. Reply: Thank you for this comment, this is an issue which is important to address. This misrepresentation of shell density in thinner material is referred to as the partial volume effect and is related to the spatial resolution and voxel number which constitute the shell wall. The partial volume effect appears at the boundary between the air and the (shell) material. Both ends of the shell is in contact with the surrounding air, and if the air has sufficiently larger volume than the material within one voxel, this voxel is drawn as low density. We agree that this could be an issue if using a low scanning resolution. Our analysis was performed with a sub-micron resolution (0.833 µm/voxel, due to size there were 5 pteropods out of 25 that were scanned with a resolution just over 1 µm). This resolution is sufficient to accurately separate the shell of the pteropod from the air that surrounds it, both internally and externally. Furthermore, with our scanning resolution we would only see this effect in shell material thinner than 1.7 µm (uses < 2 voxels). Such a thin shell wall is very limited to the internal chamber of the pteropod shell. In our study, the average shell thickness of pteropods was around 3 µm and is sufficient to accurately draw the shell wall, therefore we can say that the misrepresentation of thin shell walls as lower density is very small and/or negligible in this study. Discussion Line 411-: Cytoplasm-bearing specimens are also present in the entire water column (S7 Table), … Were the shell samples divided into with/without cytoplasm under the CT scanning? I'd like to compare the CT images of shell with/without cytoplasm individually if possible. Reply: Unfortunately, no comparison of the CT images of shells with and without cytoplasm was done for this study, but that is a point which we will include for future investigations.
Additional Information:	
Question	**Response**
Financial Disclosure Enter a financial disclosure statement that describes the sources of funding for the work included in this submission. Review the submission guidelines for detailed requirements. View published research articles from *PLOS ONE* for specific examples. This statement is required for submission and **will appear in the published article** if the submission is accepted. Please make sure it is accurate.	This work was funded by the Research Council of Norway through its Centres of Excellence scheme (grant number 223259). The XMCT analysis was funded by Japan Agency for Marine-Earth Science and Technology Grants-In-Aid for Scientific Research (KAKENHI) Grant Numbers 15H05712 and 16H04961. The water chemistry sampling and analysis was funded by the Flagship research program "Ocean Acidification and effects in northern waters" within the FRAM- High North Research Centre for Climate and the Environment. The funders had no role in study design, data collection and analysis, decision to publish, or preparation of the manuscript.

Unfunded studies Enter: *The author(s) received no specific funding for this work.* **Funded studies** Enter a statement with the following details: • Initials of the authors who received each award • Grant numbers awarded to each author • The full name of each funder • URL of each funder website • Did the sponsors or funders play any role in the study design, data collection and analysis, decision to publish, or preparation of the manuscript? • **NO** - Include this sentence at the end of your statement: *The funders had no role in study design, data collection and analysis, decision to publish, or preparation of the manuscript.* • **YES** - Specify the role(s) played. * typeset	
Competing Interests Use the instructions below to enter a competing interest statement for this submission. On behalf of all authors, disclose any competing interests that could be perceived to bias this work—acknowledging all financial support and any other relevant financial or non-financial competing interests. This statement **will appear in the published article** if the submission is accepted. Please make sure it is accurate. View published research articles from *PLOS ONE* for specific examples.	The authors have declared that no competing interests exist.

NO authors have competing interests Enter: *The authors have declared that no competing interests exist.* **Authors with competing interests** Enter competing interest details beginning with this statement: *I have read the journal's policy and the authors of this manuscript have the following competing interests: [insert competing interests here]* * typeset	
Ethics Statement Enter an ethics statement for this submission. This statement is required if the study involved: • Human participants • Human specimens or tissue • Vertebrate animals or cephalopods • Vertebrate embryos or tissues • Field research Write "N/A" if the submission does not require an ethics statement. General guidance is provided below. Consult the submission guidelines for detailed instructions. **Make sure that all information entered here is included in the Methods section of the manuscript.**	N/A

Format for specific study types **Human Subject Research (involving human participants and/or tissue)** • Give the name of the institutional review board or ethics committee that approved the study • Include the approval number and/or a statement indicating approval of this research • Indicate the form of consent obtained (written/oral) or the reason that consent was not obtained (e.g. the data were analyzed anonymously) **Animal Research (involving vertebrate animals, embryos or tissues)** • Provide the name of the Institutional Animal Care and Use Committee (IACUC) or other relevant ethics board that reviewed the study protocol, and indicate whether they approved this research or granted a formal waiver of ethical approval • Include an approval number if one was obtained • If the study involved *non-human primates*, add *additional details* about animal welfare and steps taken to ameliorate suffering • If anesthesia, euthanasia, or any kind of animal sacrifice is part of the study, include briefly which substances and/or methods were applied **Field Research** Include the following details if this study involves the collection of plant, animal, or other materials from a natural setting: • Field permit number • Name of the institution or relevant body that granted permission	
Data Availability Authors are required to make all data underlying the findings described fully available, without restriction, and from the time of publication. PLOS allows rare exceptions to address legal and ethical concerns. See the PLOS Data Policy and FAQ for detailed information.	Yes - all data are fully available without restriction

Powered by Editorial Manager® and ProduXion Manager® from Aries Systems Corporation

A Data Availability Statement describing where the data can be found is required at submission. Your answers to this question constitute the Data Availability Statement and **will be published in the article**, if accepted. **Important:** Stating 'data available on request from the author' is not sufficient. If your data are only available upon request, select 'No' for the first question and explain your exceptional situation in the text box. Do the authors confirm that all data underlying the findings described in their manuscript are fully available without restriction?	
Describe where the data may be found in full sentences. If you are copying our sample text, replace any instances of XXX with the appropriate details. • If the data are **held or will be held in a public repository**, include URLs, accession numbers or DOIs. If this information will only be available after acceptance, indicate this by ticking the box below. For example: *All XXX files are available from the XXX database (accession number(s) XXX, XXX.*). • If the data are all contained **within the manuscript and/or Supporting Information files**, enter the following: *All relevant data are within the manuscript and its Supporting Information files.* • If neither of these applies but you are able to provide **details of access elsewhere**, with or without limitations, please do so. For example: *Data cannot be shared publicly because of [XXX]. Data are available from the XXX Institutional Data Access / Ethics Committee (contact via XXX) for researchers who meet the criteria for access to confidential data.* *The data underlying the results presented in the study are available from (include the name of the third party*	All relevant data are within the manuscript and its Supporting Information files (Tables S1-10; Dataset S1-3). Water chemisty data and abundance data for planktonic foraminifera and pteropods can be found in https://doi.org/10.21335/NMDC-225800978 and https://doi.pangaea.de/10.1594/PANGAEA.904463, respectively.

and contact information or URL). • This text is appropriate if the data are owned by a third party and authors do not have permission to share the data. * typeset	
Additional data availability information:	

Dear Academic Editor,

We thank both reviewers for their constructive comments and feedback. Both anonymous reviewer #1 and anonymous reviewer #3 suggest minor revisions. We have corrected our manuscript following the reviewer's suggestions and address each comment below.

Yours sincerely,

Siri Ofstad, Katarzyna Zamelczyk, Katsunori Kimoto, Melissa Chierici, Agneta Fransson and Tine L. Rasmussen

Reviewer #1

I do not have time to scrutinise the manuscript in detail, but have read through you responses to reviewers' comments.
While most issues seem to have been acted on I must raise issue with the response to may final point regarding the shell thickness of L. helicina/Figure 8.
My observation that the only part of the shell to exhibit any variability in shell thickens was the spine was not a recommendation to measure shell thickness here! This would be the LAST place you should measure shell thickness for any environmental interpretation. The spine is structural and MUST increase in thickness as the diameter of the whorl it needs to support increases (in the same way that a tree trunk thickens are the tree gets taller). The outer wall is the area you should target and I maintain that these is no increase in thickness of the shell wall with increasing whorl number. This is worthy of note, but the spine thickness metrics and associated discussion is misguided and should be removed before this manuscript could be considered suitable for publication.

Reply: We are glad our responses and actions regarding your previous comments are satisfactory. We attempted to make the discussion points on the thickening of the spine speculative but understand that it is controversial. Therefore, Figure 8 has been edited, all whorl thickness measurements at the spine have been removed along with all mentions of it in the manuscript including the methods, supplementary tables and Figure S3.

Reviewer #3

Major comments

1. First, authors discussed about the vertical distribution of shell physical condition of living calcareous organisms against the background of the issue of ocean acidification. However, what they have done is the observation under the single environmental condition. Therefore, this study mainly reveals the growth process or ordinary life cycle of calcareous organisms that is ontogenetic process in other word. On the other hand, they did not compare the shell physical feature under the different acidification condition at different place or time. This means that it cannot discuss the impact of ocean acidification to calcification intensity of calcareous organisms from the sample set in this study. I suppose that author should clearly explain the importance for investigating the ontogenetic and growth process of these organisms. In my understanding, it would be like fine to add few sentences in Introduction that explain "what kind of knowledge is lacking in Ocean Acidification research" and "Why understanding ontogenetic and growth process of calcareous organism is necessary for Ocean Acidification research in the future".

Reply: Thank you for your in-depth comment on the overall objectives of the paper. We have now edited the introduction to make the research purposes clearer for the reader. As you suggested, we added a few sentences on why this research is relevant for ocean acidification research.

2. Second, I have something to worry about the shell samples from the surface sediments. In this study, authors also discuss about the shell samples from the surface sediment samples. However, I feel that this discussion is different from main theme of this study. I could not understand well why authors had to measure the shells in sediment sample. If they are definitely necessary in this study, authors should explain why it is necessary and what is the purpose of it. Furthermore, because some basic information of sediment samples is lack from this manuscript and figures, it is difficult to understand. The detail of samples can be quoted from other papers, but at least sediment samples location, water depth and super/under saturated to carbonate should be represented in the manuscript and/or figure of Map.

Reply: We see the surface sediment samples as a continuation of the water column story which focuses on the ontogenetic processes. The ontogenetic processes will affect how well the foraminifera will be preserved in the surface sediments. This further demonstrates the importance in studying ontogenetic and growth process of calcareous organisms. Planktonic foraminifera from surface sediments are primarily used in paleostudies, and the shell condition influences geochemical measurements. The surface sediments samples show that not all planktonic foraminifera develop a crust after gametogenesis, and experience differing degrees of dissolution of the internal chambers. The differences in these ontogenetic processes not only has the potential to effect water column ocean acidification studies, but also paleo-studies. The purpose of the surface sediment samples to the manuscript has been made clearer in the introduction, and more information on the samples has been added to the Material and Methods chapter (see reply below).

Other comments

Material and Methods

Line 128- 2.2 Sampling of marine calcifiers, and/or Figure 1 (Map)
I suggest to add more information about surface sediment sample (e.g., location, depth, etc).
Reply: The coordinates, water depth and calcite saturation at the two box-core stations has been added to section 2.2.. The location is in the same area as the plankton tows, therefore no additional information has been added to the map in Figure 1.

Results

Line 236: The water column can be divided into two……
What is reason for separating the water column at 75 m? Is this same with thermocline? It is unclear for me how does this work in the following Results and Discussion.
Reply: No actual separation of the water column has been done during for instance, statistical analysis. The word "divided" has been removed in order to avoid confusion. You are correct, the thermocline is indeed located at 75 m water depth. This is mentioned in the results section for the water chemistry because in addition to the warmer water temperature in the 0-75 m layer, the Ω saturation is elevated. This detail is relevant when we discuss the specimens sampled in the 0-50 m layer.

Line 251-252: The outer shell walls are thick and dense, while…..

This is just a comment. This is very interesting result. To me, it seems to be caused by inorganic dissolution of juvenile shell after shell calcification. But I have no idea why the shell can be dissolved in the water column such quickly. If this is due to the process of gamtogenesis, it must be very energy consuming ontogenetic process for foraminifera, because it is time consuming process to dissolve the calcified shell in the nature condition.

Reply: Thank you for your comment. Yes, this is a very interesting observation which could suggest that the internal environment is extremely corrosive following gametogenesis.

Line 314-339: 3.3.2 Planktonic Foraminifera from the surface sediments
As describe in major comments, it is better to explain why measurement of shell samples from the surface sediment is necessary.

Reply: The recently settled PF were primarily included to demonstrate the large range in calcite preservation in the 0-1 cm layer. We believe this will be of interest to the paleo-community. The preservation of the internal chambers will affect geochemical measurements, and the internal conditions were not apparent from the outer shell wall. Furthermore, by including the surface sediment samples we show an additional and promising use of the XMCT technology.

As mentioned in the reply to your previous comment the reasoning for including the surface sediment samples has been made clearer in the introduction.

Line 360-361: The way that L. helicina is distribution in the water relationship…..
Is it possible that thinner shell wall is scanned as lower CT number due to the resolution of CT scanning? I don't mind this in the case of planktic foraminifera, because they are enough thick, but I'm wondering what about the case of pteropod with very thin shell wall.

Reply: Thank you for this comment, this is an issue which is important to address. This misrepresentation of shell density in thinner material is referred to as the partial volume effect and is related to the spatial resolution and voxel number which constitute the shell wall. The partial volume effect appears at the boundary between the air and the (shell) material. Both ends of the shell is in contact with the surrounding air, and if the air has sufficiently larger volume than the material within one voxel, this voxel is drawn as low density.

We agree that this could be an issue if using a low scanning resolution. Our analysis was performed with a sub-micron resolution (0.833 μm/voxel, due to size there were 5 pteropods out of 25 that were scanned with a resolution just over 1 μm). This resolution is sufficient to accurately separate the shell of the pteropod from the air that surrounds it, both internally and externally. Furthermore, with our scanning resolution we would only see this effect in shell material thinner than 1.7 μm (uses < 2 voxels). Such a thin shell wall is very limited to the internal chamber of the pteropod shell. In our study, the average shell thickness of pteropods was around 3 μm and is sufficient to accurately draw the shell wall, therefore we can say that the misrepresentation of thin shell walls as lower density is very small and/or negligible in this study.

Discussion

Line 411-: Cytoplasm-bearing specimens are also present in the entire water column (S7 Table), …
Were the shell samples divided into with/without cytoplasm under the CT scanning? I'd like to compare the CT images of shell with/without cytoplasm individually if possible.

Reply: Unfortunately, no comparison of the CT images of shells with and without cytoplasm was done for this study, but that is a point which we will include for future investigations.

Manuscript Click here to access/download;Manuscript;Manuscript.docx

Shell density of planktonic foraminifera and pteropod species *Limacina helicina* in the Barents Sea: assessment of relationship to environmental conditions

Siri Ofstad[1*], Katarzyna Zamelczyk[1], Katsunori Kimoto[3], Melissa Chierici[4], Agneta Fransson[2], and Tine L. Rasmussen[1]

[1]CAGE – Centre for Arctic Gas Hydrate, Environment and Climate, Department of Geosciences, UiT, The Arctic University of Norway, Tromsø, Norway

[2]Norwegian Polar Institute, Fram Centre, Tromsø, Norway

[3]Japan Agency for Marine-Earth Science and Technology (JAMSTEC), Yokosuka, Japan

[4]Institute of Marine Research, Fram Centre, Tromsø, Norway

* Corresponding author

siri.ofstad@uit.no (SO)

Abstract

Planktonic calcifiers, the foraminiferal species *Neogloboquadrina pachyderma* and *Turborotalita quinqueloba*, and the thecosome pteropod *Limacina helicina* from plankton tows and surface sediments from the northern Barents Sea were studied to assess how shell density varies with depth habitat and ontogenetic processes. The shells were measured using X-ray microcomputed tomography (XMCT) scanning and compared to the physical and chemical properties of the water column and to the carbonate chemistry including calcium carbonate saturation of calcite and aragonite. Both living *L. helicina* and *N. pachyderma* increased in shell density from the surface to 300 m water depth. *Turborotalita quinqueloba* increased in shell density to 150–200 m water depth. Deeper than 150 m, *T. quinqueloba* experienced a loss of density due to internal dissolution, possibly related to gametogenesis. The shell density of recently settled (dead) specimens of planktonic foraminifera from surface sediment samples was compared to the living fauna and showed a large range of dissolution states. This dissolution was not apparent from shell-surface texture, especially for *N. pachyderma,n*which tended to be both thicker and denser than *T. quinqueloba*. *Limacina helicina* also increase in shell size with water depth and thicken the shell apex with growth. This study demonstrates that the living fauna in this specific area from the Barents Sea did not suffer from dissolution effects. Dissolution occurred after death and after settling on the sea floor. The study also shows that biomonitoring is important for the understanding of the natural variability in shell density of calcifying zooplankton.

1. Introduction

The Arctic is particularly sensitive to global warming, and this warming is greatly amplified in the Barents Sea, a large and productive shelf sea bordering the Arctic Ocean [1,2]. The Barents Sea is influenced by inflow of Atlantic Water (AW) from the south and Polar Water from the Arctic Ocean in the north, making it a hydrologically dynamic region. The two water masses mix and generate the Polar Front, a zone of very high-productivity [3]. In the northern Barents Sea there has been a substantial shift in water mass properties over the past several decades [4]. The water column in the northern Barents

Sea has become warmer and more saline, and stratification has weakened [4]. This shift is due to an increase of AW water transport, and an increase in temperature and salinity of the AW [5,6]. This 'Atlantification' of the water column will impact the productivity and structure of the Barents Sea ecosystems by displacing the Polar Front north-eastward, and allowing the advection of temperate species further into the Arctic domain [6–8]. A poleward shift of species in the Barents Sea has already been documented [9–11]. The large volume of warm and saline AW is also thought to be the main cause of the rapid decline of the winter sea ice cover [1].

The Barents Sea is one of the largest CO_2 sink areas in the Arctic region, which is mainly caused by the year-round CO_2 undersaturation and high biological production [12,13] despite the formation of sea-ice in winter. The Barents Sea CO_2 sink is predicted to double by 2065 with an associated pH decrease of up to 0.25 pH units [14]. A significant proportion of the observed CO_2 increase in the Barents Sea has been from the inflow of AW, which is rich in anthropogenic CO_2 [15]. The meltwater from sea ice or glaciers lowers the saturation state of seawater with respect to calcite (Ω_{Ca}) and aragonite (Ω_{Ar}), the two most common polymorphs of $CaCO_3$ formed by marine organisms [16–18], and is predicted to increase as a result of the progressing global warming [19]. Ocean acidification (OA) may lead to adverse effects on the ability of marine calcifiers to produce $CaCO_3$ shells [20].

Planktonic foraminifera (PF) and thecosomatous pteropods are the major calcifiers among marine zooplankton [20]. Marine calcifiers, in particular pteropods, are important prey in many marine food webs [21–24]. In addition, both PF and pteropods contribute significantly to the biological carbon pump [25–29]. Only few studies of PF and pteropod faunas for the high Arctic exists and in particular for the Barents Sea [30–32]. Planktonic foraminifera build their shells of calcite, while the polar pteropod species *Limacina helicina* build their shells of aragonite. The crystal structure of calcite is more stable than aragonite, and the tendency for the crystal structure to dissolve is linked to the Ω in the surrounding environment of the particular mineral phase. The crystal structures of aragonite and calcite are thermodynamically stable when $\Omega>1$. Both PF and *L. helicina* are sensitive to the carbonate chemistry in their environment and the extent of their calcification is commonly used as an indicator for OA [33–

40]. Furthermore, due to their long sedimentary record PF shell density has been used for paleoceanographic studies of OA and atmospheric CO_2 [41–44].

In a previous study, we documented the seasonal variability in the distribution patterns of PF and polar pteropod *L. helicina* and their environments in the northern Barents Sea [30]. Test size and abundance of both groups increased drastically from spring to summer, and in summer there was a clearer depth zonation of the individuals, possibly related to the thermal stratification [30]. Here, we extend our analysis on PF and *L. helicina* to study the shell density of the summer population.

In OA research there are few studies with focus on how the shell density of calcareous planktonic organisms varies with ontogeny, and hence, with depth habitat in the upper water column. Furthermore, ontogenetic processes like secondary calcification following gametogenesis will influence how well PF are preserved in the sedimentary record which is significant for the accuracy of studies of fossil faunas. Knowledge on the natural variability in shell density across a population of calcareous planktonic organisms will improve our ability to better document biological effects of OA. In this study, we aim to show 1) the variability in shell density of the living planktonic foraminiferal species *N. pachyderma* and *T. quinqueloba* and the pteropod *L. helicina* with shell size and water depth, 2) the interspecies differences in shell density of *N. pachyderma* and *T. quinqueloba*, 3) if any changes in the observed patterns in shell density can be related to seawater carbonate chemistry, and 4) how shell density and ontogenetic processes affect the preservation of foraminifera in the surface sediments. This study is based on X-ray microcomputed tomography (XMCT) scanning of their shells. This is a pioneer study to provide the first shell density measurements of specimens of planktonic foraminifera and *Limacina helicina* from the Arctic region.

2. Material and Methods

2.1 Study and sample collection

The Barents Sea is mainly influenced by the inflow of warm and saline Atlantic water transported in the north-eastern flowing Norwegian Atlantic current (NwAC) and the cold Arctic water transported in the

East Spitsbergen current (ESC) from the north to the south [3] (Fig 1). Once the NwAC enters the Bear Island Through it splits into two branches. A substantial part of the NwAC forms a northeast flowing current, the North Cape current, which enters the southern Barents Sea, while the remainder forms the northwest flowing West Spitsbergen current (WSC). The mean depth of the Barents Sea is 250 m and is a relatively shallow continental shelf sea adjacent to the Nordic Seas and the Arctic Ocean. The Bjørnøyrenna crater area (referred to in this study as the 'crater area') (74.91° N, 27.7° E.; Fig 1) is located in relatively deep water (~340 m depth) on the northern flank of Bear Island Trough and is characterized by high levels of methane emission [45].

Fig 1. Map of study area and main current systems in the Nordic Seas. White star indicates the crater area where plankton tows, box-cores and water sampling were conducted, detailed bathymetry can be found in Ofstad et al. [30]. Red lines are Atlantic Water inflows, blue lines are Arctic Water outflows, and green lines are coastal currents. Abbreviations: *NwAC* Norwegian Atlantic current, *WSC* West Spitsbergen current, *ESC* East Spitsbergen current, *NCC* Norwegian Coastal Current. Current systems are based on Loeng [3]. Basemap from IBCAO 3.0 [46].

Samples were collected onboard *R/V Helmer Hanssen* during the expedition CAGE 16-5, on June 29th 2016 at three stations located at 74.9° N, 27.7° E–27.8° E. No sampling permission was required at this location. This is because the study area is outside of the 12-mile limit of the Norwegian coast, meaning it is not in territorial waters, and the sampling causes no harm to the environment. The plankton sampled from the water column are not endangered or protected species. The PF and *L. helicina* were sampled with a stratified plankton net with mesh size of 64 µm (net opening 0.5 m^2; Hydro-Bios, Kiel, Germany), from five consecutive depth intervals (0–50 m, 50–100 m, 100–150 m, 150–200 m, and 200–300 m). Parallel measurements and sampling for the study of physical and chemical environment in the water column were performed at the same location using a Conductivity-Temperature-Depth (CTD)-Rosette system with seawater sampling for determination of carbonate chemistry. Empty shells found in the water column >150 m are assumed to represent recently dead specimens. Their shells were transparent, well-preserved and similar to the shells of the live specimens containing protoplasm.

2.2 Sampling of marine calcifiers

Once the plankton tows were retrieved, the samples were sieved with sea water through a 63- μm sieve and transferred into plastic bottles (250 ml) and fixed and buffered with approximately 230 ml ethanol (98%), a quarter of a teaspoon hexamethylenetetramine (≥99.0%), and stored at 2 °C. Once in the laboratory, the samples were washed over a 63- μm sieve in order to remove organic particles from the surface of the foraminiferal tests and to break up aggregations of material. All PF and *L. helicina* from the >63- μm size fraction were picked with a fine brush under a light microscope. Live (cytoplasm-bearing) planktonic foraminifera specimens were counted for each depth.

Recently settled planktonic foraminifera were collected from two box-cores located within the same area as the plankton tow stations (74.92° N, 27.77° E and 27.53° E). The water depth at both box-core stations was 330 m, and the Ω_{Ca} directly above the sediments was 1.22 [30]. The PF were collected by sampling the top sediment layer (1 cm) of the boxcore. The samples were preserved in approximately 50 ml of ethanol (96%) with rose bengal (2 g L−1 of ethanol), and stored at 2 °C. In the home laboratory, the samples were washed over a 63- μm sieve and dried in a 40 °C for at least 24 hr. Once dried, PF were picked under a light microscope with a fine brush and identified to species level. There were large pteropods in the sediment samples, but they were broken, and therefore not included in the study. The complete description of sample collection, treatment, and analysis is described in Ofstad et al. [30].

2.3 XMCT

An XMCT system (ScanXmate-DF160TSS105, Comscantecno Co. Ltd., Kanagawa, Japan) was used to quantify the shell density of individual specimens. A high-resolution setting (X-ray focus spot diameter of 0.8 μm, X-ray tube voltage of 80 kV, detector array size of 1024x1024 for the pteropods and 992x992 for the foraminifera, spatial resolution of 0.833 μm for *Limacina helicina* and 0.964 μm for the foraminifera, 1200 projections/360°, 4 s/projection) was used for 3-D quantitative densitometry of the foraminiferal and pteropod tests. One to three samples – depending on the shell size, were placed on a stage made of a quartz glass bar. Tests were mounted on the sample stage with urethane glue. A

calcite crystal ball was used to standardize the computed tomography (CT) number of each test sample and enabled us to distinguish the density distributions in the foraminiferal and pteropod tests with high resolution. In this study, a limestone particle (diameter of approximately 130 μm; 1000 in mean CT number; NIST RM8544 (NBS19)) was embedded in the sample stage, and all of the test samples were scanned with the same calcite standard. ConeCTexpress software (White Rabbit Corp., Tokyo, Japan) was used to correct and reconstruct tomography data, and the general principle of Feldkamp cone beam reconstruction was followed to reconstruct image cross sections based on filtered back projections. In order to avoid the beam hardening effect (selective attenuation of X-ray) during scan, we put the metal filter (Aluminium, 0.2 um thickness) in front of X-ray detector. Mean shell thickness was calculated by dividing the $CaCO_3$ volume by the shell surface area, both of which are parameters measured by the XMCT. The shell surface area includes both the outer areas and the surfaces of the internal chambers. A caveat with the calculated mean shell thickness is that values will decrease, when the shell material is more porous. High porosity of the shell material increases the surface area, resulting in a decrease in mean shell thickness.

Well-preserved specimens to be scanned with the XMCT were selected at random, but with the intention of having a representative size range. The complete size range of the PF and *L. helicina* specimens sampled in June 2016 from the crater area can be found in Ofstad et al. [30]. A total of 226 planktonic foraminifera shells from the water column (*N. pachyderma* n = 120, *T. quinqueloba* n = 115), 30 recently settled planktonic foraminifera shells (*N. pachyderma* n = 12, *T. quinqueloba* n = 18), and 25 *Limacina helicina* shells from all depth intervals (0–50 m, 50–100 m, 100–150 m, 150–200 m, and 200–300 m) were scanned with the XMCT (S1 Table; Fig 2). All scanned pteropod shells were either veligers, *Limacina* spp. (<300 μm, n = 7), or juveniles *L. helicina* (300–4000 μm) (n = 18) [47].

2.4 CT Number

From the 3-D scanning data of planktonic foraminiferal and *L. helicina* tests, we obtained a CT number of each volumetric pixel - referred to as a voxel, and volume (μm^3) of each individual test. The 3-D imaging software Molcer Plus (White Rabbit Corp., version 1.35) and the following equation were used

to calculate the calcite CT number:

$$\text{CT number} = \left[\left(\mu_{\text{sample}} - \mu_{\text{air}}\right)/\left(\mu_{\text{calcite STD}} - \mu_{\text{air}}\right)\right] \times 1000 \quad (1)$$

where μ_{sample}, μ_{air}, and $\mu_{\text{calciteSTD}}$ are the X-ray attenuation coefficients of the sample, calcite, and air, respectively.

The mean CT number for an entire test was calculated with the following equations:

$$\text{Mean CT number} = \frac{1}{T}\sum_{n=230}^{1000} nT_n \quad (2)$$

where n is the CT number, T_n is the total number of voxels with a specific CT number (n), and T is the total number of voxels in the whole test. The mean CT number indicates the mean density of an individual test.

2.5 CT data analysis

The shell thickness of the apex of *L. helicina* was measured by creating cross-sections using the Molcer Plus software (Version 1.35). A whorl is a single 360° revolution of the shell spiral structure. The shell apex of 16 *L. helicina* shells were measured at four locations, twice on the protoconch (first whorl), and twice between the first and second whorl (Fig S3). Careful consideration was made to take measurements at the same location for each shell for ease of comparison. Following the methods outlined by Janssen [48], the *L. helicina* shell diameters were measured and the total number of whorls were counted to the nearest quarter (S3 Fig). Additional *L. helicina* from the sampling station were measured for their shell diameter. Images were acquired by a Leica Z16 APO microscope, using the integrated Leica DFC450 camera and LAS version 4.12.0 software. The images were processed using the ruler tool in Adobe Photoshop CS6. All measurements of shell diameter and thickness performed this study are the result of three repeated measurements to diminish inaccuracies.

In order to calculate area density (area normalised weight), 111 PF shells (*T. quinqueloba* n = 54, *N. pachyderma* n = 57) shells were weighed individually using a Sartorius microbalance (model M2P,

0.1μg sensitivity). The given weight measurements are based on three repeated measurements of the single specimen. Area density is given by shell weight divided by surface area.

Isolation of the penultimate and final chamber was done on a select number of shells in order to validate the relationship with the overall CT number of the shell.

2.6 Statistical analyses

To test the relationship between any two parameters (e.g. water depth and mean shell density), a simple linear regression model was applied to the data. To test significance of correlation of shell density of the marine calcifiers with sampling intervals, a Mann-Whitney-U test was performed using the program RStudio (Version 1.2.1335) [49]. When testing variables against water depth, the maximum depth in the sampling interval was used. When testing against environmental parameters, the mean of all measurements in the sampling interval was used.

2.7 Ocean carbonate chemistry

The water chemistry data were published in Ofstad et al. [30], here we give a brief overview of the methods. Dissolved inorganic carbon (DIC) was determined using gas extraction of acidified sample followed by coulometric titration and photometric detection using a Versatile Instrument for the Determination of Titration carbonate (VINDTA 3C, Marianda, Germany). Routine analyses of Certified Reference Materials (CRM, from A. G. Dickson, Scripps Institution of Oceanography, USA) ensured the accuracy and precision of the measurements. Average standard deviation from triplicate CRM analyses was within ±1 μmol kg^{-1} for all samples. Total alkalinity (A_T) was determined from potentiometric titration with 0.1 N hydrochloric acid in a closed cell using a Versatile Instrument for the Determination of Titration Alkalinity (VINDTA, Marianda, Germany). Average standard deviation for A_T, determined from triplicate CRM measurements was ±2 μmol kg^{-1}. We used DIC, A_T, salinity, temperature, and depth for each sample as input parameters in a CO_2-chemical speciation model (CO2SYS program, version 01.05) [50,51] to calculate other parameters in the carbonate system such

as carbonate-ion concentration ($[CO_3^{2-}]$), aragonite saturation (Ω_{Ar}) and calcite saturation (Ω_{Ca}). We used the HSO_4^- dissociation constant of Dickson [52], and the CO_2-system dissociation constants (K*1 and K*2) estimated by Mehrbach et al. [53], and modified by Dickson and Millero [55].

3. Results

3.1 Hydrography and water chemistry

During the time of sampling, the predominant water masses were Atlantic Water (AW, T > 3.0°C, S > 34.65) in the top 250 m of the water column, and Transformed Atlantic Water (TAW, T = 1.0–3.0°C, S > 34.65) below 250 m, following the definitions of Cottier et al. (2005) (S1 Fig). Both Ω_{Ar} and Ω_{Ca} were supersaturated (Ω>1) throughout the entire water column, with the highest values in the surface water and lowest at the bottom (Fig 3C and Fig 8C). The water column had two distinct layers (Fig 3C and Fig 8C). The upper layer is from the sea surface to approximately 75 m water depth (Figs 3C and 4C), here, the Ω_{Ar} is 2.1–2.5, and the Ω_{Ca} is 4.0–3.0. Between 75 m and 300 m water depth the Ω_{Ar} is 1.5–2.1, and the Ω_{Ca} is 2.4–3.0, where the lowest values were observed at the bottom. The carbonate ion concentration ($[CO_3^{2-}]$) ranged between 168 μmol kg^{-1} at the surface and 105 μmol kg^{-1} at 300 m water depth. The pH ranged between 8.03 and 8.22.

3.2 Shell density from CT Number

For both *Neogloboquadrina pachyderma* and *Turborotalita quinqueloba*, the average CT number increases steadily from 684 and 632 in the 0–50 m depth interval to 762 and 793 in the 150–200 m depth interval, respectively (Fig 2). The difference in CT number between the layer of elevated Ω saturation at 0–50 m and the underlying water column when normalized for shell volume, is also significant for both PF species ($p < 0.01$), but not *L. helicina* ($p = 0.25$). For *L. helicina* the difference in shell density between the specimens in the shallow layer (0–50 m) and those found beneath is significant when not size normalized (S10 Table). *Turborotalita quinqueloba* reaches its peak shell density of 793 in the 150–200 m depth interval. Below the 150–200 m depth interval, the shell density of *T. quinqueloba* decreases.

In the 200–300 m depth interval, the average shell density of *T. quinqueloba* is 766. The outer shell walls are thick and dense, while the CT number is lower in the internal walls (Fig 3 and S2 Fig). In contrast, the shell density of *N. pachyderma* continues to increase until 200–300 m, where it reaches a peak shell density of, on average, 813 (Fig 4). Similar to *N. pachyderma*, the shell density of *L. helicina* increases with depth. At 0–50 m, *L. helicina* have an average CT number of 670, and by 200–300 m they reach a peak average density of 819 (Fig 2). Collectively, we found that the difference in shell density between sampling intervals were most significant between the shallowest (0–50 m) and deepest (200–300 m) interval (S8–10 Tables). *Turborotalita quinqueloba* showed the most significant variation between nets, and *L. helicina* the least.

Fig 2. Box-and-whisker plot of shell density with water depth for A) *Neogloboquadrina pachyderma* (n = 120), B) *Turborotalita quinqueloba* (n = 115) and c) *Limacina helicina* (n = 25) sampled from the crater area in 2016. Boxes extend from the lower to upper quartile values of the data, with a line at the median. Whiskers indicate 1.5 times the inter-quartile distance. Black dots are single measurements.

Fig 3. *Turborotalita quinqueloba* from water column. A) Texture of test surface of *Turborotalita quinqueloba* at three different depth intervals; 0–50 m, 100–150 m and 200–300 m. B) Variation in inner and outer shell density of *T. quinqueloba* as mean CT number of entire shell measured by XMCT increases. C) Mean CT number of *T. quinqueloba* (n = 115), with error bars, plotted against water depth and calcite saturation. D) *T. quinqueloba* cross-section before and after gametogenesis. Scale bars measure 100 μm.

Fig 4. *Neogloboquadrina pachyderma* from water column. A) Texture of test surface of *Neogloboquadrina pachyderma* at four different depth intervals; 0–50 m, 50–100 m, 100–150 m and 200–300 m. B) Variation in inner and outer shell density of *N. pachyderma* with mean CT number of entire shell measured by XMCT. C) Mean CT number of *N. pachyderma* (n = 120), with error bars, plotted against water depth and calcite saturation. Scale bars measure 100 μm.

Although we found a general increase in CT number and shell thickness with depth, we note a large range in CT numbers (Fig 2 and S2 Table) and mean shell thickness (S2 Table) at each sampling depth

interval. This is particularly true for *T. quinqueloba* in the shallowest depth interval 0–50 m where the CT numbers of individual specimens are evenly distributed from 539 to 826, and the mean shell thickness ranges from 2.02 to 3.25 μm. Furthermore, in the 0–50 m depth interval the average CT numbers for *N. pachyderma* and *L. helicina* ranges from 592 to 857, and 637 to 751, respectively. The shell thickness of *N. pachyderma* and *L. helicina* at the 0–50 m depth interval ranged from 1.94 to 5.28 μm, and 1.98 to 2.75 μm, respectively.

3.3 Planktonic Foraminifera

3.3.1 Planktonic Foraminifera from the water column

Both *N. pachyderma* and *T. quinqueloba* show a statistically significant positive correlation between individual shell weight, CT number, mean shell thickness and area density with water depth (S4–S5 Table). Cytoplasm-bearing specimens of both species are found in each sampling depth interval and constitute 80–100 % of XMCT scanned shells from the top 150 m (S7 Table). Below 150 m the percentage of live specimens decreases to 75 % and 78.6 % for *N. pachyderma* in the 150–200 m and 200–300 m depth interval, respectively (S7 Table). For *T. quinqueloba* there is a greater decrease in the percentage of live specimens below 150 m, with 14.3 % and 23.5 % containing a cytoplasm in the 150–200 m and 200–300 m depth interval, respectively (S7 Table). For both *T. quinqueloba* and *N. pachyderma* there is increasing formation of a layer of crust on the outer shell with depth. The texture of the shells in the shallowest samples are smooth without any calcite crust. Thereafter ridges appear that become increasingly “rough” with depth and increase in CT number (Figs 3A and 4A).

Both species undergo gradual shell thickening with depth. At 0–50 m water depth the average shell thickness of *N. pachyderma* and *T. quinqueloba* is 2.5±0.8 μm (n = 15) and 2±0.5 μm (n = 28), respectively. *Neogloboquadrina pachyderma* reaches peak thickness at 200–300 m, where the average shell thickness is 4.3±0.7 μm (n = 29). *Turborotalita quinqueloba* reaches peak thickness at 150–200 m, where the average shell thickness is 3.5±0.7 μm (n = 13). In the 200–300 m depth interval the shell of *T. quinqueloba* has decreased to 3.1±0.8 μm (n = 24). Collectively, the shell walls of *N. pachyderma*

and *T. quinqueloba* thicken by 40.8 % and 35.1 %, respectively, from their thinnest at the 0–50 m sampling interval to their peak shell thickness.

The mean shell thickness shows a strong correlation with the CT number (Fig 5; S4–S5 Table). The mean shell thickness of individual *T. quinqueloba* and *N. pachyderma* have an exponential relationship with their respective CT numbers (Figs 5A–5B). The exponential curve for *N. pachyderma* is steeper than the curve for *T. quinqueloba*. Furthermore, *N. pachyderma* (n = 120) tend to be larger, denser, and thicker than *T. quinqueloba* (n = 115), based on mean CT numbers and calcite volume (S1–S2 Table).

Fig 5. Shell thickness versus shell density. Mean shell thickness of A) *Neogloboquadrina pachyderma* and B) *Turborotalita quinqueloba* plotted versus mean shell density in the form of a CT number, fitted with an exponential model. Shells from water column samples are represented by circles, while crosses represent shells from surface sediments. Exponential model is only fitted to shells from water column. Arrow in B) is pointing to an outlier.

3.3.2 Planktonic Foraminifera from the surface sediments

In the top 1 cm of the sediments, both *N. pachyderma* and *T. quinqueloba* are found in a wide range of dissolution states. Some of the planktonic foraminiferal specimens found in the surface sediments have similar shell densities as those found in the overlying water column (Figs 6A and 6C; Figs 7A and 7C), while other specimens have undergone dissolution (Figs 6D and 6E; Figs 7E and 7F). Out of all of the *N. pachyderma* shells found in the surface sediments, there is a high proportion of low-density shells (9 out of 12, 75%), i.e. shells which can be regarded as outliers in the thickness versus density plot (Fig 5A). In contrast, low-density *T. quinqueloba* shells are in the minority (7 out of 18, 39%) (Fig 5B). The surface texture of *N. pachyderma* and *T. quinqueloba* vary in terms of CT number (Figs 6 and 7). In *T. quinqueloba*, the loss of the base features of the prominent spines is evident as the CT number reduces from 817 to 555, and the surface texture takes on a smoother appearance (Figs 6B and 6F). The surface texture of *N. pachyderma* appears to be mostly unaffected by post-depositional dissolution (Figs 7B and 7G). In the low-density shells, the calcite ridges are more prominent, giving it a more rugose texture overall (Fig 7G). In *N. pachyderma* we see a two-layered dissolution pattern (Fig 7F). There is a clear

divide between the less dense (CT number ~ 400) inner calcite, and the denser outer crust (CT number ~ 650) (Fig. 7F). Shells of both species from the surface sediments that have undergone post-depositional dissolution plot to the left of the exponential trendline (Fig 5). The external shell walls of the dissolved specimens remain at a similar thickness to those with a high-density shell (Figs 5–7). Dissolution primarily affects the CT number (Fig 5).

Fig 6. *Turborotalita quinqueloba* from surface sediments. Cross-sections of *Turborotalita quinqueloba* specimens (A,C,D,E) from surface sediment sample (0–1 cm), including surface texture of a B) high-density (n = 11) and F) low-density specimen (n = 7). Scale bars measure 100 μm.

Fig 7. *Neogloboquadrina pachyderma* from surface sediments. Cross-sections of *Neogloboquadrina pachyderma* specimens (A,C,D,E,F) from surface sediment sample (0–1 cm), including surface texture of a B) high-density (n = 3) and G) low-density specimen (n = 9). F) Close-up of shell wall cross-section. Scale bars measure 100 μm.

3.4 *Limacina helicina*

In *L. helicina* we see the same trend in the shell density with water depth as we do with the PF (Fig 2). *Limacina helicina* show a statistically significant positive correlation between shell diameter, CT number, and mean shell thickness with water depth (S6 Table). On average, the shell density of *L. helicina* increases with depth (Fig 8A). The mean density given by the CT number starts at a minimum, at 670, in the shallowest sampling interval (0–50 m) (Fig 8A). There is a steady increase until the deepest sampling interval where the mean CT number is 819 (Fig 8A). In contrast to the PF in the crater area, *L. helicina* generally increase in shell diameter with depth (Fig 8A; S6 Table). In the 0–50 m depth interval, the shells have the narrowest size range (131–457 μm), and an average size of 274 μm. The 150–200 m water depth interval has the largest range of shell sizes, 124–1190 μm (Fig 8A). The largest shells, on average, are found in the 200–300 m water depth interval and are 511 μm (Fig 8A). The number of whorls varied between 0.6 and 3.6 and is strongly correlated to the shell diameter ($p < 0.001$).

Fig 8. *Limacina helicina* from water column. A) *Limacina helicina* shell diameter (n = 175) and

density (n = 25) (given by CT number) with depth. B) Generalized shell size with depth plotted against aragonite saturation. C) Cross-sections of *L. helicina* specimens from 0–50 m (2 whorls), and 150–200 m (2.75 whorls) water depth interval. Grey boxes are shown as close-ups in E. D) Boxplot of Mann-Whitney *U* test on top shell thickness of *L. helicina* as a function of whorl number. E) Top of *L. helicina* specimens shown in C, schematic of shell thickness measurements performed on all shells. Scale bars measure 100 μm.

The way that *L. helicina* is distributed in the water column means that shell density has an inverse relationship with Ω_{Ar} ($R^2 = 0.54$, $p < 0.001$, Figs 8A–8B). The mean shell thickness also increases with depth, starting at 2.2 μm at 0–50 m water depth, to 2.8 μm at 200–300 m water depth. As the number of whorls increases, the shell apex thickens. The sum of four measurements done on the central-top part of the shell show that shells with 2.5 to 3.5 whorls is 25.9±3.1 μm, while shells with 1.5 to 2.25 whorls has a sum of 19.4±2 μm (Fig 8F).

4. Discussion

4.1 Distribution of PF, life cycles and shell density

Calcified shells are thought to have evolved as a mean for protection, and is widely found throughout the animal phyla [57]. Calcification intensity, the term often used to refer to shell density is believed to be primarily controlled by ambient seawater $\left[CO_3^{2-}\right]$ [38,58], and hence Ω, which is largely dictated by absolute $\left[CO_3^{2-}\right]$. In addition, the shell size of planktonic foraminifera appears to be controlled by temperature and food availability [36,38,59]. *Globigerina bulloides* when growing in favourable conditions, but with low Ω_{Ca} (~1.5), were found to grow large in size, with low density tests characterised by large and porous crystalline structures, suggesting that PF in some cases may prioritize shell size over shell density [36]. Furthermore, shell thickening by encrustation during ontogeny and/or gametogenic calcification is poorly understood and exhibit inter-species variation [60,61]. Encrustation of *N. pachyderma* in polar waters occurs at 50–200 m, and an increase in secondary calcification of *N.*

pachyderma has been shown to occur with depth [62]. The degree of encrustation in *N. pachyderma* is highly variable, it can amount to 50–70% of the total shell weight, and there is no consensus on which factors initiates the crust formation [62–64].

Planktonic foraminifera do not perform diel vertical migration [65], but it is hypothesized that they descend into deeper waters as they mature, and reproduce at certain water depths (see e.g. [66–68]). However, it is unclear how PF shell density changes with increasing water depth.

4.1.1 Comparison of *N. pachyderma* and *T. quinqueloba* in the water column and their preservation patterns

The dominant living planktonic foraminiferal species in the polar region are *N. pachyderma* and *T. quinqueloba* [69–73], which is reflected in our sampling area [30]. The differences in the shell density depth profile between *N. pachyderma* and *T. quinqueloba* can be explained in part by the differences in depth habitat and depth of reproduction [74,75]. Another factor, which may affect their calcification is that *T. quinqueloba* is a spinose species, while *N. pachyderma* is not. *Turborotalita quinqueloba* calcify within 25–75 m water depth, while *N. pachyderma* calcify within the much wider range of 25–280 m [74,75]. *Neogloboquadrina pachyderma* continue to calcify and apparently grow denser as they migrate to deeper depths throughout their lifecycle (Fig 4), an observation consistent with previous studies [62,76]. Not all *N. pachyderma* shells develop a secondary crust with depth, and these thin non-encrusted shells can be found throughout the water column [62,77]. In the North Pacific, shell parameters of *G. bulloides* such as the area density and outermost chamber wall thickness increase 20 % from the 0–50 m to the 100–150 m water depth interval [36]. We find similar results in the northern Barents Sea; the area density of *T. quinqueloba* increases by 50.1 % from the 0–50 m to the 100–150 m water depth interval, while the mean area density of *N. pachyderma* increases by 29.5 %. Furthermore, the CT numbers of *N. pachyderma* and *T. quinqueloba* increase by 10.2 % and 20.3 %, respectively, from the 0–50 m to the 150–200 m water depth interval. By the deepest sampling interval, 200–300 m, the CT number of *N. pachyderma* has increased by a further 6.6 % (n = 32), resulting in a total increase in CT number by 15.8 %. Below the 150–200 m water depth interval (n = 38), *T. quinqueloba* decrease in

density by 3.4%. The shallower and narrower depth habitat in the water column of *T. quinqueloba* compared to *N. pachyderma* is reflected in the faster rate of both increasing shell density and shell thickening per meter. However, we find thin low-density shells and thick high-density shells of both species in the entire water column (Fig 2). If we use thick high-density shells as a proxy for reproduction, then reproduction occurs in the entire water column. Cytoplasm-bearing specimens are also present in the entire water column (S7 Table), although in lower abundance in the deepest sampling intervals, especially *T. quinqueloba*. The increasing density curve with water depth may partly be the result of the higher presence of dead shells that have already released gametes.

The decrease in the CT number of *T. quinqueloba* from the 150–200 m depth interval to the 200–300 m depth interval likely reflects the dissolution of their internal shell walls (S1 Fig). This internal dissolution may be due to gamete formation and release (Fig 3D), which has been documented to occur in certain PF species [61]. Early culture studies on PF also showed that dissolution starts in the internal shell walls [78,79]. In preparation for the release of gametes, PF increase the Ω_{Ca} of the microenvironment adjacent to their shell [80]. Some foraminifera may do so by discharging alkaline seawater vacuoles, which would result in the internal environment of the foraminifera to become less basic [81]. Another explanation for the internal dissolution is the oxidation of internal organic matter, documented in the pteropod species *Limacina retroversa* and *L. helicina antarctica* [82]. However, this is less likely in PF shells, because they are made of calcite, which is more robust than aragonite and the proportion of soft tissue to shell size is significantly smaller than in pteropods [83]. The Ω_{Ca} is supersaturated throughout the water column (Ω_{Ca} = 2.4–4), yet there are no known Ω_{Ca} thresholds for PF. The presence of *T. quinqueloba* shells in the deepest sampling interval may also reflect a relic population. The internally dissolved shells may have a slower sinking rate than the specimens without dissolved internal walls, making them more likely to be sampled.

At our study site, PF shell density is strongly related to shell volume (S4–5 Table). In general, the larger the shell volume, the more dense it is. However, the increase in CT number with depth after size-normalization is still significant ($p < 0.01$). This means that the increase in shell density with depth is not a function of shell volume.

Our results highlight the importance of comparing PF in the same life stage, because the shell thickness and density gradually increases as they mature. The same size is not enough to eliminate ontogenetic effects (Figs 3 and 4), therefore it is also advisable to compare shells from the same sampling depth. In a study showing shell thinning in PF due to OA by comparing pre-industrial and modern shells, sampling depth may not have been the same [37]. A discrepancy in sampling depth may mean that the results simply show natural variation in shell thickness with depth.

The PF sampled from the water column in our study area did not show any signs of dissolution, both in the outer and inner shell wall (Figs 5A and 5B). The only exceptions are some specimens of *T. quinqueloba* found below 150 m water depth (Fig S2). There is a clear depth zonation in individual abundance [30], and shell density in both species. The increase in shell density with depth is in agreement with observations in the North Pacific [36], and is believed to be driven by ontogeny.

4.1.2 Comparison *N. pachyderma* and *T. quinqueloba* from the sediment and species-specific dissolution

The sedimentation rate in the northern Barents Sea ranges from 0.5–1.3 mm/yr [84], meaning that it takes anywhere from 8 to 20 years to accumulate 1 cm of sediment. The top 1 cm of sediments will therefore host PF that have settled at different times and thus can show a variable degree of dissolution (Figs 6 and 7). When PF from sediment samples are used in geochemical studies, it is often stated that the samples do not show any evidence of dissolution. The surface texture of *T. quinqueloba*, and especially that of *N. pachyderma* undergo only slight changes in their external appearance as they dissolve. The subtle dissolution in the surface texture may go undetected under a light microscope if all chambers are intact, which was the case for the samples used in this study. The post-depositional dissolution found in some of the specimens (Figs 6D–6E and Figs 7D–7F) is likely to alter the original chemical composition of their tests, mainly the Mg/Ca ratio, and the oxygen and carbon isotopic composition [85,86]. The higher percentage of low-density *N. pachyderma* shells (75%) compared to *T. quinqeloba* (39%) suggests that fewer low-density *T. quinqeuloba* shells remain intact in the surface sediments, which may lead to an underrepresentation of *T. quinqueloba* in the sediment records.

462 Selective dissolution of *T. quinqueloba* is also likely because of the extensive internal dissolution in the
463 low-density shells (Figs 6D and 6E), which could lead to a collapse of the entire shell resulting in
464 fragmentation.

465 The inter-species differences in the manifestation of post-depositional dissolution is thought to be
466 primarily due to the magnesium content in the calcite structure [87], thus also suggesting that the
467 calcification process is species-specific. *Neogloboquadrina pachyderma* consistently rank as one of the
468 planktonic foraminiferal species most resistant to dissolution, regardless of the region they are found,
469 while *T. quinqueloba* has a low resistance to dissolution [87,88]. The exponential curve for *N.*
470 *pachyderma* shell thickness versus CT number (Fig 5A) is steeper than that of *T. quinqueloba* (Fig 5B).
471 The steeper *N. pachyderma* curve suggests that they calcify more than *T. quinqueloba*, leading to a
472 thicker crust. The ability to build a thicker and denser crust may have a number of different explanations.
473 Firstly, there could be a difference in lifecycle length between *N. pachyderma* and *T. quinqueloba*.
474 *Neogloboquadrina pachyderma* may have a longer lifecycle than *T. quinqueloba* meaning that they
475 could calcify over a longer period of time and build thicker and denser shells. Individuals of *N.*
476 *pachyderma* have been kept alive in culture for up to 200 days [89,90]. The tendency of *N. pachyderma*
477 to build thicker and denser shells may be due to a naturally higher calcification rate, rather than a longer
478 lifecycle compared to *T. quinqueloba*. The two species may also have very different calcification
479 strategies because, unlike *N. pachyderma*, *T. quinqueloba* builds numerous spines on most of its
480 chambers at the expense of chamber walls resulting in thinner shells.

481 The two-layered dissolution pattern seen in *N. pachyderma* highlights their higher degree of resistance
482 to dissolution (Fig 7F). A similar pattern was also found in *G. bulloides* [91]. The denser outer calcite
483 of *G. bulloides* was resistant to dissolution and remained well preserved in water undersaturated with
484 respect to calcite, while the Mg-rich inner calcite dissolved [91]. This mechanism of selective
485 dissolution likely skews the sediment record to favor species with a dense outer calcite layer. Following
486 dissolution in the surface sediments, the thickness of the shell walls remains intact while the whole shell
487 gets a more porous crystalline structure, resulting in a lower mean CT number (Figs 6 and 7). In our
488 study, the dissolved shells from the surface sediments plotted to the left of the trend line showcase this

phenomenon (Figs 5A–5B), suggesting that the comparison between CT number and shell thickness can be used as a tool to identify shells which have undergone either post-depositional dissolution or calcified in low Ω_{Ca} waters [92]. However, outliers may occur if specimens have an unusual morphology. A *T. quinqueloba* with an abnormally large and low-density final chamber plotted significantly to the left of the other shells from the water column (Fig 5B). Large, yet low-density shells may be found when PF calcify in low Ω_{Ca} waters, and shift their ecological strategy to favor shell size over shell density [36], although, *T. quinqueloba* has been shown to present a large phenotypic variation related to changes in sea surface temperature [93].

4.2 *Limacina helicina*

4.2.1 Distribution in the water column and shell density

In contrast to PF, *L. helicina* do perform diel vertical migrations. Mature individuals diurnally migrate in the upper 200 m of the water column, while veligers and juveniles migrate in the top 50 m [94]. Like PF, it is also not known how the shell density of *L. helicina* changes with depth and increasing number of whorls. There is a skewness towards numerous small individuals at the surface, which is in agreement with previous findings in the polar region [95]. Because they migrate vertically, *L. helicina* showed less of a vertical zonation in shell density through the water column (S8–10 Tables). The statistical significance in the increase in shell density with depth is driven by the low-density, smaller specimens in the 0–50 m depth interval (S10 Table). This is an observation consistent with their distribution in the water column [94]. The dominance of small individuals at the surface is likely because they have not developed their swimming wings and must therefore stay in the food-rich layer for growth. Once they have developed their wings they are able to migrate deeper in order to avoid predators, and this predation risk is likely what controls the vertical distribution of *Limacina helicina* [96].

4.2.2 Dissolution of *L. helicina*, ontogeny, and future outlook

The connection between low Ω_{Ar} and shell damage in *L. helicina* has been confirmed by observations

513 from marine environments with large natural gradients in the carbonate chemistry [97]. However, recent
514 studies on the periostracum of *L. helicina* suggests that they may not be as sensitive to OA as previously
515 claimed [98,99]. Further, an increased food supply may reduce or even negate the effects of living in
516 low-Ω waters [100,101]. In the Arctic, *L. helicina* juveniles may experience waters with lowest [CO_3^{2-}]
517 and Ω_{Ar} during fall and winter, and it is unclear whether they calcify during this time or await elevated
518 saturation states at the onset of CO_2 uptake by phytoplankton production in spring [18]. Seasonal decline
519 in carbonate parameters was found to coincide with a higher proportion of pteropod shell dissolution in
520 the North Sea [100]. *Limacina helicina* shell dissolution has been recorded at a Ω_{Ar} of 1.4 [97], and
521 greatly reduced calcification at Ω_{Ar}<1.2 [101]. An Ω_{Ar} of 1.4 is close to the values we observe at the
522 bottom waters in our study area. Moreover, our saturation states are based on a summer situation when
523 the surface water has higher saturation states than what we would expect in fall and winter.

524 The increase in the thickness of their shell apex with growth could mean that they are more resistant to
525 dissolution if the Ω_{Ar} at out study site decreases in fall and winter (Figs 8D and 8E), and their depth
526 habitat deepens with growth. In the surface water (0–50 m) during the summer, the Ω_{Ar} conditions are
527 favourable (Fig 8B), allowing the small, low-density individuals to prioritize the growth of their
528 muscles. Their thin and delicate shells during this stage of their life cycle will be less compromised with
529 the higher Ω_{Ar}. It is possible that the thickening of the shell apex with increasing whorl number could
530 be linked to re-directing the energy to calcification after finalizing the development of their soft body.
531 It has been demonstrated that *L. helicina* can add new shell material after damage [98], and as long as
532 the Ω_{Ar} is ≥1.2 ongoing thickening can occur over the entire shell, including the protoconch [101]. The
533 repair mechanism of *L. helicina* and ongoing thickening means that they can choose specific areas of
534 their shell to thicken after the initial calcification as part of a resilience strategy to environmental stress.
535 Instances of over-calcification as a reaction to low Ω values have been found in barnacles [102] and
536 coccolithophores [103,104], further suggesting that some calcifiers can re-direct energy for calcification
537 when their shells are vulnerable.

538 Longer term studies using the techniques described here could shed light on the natural variability in the
539 shell properties of *L. helicina* throughout their life cycle. Topics which could be addressed are to what

extent calcification intensity varies with Ω_{Ar} and nutrients, and if specimens living in low Ω_{Ar} environments have adapted by building of thicker and denser shells. One could also investigate if there are geographical variations in whorl thickness depending on seasonality and chemical environment. Furthermore, with the ongoing climate change, water temperatures in the Barents Sea have increased [4] and are projected to continue to increase globally [105]. Synergistic effects of OA and warming have been demonstrated to be especially lethal for juvenile *L. helicina* [106,107], highlighting the need for a better understanding of the *L. helicina* calcification strategy.

5. Conclusions

The application of the XMCT scanning technique on the extant planktonic calcifying foraminiferal (PF) species *Neogloboquadrina pachyderma* and *Turborotalita quinqueloba* and the pteropod species *Limacina helicina* retrieved from stratified plankton net samples from the northern Barents Sea have provided us with a unique dataset to better understand the shell density distribution with depth and ontogeny of these species at high Arctic latitudes. We found that both PF and *L. helicina* increase in shell density with depth, however there were inter-species differences in the PF due to depth habitat and reproduction. *Neogloboquadrina pachyderma* tends to be both thicker and denser than *T. quinqueloba*, and continues to increase in density until the deepest sampling interval 200–300 m. *Turborotalita quinqueloba* decrease in shell density below the depth interval 150–200 m, this loss may be due to internal dissolution associated with gamete release or bacterial degradation of the cytoplasm. Our results highlight the importance of sampling at the same water depth interval when comparing PF calcification intensity. In the surface sediments (0–1 cm) the shell preservation state was highly variable in both planktonic foraminiferal species with little alteration of the surface shell texture. In the surface sediments, *N. pachyderma* appeared more resilient towards post-depositional dissolution. In this area from the Barents Sea, the PF did not suffer from dissolution effects. Dissolution occurred after death and after settling on the sea floor. We observed that *L. helicina* thickens their shell apex as the number of whorls increase. There was a weaker zonation in shell density through the water column compared to PF, which is probably due to vertical migration. We recommend longer-term studies on planktonic

calcifiers using the XMCT scanning technique. Longer studies in different carbonate chemistry environments would provide even greater insight on the natural variability in shell density. This knowledge is important in order to use PF and *L. helicina* as biological indicators for ocean acidification and to predict future developments in food webs. It is also important in the use of PF as paleo-proxies.

Acknowledgements

We thank the captain and crew of the R/V *Helmer Hanssen*, without whom this work would not have been possible. We thank Dr. Arunima Sen for help with statistical analysis. We are very grateful to Dr. Brett Metcalfe and two Anonymous reviewers for their comments that greatly helped us improve the manuscript. The study was supported by the Centre for Arctic Gas Hydrate, Environment and Climate (CAGE).

Author Contributions

Conceptualization: Siri Ofstad.

Data Curation: Siri Ofstad.

Formal analysis: Siri Ofstad, Katsunori Kimoto.

Funding acquisition: Tine L. Rasmussen, Katsunori Kimoto, Melissa Chierici, Agneta Fransson.

Investigation: Siri Ofstad, Katarzyna Zamelczyk, Katsunori Kimoto.

Resources: Katsunori Kimoto, Melissa Chierici, Agneta Fransson, Tine L. Rasmussen.

Supervision: Katarzyna Zamelczyk, Tine L. Rasmussen.

Validation: Katarzyna Zamelczyk, Katsunori Kimoto, Melissa Chierici, Agneta Fransson, Tine L. Rasmussen.

Visualization: Siri Ofstad.

Writing – original draft: Siri Ofstad.

Writing – review & editing: Siri Ofstad, Katarzyna Zamelczyk, Katsunori Kimoto, Melissa Chierici, Agneta Fransson, Tine L. Rasmussen.

Financial Disclosure Statement

This work was funded by the Research Council of Norway through its Centres of Excellence scheme (grant number 223259). The XMCT analysis was funded by Japan Agency for Marine-Earth Science and Technology Grants-In-Aid for Scientific Research (KAKENHI) Grant Numbers 15H05712 and 16H04961. The water chemistry sampling and analysis was funded by the Flagship research program "Ocean Acidification and effects in northern waters" within the FRAM- High North Research Centre for Climate and the Environment. The funders had no role in study design, data collection and analysis, decision to publish, or preparation of the manuscript. The publication charges for this article have been funded by a grant from the publication fund of UiT - The Arctic University of Norway.

Data Set

The CTD and carbonate chemistry data from the crater area in June 2016 is available at Norwegian Marine Data Center (https://doi.org/10.21335/NMDC- 225800978). All other data is available in the supporting information file (S1-10 Table, S1-3 Dataset).

References

1. Årthun M, Eldevik T, Smedsrud LH, Skagseth Ø, Ingvaldsen RB. Quantifying the Influence of Atlantic Heat on Barents Sea Ice Variability and Retreat. J Clim. 2012;25(13): 4736–4743. doi:10.1175/JCLI-D-11-00466.1

2. Smedsrud LH, Esau I, Ingvaldsen RB, Eldevik T, Haugan PM, Li C, et al. The role of the Barents Sea in the Arctic climate system. 2013;5(2012): 415–449. doi:10.1002/rog.20017.1.INTRODUCTION

3. Loeng H. Features of the physical oceanographic conditions of the Barents Sea. Polar Res.

1991;10(1): 5–18. doi:10.1111/j.1751-8369.1991.tb00630.x

4. Lind S, Ingvaldsen RB, Furevik T. Arctic warming hotspot in the northern Barents Sea linked to declining sea-ice import. Nat Clim Chang. 2018;8(7): 634–639. doi:10.1038/s41558-018-0205-y

5. Skagseth Ø, Furevik T, Ingvaldsen R, Loeng H, Mork KA, Orvik KA, et al. Volume and Heat Transports to the Arctic Ocean Via the Norwegian and Barents Seas. In: Dickson RR, Meincke J, Rhines P, editors. Arctic-Subarctic Ocean Fluxes: Defining the Role of the Northern Seas in Climate. Dordrecht: Springer Netherlands; 2008. pp. 45–64. doi:10.1007/978-1-4020-6774-7_3

6. Oziel L, Sirven J, Gascard JC. The Barents Sea frontal zones and water masses variability (1980-2011). Ocean Sci. 2016;12(1): 169–184. doi:10.5194/os-12-169-2016

7. Wassmann P, Kosobokova KN, Slagstad D, Drinkwater KF, Hopcroft RR, Moore SE, et al. The contiguous domains of Arctic Ocean advection: Trails of life and death. Prog Oceanogr. 2015;139: 42–65. doi:10.1016/j.pocean.2015.06.011

8. Dalpadado P, Ingvaldsen RB, Stige LC, Bogstad B, Knutsen T, Ottersen G, et al. Climate effects on Barents Sea ecosystem dynamics. ICES J Mar Sci. 2012;69(7): 1303–1316. doi:10.1093/icesjms/fss063

9. Neukermans G, Oziel L, Babin M. Increased intrusion of warming Atlantic water leads to rapid expansion of temperate phytoplankton in the Arctic. Glob Chang Biol. 2018;24(6): 2545–2553. doi:10.1111/gcb.14075

10. Fossheim M, Primicerio R, Johannesen E, Ingvaldsen RB, Aschan MM, Dolgov A V. Recent warming leads to a rapid borealization of fish communities in the Arctic. Nat Clim Chang. 2015;5(7): 673–677. doi:10.1038/nclimate2647

11. Bjørklund KR, Kruglikova SB, Anderson OR. Modern incursions of tropical Radiolaria into the Arctic Ocean. J Micropalaeontology. 2012;31(2): 139–158. doi:10.1144/0262-821X11-030

12. Fransson A, Chierici M, Anderson LG, Bussmann I, Kattner G, Peter Jones E, et al. The importance of shelf processes for the modification of chemical constituents in the waters of the Eurasian Arctic Ocean: Implication for carbon fluxes. Cont Shelf Res. 2001;21(3): 225–242. doi:10.1016/S0278-4343(00)00088-1

13. Bates NR, Mathis JT. The Arctic Ocean marine carbon cycle: evaluation of air-sea CO2 exchanges, ocean acidification impacts and potential feedbacks. Biogeosciences. 2009;6(11): 2433–2459. doi:10.5194/bg-6-2433-2009

14. Skogen MD, Olsen A, Børsheim KY, Sandø AB, Skjelvan I. Modelling ocean acidification in the Nordic and Barents Seas in present and future climate. J Mar Syst. 2014;131: 10–20. doi:10.1016/j.jmarsys.2013.10.005

15. Omar A, Johannessen T, Kaltin S, Olsen A. Anthropogenic increase of oceanic pCO2 in the Barents Sea surface water. J Geophys Res Ocean. 2003;108(C12): 1–8. doi:10.1029/2002JC001628

16. Evans W, Mathis JT, Cross JN. Calcium carbonate corrosivity in an Alaskan inland sea. Biogeosciences. 2014;11: 365–379. doi:10.5194/bg-11-365-2014

17. Fransson A, Chierici M, Nomura D, Granskog MA, Kristiansen S, Martma T, et al. Effect of glacial drainage water on the CO2 system and ocean acidification state in an Arctic tidewater-glacier fjord during two contrasting years. J Geophys Res Ocean. 2015;120.

doi:10.1002/2014JC010320

18. Fransson A, Chierici M, Hop H, Findlay HS, Kristiansen S, Wold A. Late winter-to-summer change in ocean acidification state in Kongsfjorden, with implications for calcifying organisms. Polar Biol. 2016;39(10): 1841–1857. doi:10.1007/s00300-016-1955-5

19. Piquet AMT, Van De Poll WH, Visser RJW, Wiencke C, Bolhuis H, Buma AGJ. Springtime phytoplankton dynamics in Arctic Krossfjorden and Kongsfjorden (Spitsbergen) as a function of glacier proximity. Biogeosciences. 2014;11(8): 2263–2279. doi:10.5194/bg-11-2263-2014

20. Fabry VJ, Seibel BA, Feely RA, Orr JC. Impacts of ocean acidification on marine fauna and ecosystem processes. ICES J Mar Sci. 2008;65(3): 414–432. doi:10.1093/icesjms/fsn048

21. Larson RJ, Harbison GR. Source and Fate of Lipids in Polar Gelatinous Zooplankton. Arctic. 1989;42(4): 339–346. doi:10.14430/arctic1675

22. Hunt BPV, Pakhomov EA, Hosie GW, Siegel V, Ward P, Bernard K. Pteropods in Southern Ocean ecosystems. Prog Oceanogr. 2008;78(3): 193–221. doi:10.1016/j.pocean.2008.06.001

23. Weslawski JM, Hacquebord L, Stempniewicz L, Malinga M. Greenland whales and walruses in the Svalbard food web before and after exploitation. Oceanologia. 2000;42(1): 37–56.

24. Willette TM, Cooney RT. Ecological processes influencing mortality of juvenile pink salmon (Oncorhynchus gorbuscha) in Prince William Sound, Alaska. Fish Oceanogr. 2001;10: 14–41. doi:10.1046/j.1054-6006.2001.00043.x

25. Bathmann U V., Noji TT, von Bodungen B. Sedimentation of pteropods in the Norwegian Sea in autumn. Deep Res. 1991;38(10): 1341–1360. doi:10.1016/0198- 0149(91)90031- A

26. Schiebel R. Planktic foraminiferal sedimentation and the marine calcite budget. Global Biogeochem Cycles. 2002;16(4): 1–21. doi:10.1029/2001GB001459

27. Meilland J, Schiebel R, Lo Monaco C, Sanchez S, Howa H. Abundances and test weights of living planktic foraminifers across the Southwest Indian Ocean: Implications for carbon fluxes. Deep Res Part I Oceanogr Res Pap. 2018;131(March 2017): 27–40. doi:10.1016/j.dsr.2017.11.004

28. Meilland J, Fabri-Ruiz S, Koubbi P, Monaco C Lo, Cotte C, Hosie GW, et al. Planktonic foraminiferal biogeography in the Indian sector of the Southern Ocean: Contribution from CPR data. Deep Res Part I Oceanogr Res Pap. 2016;110: 75–89. doi:10.1016/j.dsr.2015.12.014

29. Manno C, Accornero A, Umani SF. Importance of the contribution of Limacina helicina faecal pellets to the carbon pump in Terra Nova Bay (Antarctica). J Plankton Res. 2010;32(2): 145–152. doi:10.1093/plankt/fbp108

30. Ofstad S, Meilland J, Zamelczyk K, Chierici M. Development, Productivity, and Seasonality of Living Planktonic Foraminiferal Faunas and Limacina helicina in an Area of Intense Methane Seepage in the Barents Sea. J Geophys Res Biogeosciences. 2020;125(2): 1–24. doi:10.1029/2019JG005387

31. Meilland J, Howa H, Hulot V, Demangel I, Salaün J, Garlan T. Population dynamics of modern planktonic foraminifera in the western Barents Sea. Biogeosciences. 2020;17(6): 1437–1450.

32. Kacprzak P, Panasiuk A, Wawrzynek J, Weydmann A. Distribution and abundance of pteropods in the western Barents Sea. Oceanol Hydrobiol Stud. 2017;46(4): 393–404. doi:10.1515/ohs-2017-0039

33. Howes EL, Eagle RA, Gattuso JP, Bijma J. Comparison of Mediterranean pteropod shell biometrics and ultrastructure from historical (1910 and 1921) and present day (2012) samples provides baseline for monitoring effects of global change. PLoS One. 2017;12(1): 1–23. doi:10.1371/journal.pone.0167891

34. Oakes RL, Sessa JA. Assessing annual variability in the shell thickness of the pteropod Heliconoides inflatus in the Cariaco Basin using micro-CT scanning. 2019(October).

35. Beer CJ, Schiebel R, Wilson PA. Testing planktic foraminiferal shell weight as a surface water [CO2-3] proxy using plankton net samples. Geology. 2010;38(2): 103–106. doi:10.1130/G30150.1

36. Iwasaki S, Kimoto K, Sasaki O, Kano H, Uchida H. Sensitivity of planktic foraminiferal test bulk density to ocean acidification. 2019;(June): 1–9. doi:10.1038/s41598-019-46041-x

37. Fox L, Stukins S, Hill T, Miller CG. Quantifying the Effect of Anthropogenic Climate Change on Calcifying Plankton. Sci Rep. 2020;10(1620): 1–9. doi:10.1038/s41598-020-58501-w

38. Osborne EB, Thunell RC, Marshall BJ, Holm JA, Tapa EJ, Benitez-Nelson C, et al. Calcification of the planktonic foraminifera Globigerina bulloides and carbonate ion concentration: Results from the Santa Barbara Basin. Paleoceanography. 2016;31(8): 1083–1102. doi:10.1002/2016PA002933

39. Marshall BJ, Thunell RC, Henehan MJ, Astor Y, Wejnert KE. Planktonic foraminiferal area density as a proxy for carbonate ion concentration: A calibration study using the Cariaco Basin ocean time series. Paleoceanography. 2013;28(2): 363–376. doi:10.1002/palo.20034

40. de Moel H, Ganssen GM, Peeters FJC, Jung SJA, Kroon D, Brummer GJA, et al. Planktic foraminiferal shell thinning in the Arabian Sea due to anthropogenic ocean acidification? Biogeosciences. 2009;6(9): 1917–1925. doi:10.5194/bg-6-1917-2009

41. Barker S, Elderfield H. Foraminiferal Calcification Response to Glacial-Interglacial Changes in Atmospheric CO2. Science (80-). 2002;297(5582): 833–836. doi:10.1126/science.1072815

42. Todd C. Planktic foraminiferal test size and weight response to the late Pliocene environment Planktic Foraminiferal Test Size and Weight Response to the Late Pliocene Environment. Paleoceanogr Paleoclimatology. 2020;35(1): e2019PA003738. doi:10.1029/2019PA003738

43. Naik SS, Naidu PD, Govil P, Godad S. Relationship between weights of planktonic foraminifer shell and surface water CO3= concentration during the Holocene and Last Glacial Period. Mar Geol. 2010;275(1–4): 278–282. doi:10.1016/j.margeo.2010.05.004

44. Gonzalez-Mora B, Sierro FJ, Flores JA. Controls of shell calcification in planktonic foraminifers. Quat Sci Rev. 2008;27: 956–961. doi:10.1016/j.quascirev.2008.01.008

45. Andreassen K, Hubbard A, Winsborrow MCM, Patton H, Vadakkepuliyambatta S, Plaza-Faverola A, et al. Massive blow-out craters formed by hydrate-controlled methane expulsion from the Arctic seafloor. Science (80-). 2017;356(6341): 948–953. doi:10.1126/science.aal4500

46. Jakobsson M, Mayer L, Coakley B, Dowdeswell JA, Forbes S, Fridman B, et al. The International Bathymetric Chart of the Arctic Ocean (IBCAO) Version 3.0. Geophys Res Lett. 2012;39(12). doi:10.1029/2012GL052219

47. Lalli CM, Wells FE. Reproduction in the genus Limacina (Opisthobranchia Thecosomata). J Zool. 1978;186(1): 95–108. doi:10.1111/j.1469-7998.1978.tb03359.x

48. Janssen AW. Holoplanktonic Mollusca (Gastropoda: Pterotracheoidea, Janthinoidea, Thecosomata and Gymnosomata) from the Pliocene of Pangasinan (Luzon, Philippines). Scr Geol. 2007;135: 29–177.

49. RStudio Team. RStudio: Integrated Development for R. RStudio, Inc. Boston, MA; 2015. Available: http://www.rstudio.com/

50. Pierrot DE, Wallace DWR. MS Excel program developed for CO2 system calculations. Oak Ridge, Tenn.: ORNL/CDIAC-105, Carbon Dioxide Inf. Anal. Cent., Oak Ridge Natl. Lab., U.S. Dep. of Energy; 2006.

51. Lewis E, Wallace DWR. CO2SYS-Program developed for CO2 system calculations, ORNL/CDIAC-105. Oak Ridge, Tenn.: Carbon Dioxide Inf. Anal. Cent., Oak Ridge Natl. Lab.; 1998. doi:10.2172/639712

52. Dickson AG. Thermodynamics of the dissociation of boric acid in synthetic seawater from 273.15 to 318.15 K. Deep Sea Res Part A Oceanogr Res Pap. 1990;37(5): 755–766. doi:10.1016/0198-0149(90)90004-F

53. Mehrbach C, Culberson CH, Hawley JE, Pytkowicx RM. Measurement of the Apparent Dissociation Constants of Carbonic Acid in Seawater At Atmospheric Pressure. Limnol Oceanogr. 1973;18(6): 897–907. doi:10.4319/lo.1973.18.6.0897

54. Dickson A, Millero F. A Comparison of the Equilibrium Constants for the Dissociation of Carbonic Acid in Seawater Media. Deep Sea Research Part A. Oceanographic Research Papers. 1987. doi:10.1016/0198-0149(87)90021-5

55. Dickson A, Millero F. A Comparison of the Equilibrium Constants for the Dissociation of Carbonic Acid in Seawater Media. Deep Sea Research Part A. Oceanographic Research Papers. 1987. doi:10.1016/0198-0149(87)90021-5

56. Cottier F, Tverberg V, Inall M, Svendsen H, Nilsen F, Griffiths C. Water mass modification in an Arctic fjord through cross-shelf exchange: The seasonal hydrography of Kongsfjorden, Svalbard. J Geophys Res Ocean. 2005;110(12): 1–18. doi:10.1029/2004JC002757

57. Bengtson S. The advent of skeletons. Early life on earth. New York, NY: Nobel symposium No. 84. Columbia University Press; 1994. pp. 412–425.

58. Weinkauf MFG, Moller T, Koch MC, Kucera M. Calcification intensity in planktonic foraminifera reflects ambient conditions irrespective of environmental stress. Biogeosciences. 2013;10(10): 6639–6655. doi:10.5194/bg-10-6639-2013

59. Manno C, Morata N, Bellerby R. Effect of ocean acidification and temperature increase on the planktonic foraminifer Neogloboquadrina pachyderma (sinistral). Polar Biol. 2012;35(9): 1311–1319. doi:10.1007/s00300-012-1174-7

60. Steinhardt J, Nooijer LJ De, Brummer GJ, Reichart G. Profiling planktonic foraminiferal crust formation. Geochemistry Geophys Geosystems. 2015;18(1–2): 1541–1576. doi:10.1002/2014GC005684.Key

61. Caron DA, Anderson OR, Lindsey JL, Faber WW, Lin EE. Effects of Gametogenesis on Test Structure and Dissolution of Some Spinose Planktonic Foraminifera and Implications for Test Preservation. Mar Micropaleontol. 1990;16(1–2): 93–116. doi:10.1016/0377-8398(90)90031-G

62. Kohfeld KE, Fairbanks RG, Smith SL, Walsh ID. Neogloboquadrina pachyderma (sinistral coiling) as paleoceanographic tracers in polar oceans: Evidence from Northeast Water Polynya

plankton tows, sediment traps, and surface sediments. Paleoceanography. 1996;11(6): 679–699. doi:10.1029/96PA02617

63. Arikawa R. Distribution and Taxonomy of Globigerina pachyderma (Ehrenberg) off the Sanriku Coast, Northeast Honshu, Japan. Tohoku Univ Sci Rep Ser Geol. 1983;53: 103–157.

64. Stangeew E. Distribution and Isotopic Composition of Living Planktonic Foraminifera N. pachyderma (sinistral) and T. quinqueloba in the High Latitude North Atlantic. Christian-Albrechts-Universität, Kiel. 2001. Available: https://macau.uni-kiel.de/rsc/thumbnail/diss_mods_00000464.png

65. Meilland J, Siccha M, Weinkauf MFG, Jonkers L, Morard R. Highly replicated sampling reveals no species-specific vertical habitats in diurnal vertical migration but stable planktonic foraminifera. J Plankton Res. 2019;41(2): 127–141. doi:10.1093/zoolinnean/zly093

66. Bijma J, Erez J, Hemleben C. Lunar and semi-lunar reproductive cycles in some spinose planktonic foraminifers. J Foraminifer Res. 1990;20(2): 117–127. doi:10.2113/gsjfr.20.2.117

67. Hemleben C, Spindler M, Anderson OR. Modern Planktonic Foraminifera. 1st ed. Springer-Verlag New York; 1989. doi:10.1007/978-1-4612-3544-6

68. Schiebel R, Bijma J, Hemleben C. Population dynamics of the planktic foraminifer Globigerina bulloides from the eastern North Atlantic. Deep Res Part I Oceanogr Res Pap. 1997;44(9–10): 1701–1713. doi:10.1016/S0967-0637(97)00036-8

69. Carstens J, Hebbeln D, Wefer G. Distribution of planktic foraminifera at the ice margin in the Arctic (Fram Strait). Mar Micropaleontol. 1997;29(3–4): 257–269. doi:10.1016/S0377-8398(96)00014-X

70. Eynaud F. Planktonic foraminifera in the arctic: Potentials and issues regarding modern and quaternary populations. IOP Conf Ser Earth Environ Sci. 2011;14(1). doi:10.1088/1755-1315/14/1/012005

71. Jensen S. Planktische Foraminiferen im Europäischen Nordmeer: Verbreitung und Vertikalfluß sowie ihre Entwicklung während der letzten 15000 Jahre. Berichte Sonderforschungsbereich 313, Univ Kiel. 1998;75(75): 1–105.

72. Pados T, Spielhagen RF. Species distribution and depth habitat of recent planktic foraminifera in Fram Strait, Arctic Ocean. Polar Res. 2014;33(1): 22483. doi:10.3402/polar.v33.22483

73. Volkmann R. Planktic Foraminifers in the Outer Laptev Sea and the Fram Strait-Modern Distribution and Ecology. J Foraminifer Res. 2000;30(3): 157–176. doi:10.2113/0300157

74. Simstich J, Sarnthein M, Erlenkeuser H. Paired δ18O signals of Neogloboquadrina pachyderma (s) and Turborotalita quinqueloba show thermal stratification structure in Nordic Seas. Mar Micropaleontol. 2003;48(1–2): 107–125. doi:10.1016/S0377-8398(02)00165-2

75. Greco M, Jonkers L, Kretschmer K, Bijma J, Kucera M. Variable habitat depth of the planktonic foraminifera Neogloboquadrina pachyderma in the northern high latitudes explained by sea-ice and chlorophyll concentration. Biogeosciences. 2019;16(17): 3425–3437. doi:10.5194/bg-16-3425-2019

76. Carstens J, Wefer G. Recent distribution of planktonic foraminifera in the Nansen Basin, Arctic Ocean. Deep Res. 1992;39.

77. Kozdon R, Ushikubo T, Kita NT, Spicuzza M, Valley JW. Intratest oxygen isotope variability

in the planktonic foraminifer N . pachyderma: Real vs . apparent vital effects by ion microprobe. Chem Geol. 2009;258(3–4): 327–337. doi:10.1016/j.chemgeo.2008.10.032

78. Brown SJ, Elderfield H. Variations in Mg/Ca and Sr/Ca ratios of planktonic foraminifera caused by postdepositional dissolution: Evidence of shallow Mg-dependent dissolution. Paleoceanography. 1996;11(5): 543–551. doi:10.1029/96PA01491

79. Hecht AD, Eslinger E V, Garmon LB. Experimental studies on the dissolution of planktonic foraminifera. In: Sliter W V, Bé AWH, Berger WH, editors. Dissolution of Deep-sea Carbonates. Cushman Foundation for Foraminiferal Research; 1975. pp. 59–69.

80. Hamilton CP, Spero HJ, Bijma J, Lea DW. Geochemical investigation of gametogenic calcite addition in the planktonic foraminifera Orbulina universa. Mar Micropaleontol. 2008;68(3–4): 256–267. doi:10.1016/j.marmicro.2008.04.003

81. Erez J. The Source of Ions for Biomineralization in Foraminifera and Their Implications for Paleoceanographic Proxies. Rev Mineral Geochemistry. 2003;54(1): 115–149. doi:10.2113/0540115

82. Oakes RL, Peck VL, Manno C, Bralower TJ. Degradation of Internal Organic Matter is the Main Control on Pteropod Shell Dissolution After Death. Global Biogeochem Cycles. 2019;33(6): 749–760. doi:10.1029/2019GB006223

83. Watanabe E, Onodera J, Harada N, Honda MC, Kimoto K, Kikuchi T, et al. Enhanced role of eddies in the Arctic marine biological pump. Nat Commun. 2014;5(1): 3950. doi:10.1038/ncomms4950

84. Zaborska A, Carroll J, Papucci C, Torricelli L, Carroll ML, Walkusz-Miotk J, et al. Recent sediment accumulation rates for the Western margin of the Barents Sea. Deep Res II. 2008;55(20–11): 2352–2360. doi:10.1016/j.dsr2.2008.05.026

85. Wu G, Berger WH. Planktonic foraminifera: Differential dissolution and the Quaternary stable isotope Record in the west equatorial Pacific. Paleoceanography. 1989;4(2): 181–198. doi:10.1029/PA004i002p00181

86. Nürnberg D. Magnesium in tests of Neogloboquadrina pachyderma sinistral from high northern and southern latitudes. J Foraminifer Res. 1995;25(4): 350–368. doi:10.2113/gsjfr.25.4.350

87. Petro SM, Pivel MAG, Coimbra JC. Foraminiferal solubility rankings: A contribution to the search for consensus. J Foraminifer Res. 2018;48(4): 301–313. doi:10.2113/gsjfr.48.4.301

88. Malmgren BA. Ranking of dissolution susceptibility of planktonic foraminifera at high latitudes of the South Atlantic Ocean. Mar Micropaleontol. 1983;8(3): 183–191. doi:10.1016/0377-8398(83)90023-3

89. Spindler M. On the salinity tolerance of the planktonic foraminifera Neogloboquadrina pachyderma from Antarctic sea ice. Proc NIPR Symp Polar Biol. 1996;9: 85–91.

90. Kimoto K. Planktic Foraminifera. In: Ohtsuka S, Suzaki T, Horiguchi T, Suzuki N, Not F, editors. Marine protists: diversity and dynamics. Tokyo: Springer Japan; 2015. pp. 129–178. doi:10.1007/978-4-431-55130-0

91. Iwasaki S, Kimoto K, Sasaki O, Kano H, Honda MC, Okazaki Y. Observation of the dissolution process of Globigerina bulloides tests (planktic foraminifera) by X-ray microcomputed tomography. Paleoceanography. 2015;30(4): 317–331. doi:10.1002/2014PA002639

862 92. Johnstone HJH, Schulz M, Barker S, Elderfield H. Inside story: An X-ray computed
863 tomography method for assessing dissolution in the tests of planktonic foraminifera. Mar
864 Micropaleontol. 2010;77(1–2): 58–70. doi:10.1016/j.marmicro.2010.07.004

865 93. Kroon D, Wouters P, Moodley L, Ganssen G, Troelstra SR. Phenotypic variation of
866 Turborotalita quinqueloba (Natland) tests in living populations and in the Pleistocene of an
867 eastern Mediterranean piston core. In: Brummer GJA, Kroon D, editors. Planktonic
868 Foraminifers as Tracers of Ocean-Climate History. Amsterdam: Free Univ. Press; 1988. pp.
869 131–143.

870 94. Falk-Petersen S, Leu E, Berge J, Kwasniewski S, Røstad A, Keskinen E, et al. Vertical
871 migration in high Arctic waters during autumn 2004. Deep Res II. 2008;55: 2275–2284.
872 doi:10.1016/j.dsr2.2008.05.010

873 95. Kobayashi HA. Growth Cycle and Related Vertical Distribution of the Thecosomatous
874 Pteropod Spiratella (" Limacina ") helicina in the Central Arctic Ocean. Mar Biol. 1974;26:
875 295–301. doi:10.1007/BF00391513

876 96. Lampert W. The Adaptive Significance of Diel Vertical Migration of Zooplankton. Funct Ecol.
877 1989;3(1): 21–27. doi:10.2307/2389671

878 97. Bednaršek N, Ohman MD. Changes in pteropod distributions and shell dissolution across a
879 frontal system in the California Current System. Mar Ecol Prog Ser. 2015;523: 93–103.
880 doi:10.3354/meps11199

881 98. Peck VL, Oakes RL, Harper EM, Manno C, Tarling GA. Pteropods counter mechanical
882 damage and dissolution through extensive shell repair. Nat Commun. 2018;9(1): 264.
883 doi:10.1038/s41467-017-02692-w

884 99. Peck VL, Tarling GA, Manno C, Harper EM, Tynan E. Outer organic layer and internal repair
885 mechanism protects pteropod Limacina helicina from ocean acidification. Deep Res Part II Top
886 Stud Oceanogr. 2016;127: 41–52. doi:10.1016/j.dsr2.2015.12.005

887 100. León P, Bednaršek N, Walsham P, Cook K, Hartman SE, Wall-Palmer D, et al. Relationship
888 between shell integrity of pelagic gastropods and carbonate chemistry parameters at a Scottish
889 Coastal Observatory monitoring site. ICES J Mar Sci. 2020;77(1): 436–450.
890 doi:10.1093/icesjms/fsz178

891 101. Bednaršek N, Feely RA, Tolimieri N, Hermann AJ, Siedlecki SA, Waldbusser GG, et al.
892 Exposure history determines pteropod vulnerability to ocean acidification along the US West
893 Coast article. Sci Rep. 2017;7(1): 1–12. doi:10.1038/s41598-017-03934-z

894 102. McDonald MR, McClintock JB, Amsler CD, Rittschof D, Angus RA, Orihuela B, et al. Effects
895 of ocean acidification over the life history of the barnacle Amphibalanus amphitrite. Mar Ecol
896 Prog Ser. 2009;385: 179–187. doi:10.3354/meps08099

897 103. Smith HEK, Tyrrell T, Charalampopoulou A, Dumousseaud C, Legge OJ. Predominance of
898 heavily calcified coccolithophores at low CaCO3 saturation during winter in the Bay of Biscay.
899 Proc Natl Acad Sci. 2012;109(23): 8845–8849. doi:10.1073/pnas.1117508109

900 104. Rigual-Hernán AS, Trull TW, Flores JA, No SD, Eriksen R. Full annual monitoring of
901 Subantarctic Emiliania huxleyi populations reveals highly calcified conditions. Sci Rep.
902 2020;10: 2594. doi:10.1038/s41598-020-59375-8

903 105. IPCC. Climate Change 2013: The Physical Science Basis. Contribution of Working Group I to
904 the Fifth Assessment Report of the Intergovernmental Panel on Climate Change. Stocker TF,

Qin D, Plattner G-K, Tignor M, Allen SK, Boschung J, et al., editors. Cambridge University Press. Cambridge, United Kingdom and New York, NY, USA: Cambridge University Press; 2013. doi:10.1017/CBO9781107415324

106. Lischka S, Riebesell U. Synergistic effects of ocean acidification and warming on overwintering pteropods in the Arctic. Glob Chang Biol. 2012;18(12): 3517–3528. doi:10.1111/gcb.12020

107. Lischka S, Büdenbender J, Boxhammer T, Riebesell U. Impact of ocean acidification and elevated temperatures on early juveniles of the polar shelled pteropod Limacina helicina: Mortality, shell degradation, and shell growth. Biogeosciences. 2011;8(4): 919–932. doi:10.5194/bg-8-919-2011

108. Janssen AW. Holoplanktonic Mollusca (Gastropoda: Pterotracheoidea, Janthinoidea, Thecosomata and Gymnosomata) from the Pliocene of Pangasinan (Luzon, Philippines). Scr Geol. 2007;(135): 29–177.

Supporting Information

Fig S1. Temperature and salinity profile at study area.

Fig S2. Cross-sections of *Turborotalita quinqueloba* found in the 200–300 m water depth interval.

Scale bars measure 100 μm.

Fig S3. Annotated *Limacina helicina* to demonstrate measurement of physical parameters. More details on whorl counting method can be found in Janssen [48]. Wall thickness measurements were done along a cross-section (blue), and diameter measured along white stippled line. Black circles show location of shell thickness measurements. The shell in the figure has 3.5 whorls.

Table S1. Plankton tow sampling depth for planktonic foraminifera, ambient seawater characteristics and calcite volume at the crater area in June 2016.

Table S2. CT Number and shell thickness of *Neogloboquadrina pachyderma*, *Turborotalita quinqueloba* and *Limacina helicina* at each depth interval.

Table S3. Plankton tow sampling depth for *Limacina helicina*, ambient seawater characteristics and calcite volume at the crater area in June 2016.

Table S4. Linear regression analysis of *Neogloboquadrina pachyderma* shell properties and environment.

Table S5. Linear regression analysis of *Turborotalita quinqueloba* shell properties and environment.

Table S6. Linear regression analysis of *Limacina helicina* shell properties and environment.

Table S7. Percentage of *Neogloboquadrina pachyderma* and *Turborotalita quinqueloba* shells containing cytoplasm.

Table S8. ***Neogloboquadrina pachyderma*** **significance test (p-value) in CT number between depth intervals.**

Table S9. ***Turborotalita quinqueloba*** **significance test (p-value) in CT number between depth intervals.**

Table S10. ***Limacina helicina*** **significance test (p-value) in CT number between depth intervals.**

S1 Dataset. Raw X-ray microcomputed tomography (XMCT) data of planktonic foraminifera ***Neogloboquadrina pachyderma*** **and** ***Turborotalita quinqueloba*** **from the surface sediments.**

S2 Dataset. Raw X-ray microcomputed tomography (XMCT) data of ***Limacina helicina*** **from plankton tows, including whorl count and shell apex thickness.**

S3 Dataset. Raw X-ray microcomputed tomography (XMCT) data of planktonic foraminifera ***Neogloboquadrina pachyderma*** **and** ***Turborotalita quinqueloba*** **from plankton tows.**

Fig 2

Click here to access/download;Figure;Fig2.tif

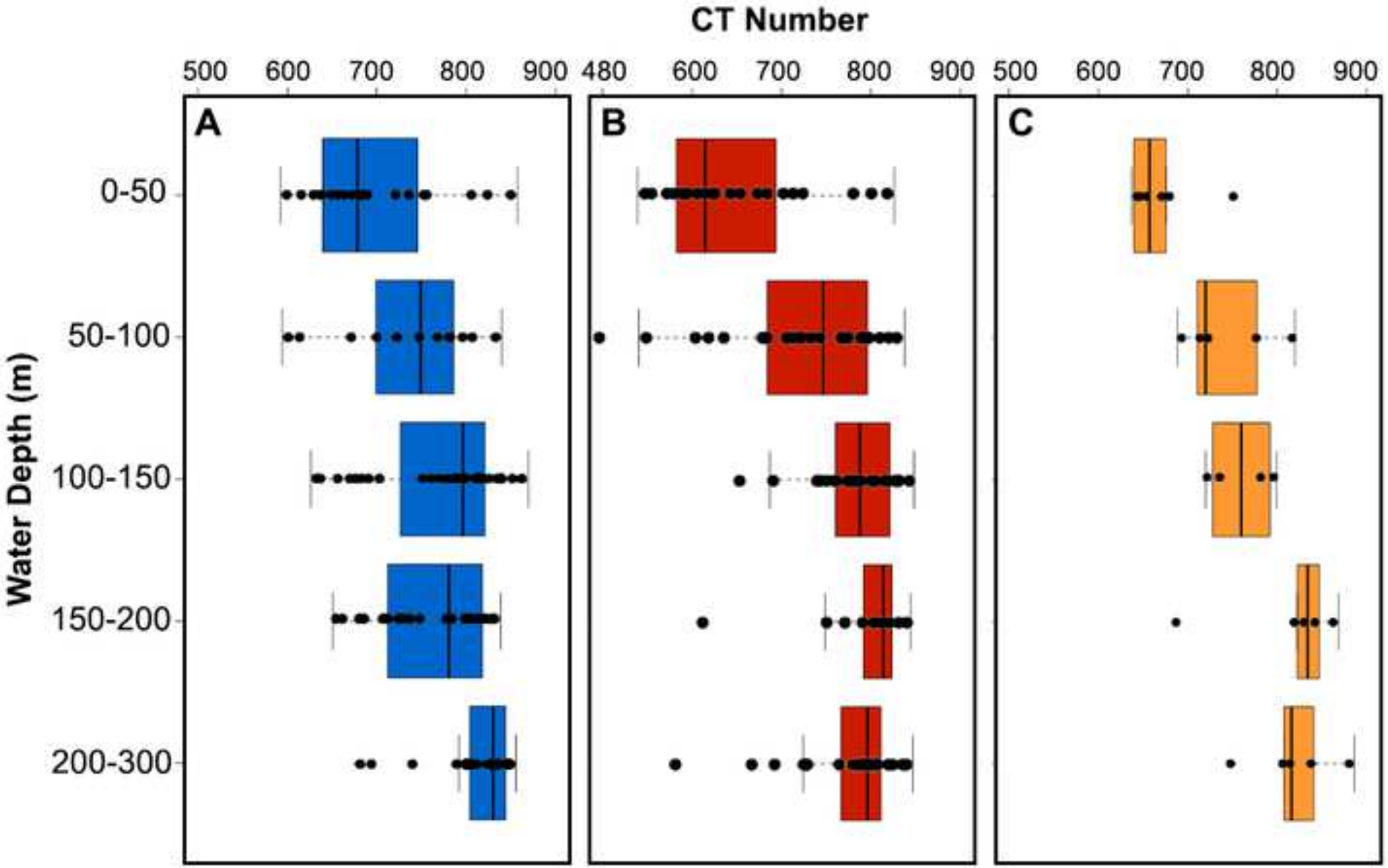

Fig 3

Click here to access/download;Figure;Fig3.tif

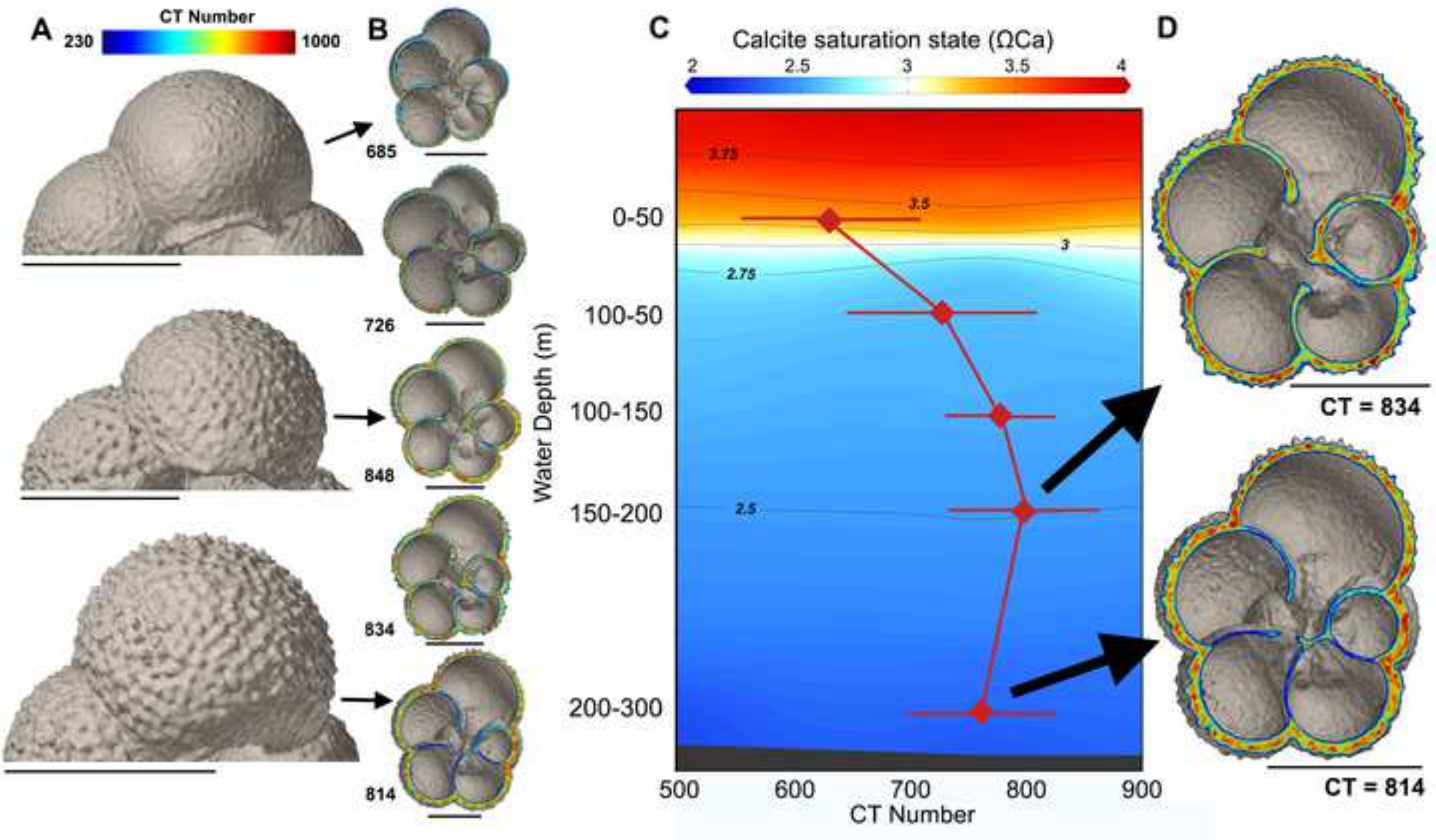

Fig 4

Click here to access/download;Figure;Fig4.tif

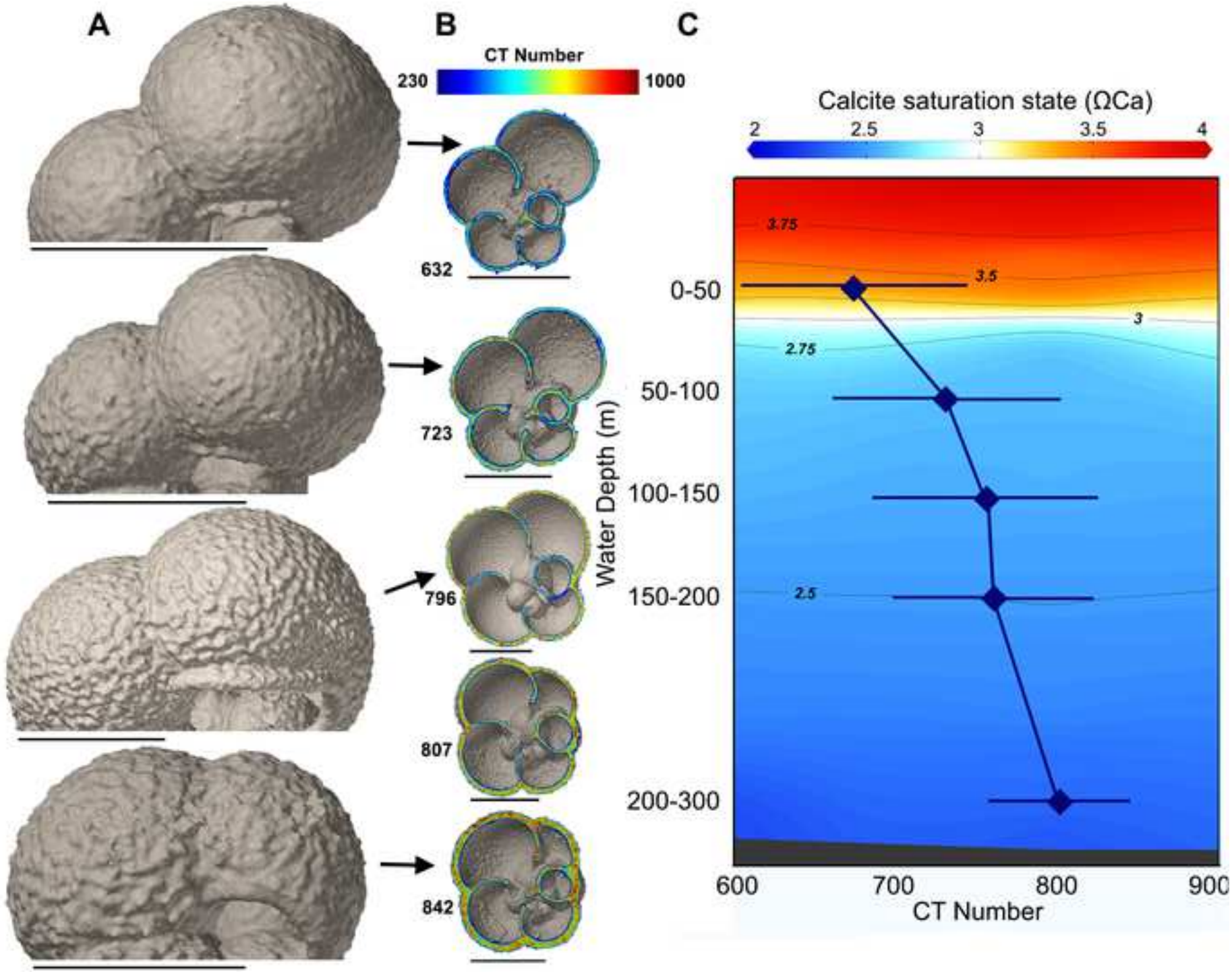

Fig 1

Click here to access/download;Figure;Fig1.tif

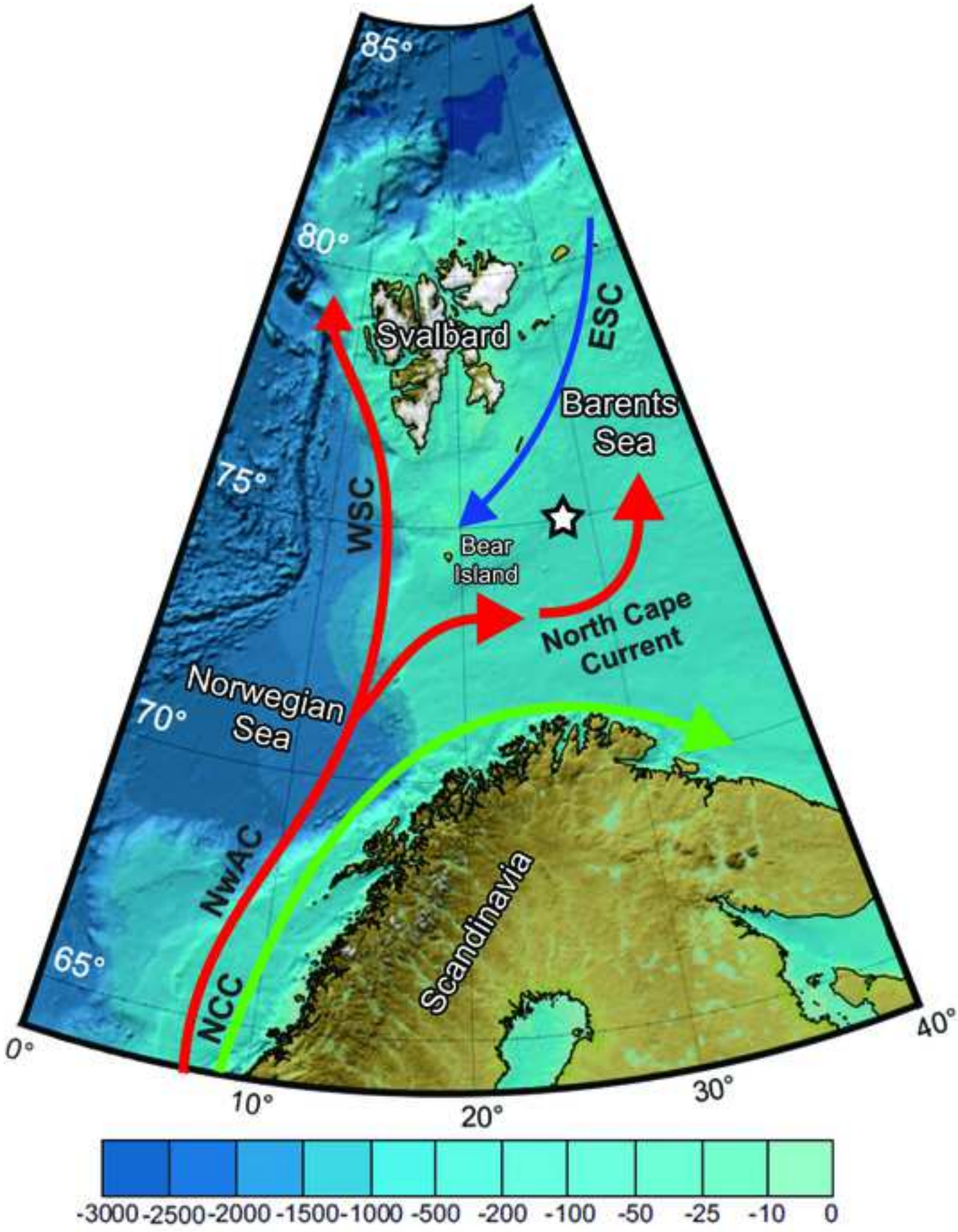

Figure 8

Click here to access/download;Figure;Fig8.tif

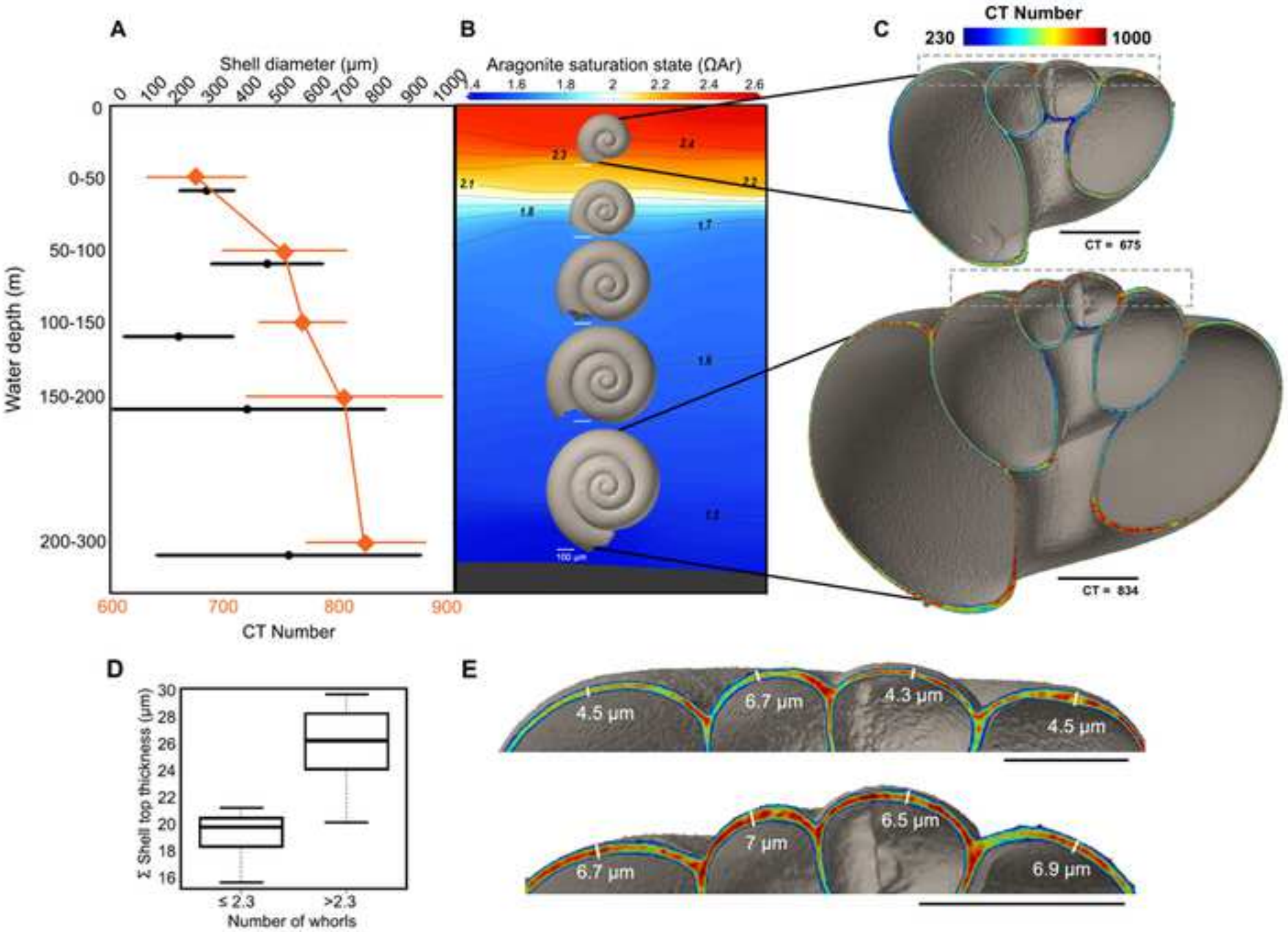

Figure 5

Click here to access/download;Figure;Fig5.tif

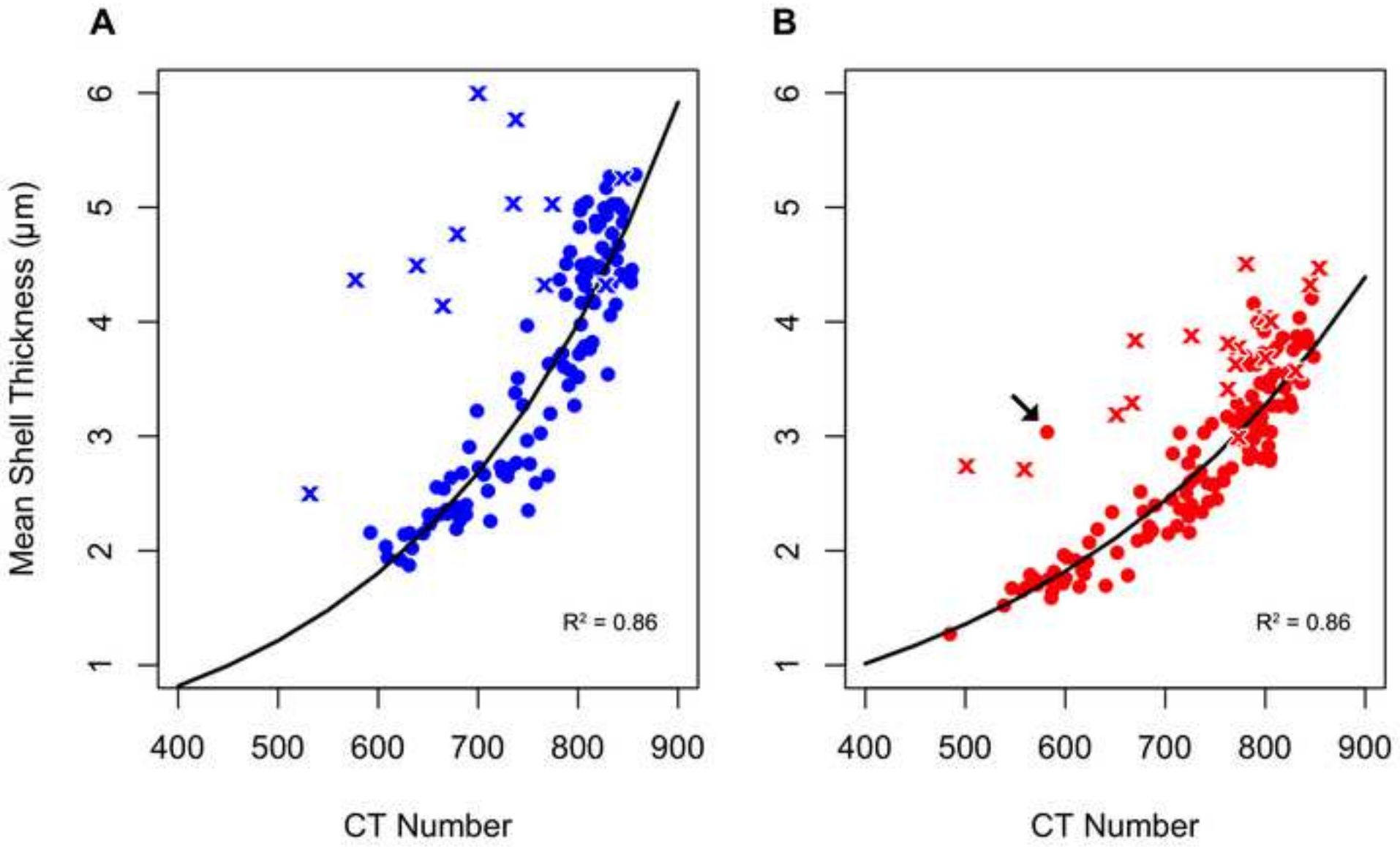

Figure 6

Click here to access/download;Figure;Fig6.tif

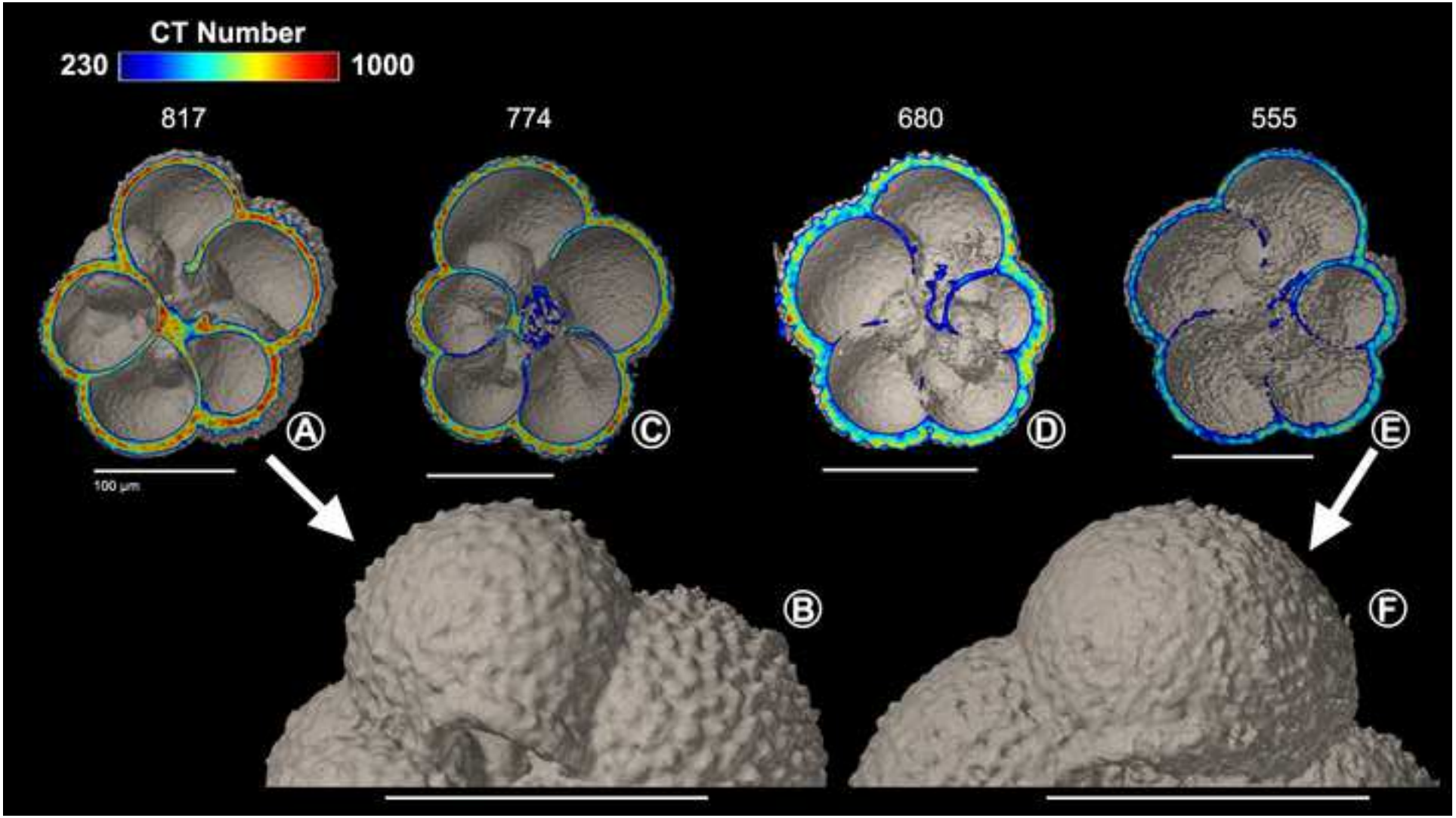

Figure 7

Click here to access/download;Figure;Fig7.tif

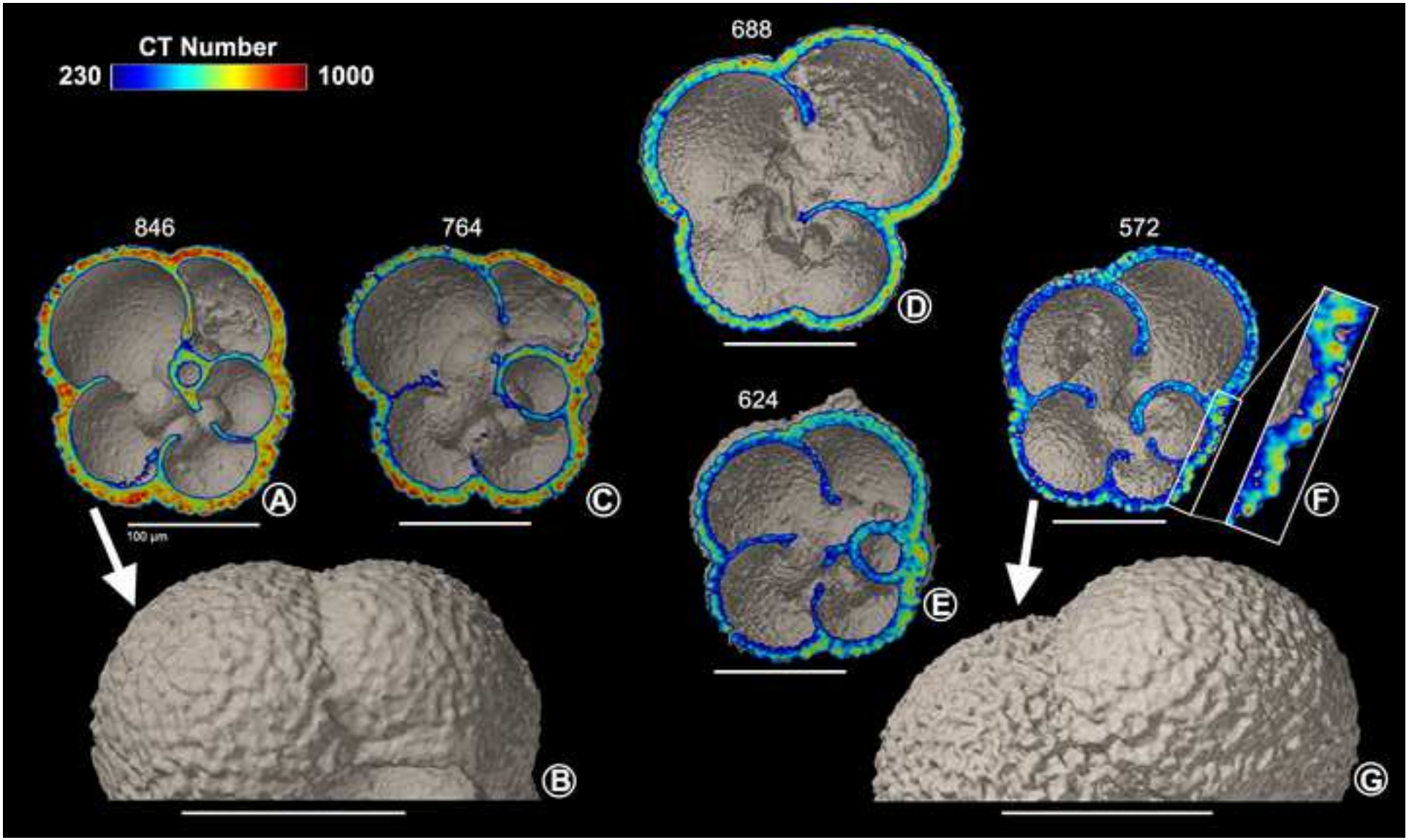

Fig S1

Click here to access/download
Supporting Information
FigS1.tif

Figure S3

Click here to access/download
Supporting Information
FigS3.tif

Figure S2

Click here to access/download
Supporting Information
FigS2.tif

Click here to access/download
Supporting Information
Supporting-information-Ofstadetal.xlsx

Shell density of planktonic foraminifera and pteropod species *Limacina helicina* in the Barents Sea: assessment of relationship to environmental conditions

Siri Ofstad[1*], Katarzyna Zamelczyk[1], Katsunori Kimoto[3], Melissa Chierici[4], Agneta Fransson[2], and Tine L. Rasmussen[1]

[1]CAGE – Centre for Arctic Gas Hydrate, Environment and Climate, Department of Geosciences, UiT, The Arctic University of Norway, Tromsø, Norway

[2]Norwegian Polar Institute, Fram Centre, Tromsø, Norway

[3]Japan Agency for Marine-Earth Science and Technology (JAMSTEC), Yokosuka, Japan

[4]Institute of Marine Research, Fram Centre, Tromsø, Norway

* Corresponding author

siri.ofstad@uit.no (SO)

Abstract

Planktonic calcifiers, the foraminiferal species *Neogloboquadrina pachyderma* and *Turborotalita quinqueloba*, and the thecosome pteropod *Limacina helicina* from plankton tows and surface sediments from the northern Barents Sea were studied to assess how shell density ~~the relationship between~~varies with depth ~~distribution and their shell densit~~habitat and ontogenetic processes~~y. Possible effects of ocean acidification were also investigated~~. The shells were measured using X-ray microcomputed tomography (XMCT) scanning and compared to the physical and chemical properties of the water column and to the carbonate chemistry including calcium carbonate saturation of calcite and aragonite. Both living *L. helicina* and *N. pachyderma* increased in shell density from the surface to 300 m water depth. *Turborotalita quinqueloba* increased in shell density to 150–200 m water depth.~~,~~ Deeper than 150 m, *T. quinqueloba* experienced a loss of density due to internal dissolution, possibly related to gametogenesis. The shell density of recently settled (dead) specimens of planktonic foraminifera from surface sediment samples was compared to the living fauna and showed a large range of dissolution states. This dissolution was not apparent from shell-surface texture, especially for *N. pachyderma*, which tended to be both thicker and denser than *T. quinqueloba*. ~~–~~*Limacina helicina* also increase in shell size with water depth and thicken the shell apex with growth. This study demonstrates that the living fauna in this specific area from the Barents Sea did not suffer from dissolution effects. Dissolution occurred after death and after settling on the sea floor. The study also shows that biomonitoring is important for the understanding of the natural variability in shell density of calcifying zooplankton.

1. Introduction

The Arctic is particularly sensitive to global warming, and this warming is greatly amplified in the Barents Sea, a large and productive shelf sea bordering the Arctic Ocean [1,2]. The Barents Sea is influenced by inflow of Atlantic Water (AW) from the south and Polar Water from the Arctic Ocean in the north, making it a hydrologically dynamic region. The two water masses mix and generate the Polar Front, a zone of very high-productivity [3]. In the northern Barents Sea there has been a substantial shift

in water mass properties over the past several decades [4]. The water column in the northern Barents Sea has become warmer and more saline, and stratification has weakened [4]. This shift is due to an increase of AW water transport, and an increase in temperature and salinity of the AW [5,6]. Thise 'Atlantification' of the water column will impact the productivity and structure of the Barents Sea ecosystems by displacing the Polar Front north-eastward, and allowing the advection of temperate species further into the Arctic domain [6–8]. A poleward shift of species in the Barents Sea has already been documented [9–11]. The large volume of warm and saline AW is also thought to be the main cause of the rapid decline of the winter sea ice cover [1].

The Barents Sea is one of the largest CO_2 sink areas in the Arctic region, which is mainly caused by the year-round CO_2 undersaturation and high biological production [12,13] despite the formation of sea-ice in winter. The Barents Sea CO_2 sink is predicted to double by 2065 with an associated pH decrease of up to 0.25 pH units [14]. A significant proportion of the observed CO_2 increase in the Barents Sea has been from the inflow of AW, which is rich in anthropogenic CO_2 [15]. The meltwater from sea ice or glaciers lowers the saturation state of seawater with respect to calcite (Ω_{Ca}) and aragonite (Ω_{Ar}), the two most common polymorphs of $CaCO_3$ formed by marine organisms [16–18], and is predicted to increase as a result of the progressing global warming [19]. Ocean acidification (OA) may lead to adverse effects on the ability of marine calcifiers to produce $CaCO_3$ shells [20].

Planktonic foraminifera (PF) and thecosomatous pteropods are the major calcifiers among marine zooplankton [20]. Marine calcifiers, in particular pteropods, are important prey in many marine food webs [21–24]. In addition, both PF and pteropods contribute significantly to the biological carbon pump [25–29]. Only few studies of PF and pteropod faunas for the high Arctic exists and in particular for the Barents Sea [30–32]. Planktonic foraminifera build their shells of calcite, while the polar pteropod species *Limacina helicina* build their shells of aragonite. The crystal structure of calcite is more stable than aragonite, and the tendency for the crystal structure to dissolve is linked to the Ω in the surrounding environment of the particular mineral phase. The crystal structures of aragonite and calcite are thermodynamically stable when $\Omega>1$. Both PF and *L. helicina* are sensitive to the carbonate chemistry in their environment and the extent of their calcification is commonly used as an indicator for OA [33–

40]. Furthermore, due to their long sedimentary record PF shell density has been used for paleoceanographic studies of OA and atmospheric CO_2 [41–44].

In a previous study, we documented the seasonal variability in the distribution patterns of PF and polar pteropod *L. helicina* and their environments in the northern Barents Sea [30]. Test size and abundance of both groups increased drastically from spring to summer, and in summer there was a clearer depth zonation of the individuals, possibly related to the thermal stratification [30]. Here, we extend our analysis on PF and *L. helicina* to study the shell density of the summer population.

In OA research there are few studies with focus on how the shell density of calcareous planktonic organisms varies with ontogeny, and hence, with depth habitat in the upper water column. Furthermore, ontogenetic processes like secondary calcification following gametogenesis will influence how well PF are preserved in the sedimentary record which is significant for the accuracy of studies of fossil faunas. Knowledge on the natural variability in shell density across a population of calcareous planktonic organisms will improve our ability to better document biological effects of OA. In this study, we aim to show 1) the variability in shell density of the living planktonic foraminiferal species *N. pachyderma* and *T. quinqueloba* and the pteropod *L. helicina* with shell size and water depth, 2) the interspecies differences in shell density of *N. pachyderma* and *T. quinqueloba*, ~~and~~ 3) if any changes in the observed patterns in shell density can be related to seawater carbonate chemistry, and 4) how shell density and ontogenetic processes affect the preservation of foraminifera in the surface sediments. ~~–~~ This study is based on X-ray microcomputed tomography ~~technique~~ (XMCT) scanning of their shells. This is a pioneer study to provide the first shell density measurements of specimens of planktonic foraminifera and *Limacina helicina* from the Arctic region.

2. Material and Methods

2.1 Study and sample collection

Formatted: Font color: Text 1, Pattern: Clear (White)

Formatted: Normal (Web)

Formatted: English (United States)

Formatted: Font color: Text 1, Pattern: Clear (White)

The Barents Sea is mainly influenced by the inflow of warm and saline Atlantic water transported in the north-eastern flowing Norwegian Atlantic current (NwAC) and the cold Arctic water transported in the East Spitsbergen current (ESC) from the north to the south [3] (Fig 1). Once the NwAC enters the Bear Island Through it splits into two branches. A substantial part of the NwAC forms a northeast flowing current, the North Cape current, which enters the southern Barents Sea, while the remainder forms the northwest flowing West Spitsbergen current (WSC). The mean depth of the Barents Sea is 250 m and is a relatively shallow continental shelf sea adjacent to the Nordic Seas and the Arctic Ocean. The Bjørnøyrenna crater area (referred to in this study as the 'crater area') (74.91° N, 27.7° E.; Fig 1) is located in relatively deep water (~340 m depth) on the northern flank of Bear Island Trough and is characterized by high levels of methane emission [45].

Fig 1. Map of study area and main current systems in the Nordic Seas. White star indicates the crater area where plankton tows, box-cores and water sampling were conducted, detailed bathymetry can be found in Ofstad et al. [30]. Red lines are Atlantic Water inflows, blue lines ~~are~~ Arctic Water outflows, and green lines are coastal currents. Abbreviations: *NwAC* Norwegian Atlantic current, *WSC* West Spitsbergen current, *ESC* East Spitsbergen current, *NCC* Norwegian Coastal Current. Current systems are based on Loeng [3]. Basemap from IBCAO 3.0 [46].

Samples were collected onboard *R/V Helmer Hanssen* during the expedition CAGE 16-5, on June 29th 2016 at three stations located at 74.9° N, 27.7° E–27.8° E. No sampling permission was required at this location~~,~~. T~~t~~his is because the study area is outside of the 12-mile limit of the Norwegian coast, meaning it is not in territorial waters, and the sampling causes no harm to the environment. ~~,~~The plankton sampled from the water column are not endangered or protected species. The PF and *L. helicina* were sampled with a stratified plankton net with mesh size of 64 µm (net opening 0.5 m^2; Hydro-Bios, Kiel, Germany), from five consecutive depth intervals (0–50 m, 50–100 m, 100–150 m, 150–200 m, and 200–300 m). ~~The plankton sampled from the water column are not endangered or protected species.~~ Parallel measurements and sampling for the study of physical and chemical environment in the water column were performed at the same location using a Conductivity-Temperature-Depth (CTD)-Rosette system

with seawater sampling for determination of carbonate chemistry. Empty shells found in the water column >150 m are assumed to represent recently dead specimens. Their shells were transparent, well-preserved and similar to the shells of the live specimens containing protoplasm.

2.2 Sampling of marine calcifiers

Once the plankton tows were retrieved, the samples were sieved with sea water through a 63- µm sieve and transferred into plastic bottles (250 ml) and fixed and buffered with approximately 230 ml ethanol (98%), a quarter of a teaspoon hexamethylenetetramine (≥99.0%), and stored at 2 °C. Once in the laboratory, the samples were washed over a 63- µm sieve in order to remove organic particles from the surface of the foraminiferal tests and to break up aggregations of material. All PF and *L. helicina* from the >63- µm size fraction were picked with a fine brush under a light microscope. Live (cytoplasm-bearing) planktonic foraminifera specimens were counted for each depth.

Recently settled planktonic ~~calcifiers~~ foraminifera were collected from two box-cores located within the same area as the plankton tow stations (74.92° N, 27.77° E and 27.53° E). The water depth at both box-core stations was 330 m, and the Ω_{Ca} directly above the sediments was 1.22 [30]. The PF were collected by ~~by~~ sampling the top sediment layer (1 cm) of ~~a~~ the boxcore. The samples were preserved in approximately 50 ml of ethanol (96%) with rose bengal (2 g L−1 of ethanol), and stored at 2 °C. In the home laboratory, the samples were washed over a 63- µm sieve and dried in a 40 °C for at least 24 hr. Once dried, PF were picked under a light microscope with a fine brush and identified to species level. There were large pteropods in the sediment samples, but they were broken, and therefore not included in the study. The complete description of sample collection, treatment, and analysis is described in Ofstad et al. [30].

Formatted: English (United States)

2.3 XMCT

An XMCT system (ScanXmate-DF160TSS105, Comscantecno Co. Ltd., Kanagawa, Japan) was used to quantify the shell density of individual specimens. A high-resolution setting (X-ray focus spot diameter of 0.8 µm, X-ray tube voltage of 80 kV, detector array size of 1024x1024 for the pteropods

and 992x992 for the foraminifera, spatial resolution of 0.833 μm for *Limacina helicina* and 0.964 μm for the foraminifera, 1200 projections/360°, 4 s/projection) was used for 3-D quantitative densitometry of the foraminiferal and pteropod tests. One to three samples – depending on the shell size, were placed on a stage made of a quartz glass bar. Tests were mounted on the sample stage with urethane glue. A calcite crystal ball was used to standardize the computed tomography (CT) number of each test sample and enabled us to distinguish the density distributions in the foraminiferal and pteropod tests with high resolution. In this study, a limestone particle (diameter of approximately 130 μm; 1000 in mean CT number; NIST RM8544 (NBS19)) was embedded in the sample stage, and all of the test samples were scanned with the same calcite standard. ConeCTexpress software (White Rabbit Corp., Tokyo, Japan) was used to correct and reconstruct tomography data, and the general principle of Feldkamp cone beam reconstruction was followed to reconstruct image cross sections based on filtered back projections. In order to avoid the beam hardening effect (selective attenuation of X-ray) during scan, we put the metal filter (Aluminium, 0.2 um thickness) in front of X-ray detector. Mean shell thickness was calculated by dividing the $CaCO_3$ volume by the shell surface area, both of which are parameters measured by the XMCT. The shell surface area includes both the outer areas and the surfaces of the internal chambers. A caveat with the calculated mean shell thickness is that values will decrease, when the shell material is more porous. High porosity of the shell material increases the surface area, resulting in a decrease in mean shell thickness.

Well-preserved specimens to be scanned with the XMCT were selected at random, but with the intention of having a representative size range. The complete size range of the PF and *L. helicina* specimens sampled in June 2016 from the crater area can be found in Ofstad et al. [30]. A total of 226 planktonic foraminifera shells from the water column (*N. pachyderma* n = 120, *T. quinqueloba* n = 115), 30 recently settled planktonic foraminifera shells (*N. pachyderma* n = 12, *T. quinqueloba* n = 18), and 25 *Limacina helicina* shells from all depth intervals (0–50 m, 50–100 m, 100–150 m, 150–200 m, and 200–300 m) were scanned with the XMCT (S1 Table; Fig 2). All scanned pteropod shells were either veligers, *Limacina* spp. (<300 μm, n = 7), or juveniles *L. helicina* (300–4000 μm) (n = 18) [47].

2.4 CT Number

From the 3-D scanning data of planktonic foraminiferal and *L. helicina* tests, we obtained a CT number of each volumetric pixel - referred to as a voxel, and volume (μm^3) of each individual test. The 3-D imaging software Molcer Plus (White Rabbit Corp., version 1.35) and the following equation were used to calculate the calcite CT number:

$$\text{CT number} = \left[\left(\mu_{\text{sample}} - \mu_{\text{air}}\right)/\left(\mu_{\text{calcite STD}} - \mu_{\text{air}}\right)\right] \times 1000 \quad (1)$$

where μ_{sample}, μ_{air}, and $\mu_{\text{calciteSTD}}$ are the X-ray attenuation coefficients of the sample, calcite, and air, respectively.

The mean CT number for an entire test was calculated with the following equations:

$$\text{Mean CT number} = \frac{1}{T}\sum_{n=230}^{1000} nT_n \quad (2)$$

where n is the CT number, T_n is the total number of voxels with a specific CT number (n), and T is the total number of voxels in the whole test. The mean CT number indicates the mean density of an individual test.

2.5 CT data analysis

The shell thickness of the apex of ~~individual~~ *L. helicina* ~~whorls and apex~~ was measured by creating cross-sections using the Molcer Plus software (Version 1.35). A whorl is a single 360° revolution of the shell spiral structure. ~~The whorl measurements were done on a total of 23 *L. helicina* shells (S3 Fig) and are the result of three repeated measurements.~~ The shell apex of 16 *L. helicina* shells were measured at four locations, twice on the protoconch (first whorl), and twice between the first and second whorl (Fig S3). Careful consideration was made to take measurements at the same location for each shell for ease of comparison. Following the methods outlined by Janssen [48], the *L. helicina* shell diameters were measured and the total number of whorls were counted to the nearest quarter (S3 Fig). Additional *L. helicina* from the sampling station were measured for their shell diameter. Images were acquired by a Leica Z16 APO microscope, using the integrated Leica DFC450 camera and LAS version 4.12.0 software. The images were processed using the ruler tool in Adobe Photoshop CS6. All measurements

of shell diameter and thickness performed this study are the result of three repeated measurements to diminish inaccuracies.

In order to calculate area density (area normalised weight), 111 PF shells (*T. quinqueloba* n = 54, *N. pachyderma* n = 57) shells were weighed individually using a Sartorius microbalance (model M2P, 0.1µg sensitivity). The given weight measurements are based on three repeated measurements of the single specimen. Area density is given by shell weight divided by surface area.

Isolation of the penultimate and final chamber was done on a select number of shells in order to validate the relationship with the overall CT number of the shell.

2.6 Statistical analyses

To test the relationship between any two parameters (e.g. water depth and mean shell density), a simple linear regression model was applied to the data. To test significance of correlation of shell density of the marine calcifiers with sampling intervals, a Mann-Whitney-U test was performed using the program RStudio (Version 1.2.1335) [49]. When testing variables against water depth, the maximum depth in the sampling interval was used. When testing against environmental parameters, the mean of all measurements in the sampling interval was used.

2.7 Ocean carbonate chemistry

The water chemistry data were published in Ofstad et al. [30], here we give a brief overview of the methods. Dissolved inorganic carbon (DIC) was determined using gas extraction of acidified sample followed by coulometric titration and photometric detection using a Versatile Instrument for the Determination of Titration carbonate (VINDTA 3C, Marianda, Germany). Routine analyses of Certified Reference Materials (CRM, from A. G. Dickson, Scripps Institution of Oceanography, USA) ensured the accuracy and precision of the measurements. Average standard deviation from triplicate CRM analyses was within ±1 µmol kg^{-1} for all samples. Total alkalinity (A_T) was determined from potentiometric titration with 0.1 N hydrochloric acid in a closed cell using a Versatile Instrument for the

Determination of Titration Alkalinity (VINDTA, Marianda, Germany). Average standard deviation for A_T, determined from triplicate CRM measurements was ±2 μmol kg^{-1}. We used DIC, A_T, salinity, temperature, and depth for each sample as input parameters in a CO_2-chemical speciation model (CO2SYS program, version 01.05) [50,51] to calculate other parameters in the carbonate system such as carbonate-ion concentration ($[CO_3^{2-}]$), aragonite saturation (Ω_{Ar}) and calcite saturation (Ω_{Ca}). We used the HSO_4^- dissociation constant of Dickson [52], and the CO_2-system dissociation constants (K*1 and K*2) estimated by Mehrbach et al. [53], and modified by Dickson and Millero [55].

3. Results

3.1 Hydrography and water chemistry

During the time of sampling, the predominant water masses were Atlantic Water (AW, T > 3.0°C, S > 34.65) in the top 250 m of the water column, and Transformed Atlantic Water (TAW, T = 1.0–3.0°C, S > 34.65) below 250 m, following the definitions of Cottier et al. (2005) (S1 Fig). Both Ω_{Ar} and Ω_{Ca} were supersaturated (Ω>1) throughout the entire water column, with the highest values in the surface water and lowest ~~in~~ at the bottom (Fig 3C and Fig 8C). The water column ~~can be divided into~~had two distinct layers (Fig 3C and Fig 8C). The upper layer is from the sea surface to approximately 75 m water depth (Figs 3C and 4C), here, the Ω_{Ar} is 2.1–2.5, and the Ω_{Ca} is 4.0–3.0. Between 75 m and 300 m water depth the Ω_{Ar} is 1.5–2.1, and the Ω_{Ca} is 2.4–3.0, where the lowest values were observed at the bottom. The carbonate ion concentration ($[CO_3^{2-}]$) ranged between 168 μmol kg^{-1} at the surface and 105 μmol kg^{-1} at 300 m water depth. The pH ranged between 8.03 and 8.22.

3.2 Shell density from CT Number

For both *Neogloboquadrina pachyderma* and *Turborotalita quin~~e~~queloba*, the average CT number increases steadily from 684 and 632 in the 0–50 m depth interval to 762 and 793 in the 150–200 m depth interval, respectively (Fig 2). The difference in CT number between the layer of elevated Ω saturation at 0–50 m and the underlying water column when normalized for shell volume, is also significant for

both PF species ($p < 0.01$), but not *L. helicina* ($p = 0.25$). For *L. helicina* the difference in shell density between the specimens in the shallow layer (0–50 m) and those found beneath is significant when not size normalized (S10 Table). *Turborotalita quinqueloba* reaches its peak shell density of 793 in the 150–200 m depth interval. Below the 150–200 m depth interval, the shell density of *T. quinqueloba* decreases. In the 200–300 m depth interval, the average shell density of *T. quinqueloba* is 766. The outer shell walls are thick and dense, while the CT number is lower in the internal walls (Fig 3 and S2 Fig). In contrast, the shell density of *N. pachyderma* continues to increase until 200–300 m, where it reaches a peak shell density of, on average, 813 (Fig 4). Similar to *N. pachyderma*, the shell density of *L. helicina* increases with depth. At 0–50 m, *L. helicina* have an average CT number of 670, and by 200–300 m they reach a peak average density of 819 (Fig 2). Collectively, we found that the difference in shell density between sampling intervals were most significant between the shallowest (0–50 m) and deepest (200–300 m) interval (S8–10 Tables). *Turborotalita quinqueloba* showed the most significant variation between nets, and *L. helicina* the least.

Fig 2. Box-and-whisker plot of shell density with water depth for A) *Neogloboquadrina pachyderma* (n = 120), B) *Turborotalita quinqueloba* (n = 115) and c) *Limacina helicina* (n = 25) sampled from the crater area in 2016. Boxes extend from the lower to upper quartile values of the data, with a line at the median. Whiskers indicate 1.5 times the inter-quartile distance. Black dots are single measurements.

Fig 3. *Turborotalita quinqueloba* from water column. A) Texture of test surface of *Turborotalita quinqueloba* at three different depth intervals; 0–50 m, 100–150 m and 200–300 m. B) Variation in inner and outer shell density of *T. quinqueloba* as mean CT number of entire shell measured by XMCT increases. C) Mean CT number of *T. quinqueloba* (n = 115), with error bars, plotted against water depth and calcite saturation. D) *T. quinqueloba* cross-section before and after gametogenesis. Scale bars measure 100 μm.

Fig 4. *Neogloboquadrina pachyderma* from water column. A) Texture of test surface of *Neogloboquadrina pachyderma* at four different depth intervals; 0–50 m, 50–100 m, 100–150 m and 200–300 m. B) Variation in inner and outer shell density of *N. pachyderma* with mean CT number of

entire shell measured by XMCT. C) Mean CT number of *N. pachyderma* (n = 120), with error bars, plotted against water depth and calcite saturation. Scale bars measure 100 µm.

Although we found a general increase in CT number and shell thickness with depth, we note a large range in CT numbers (Fig 2 and S2 Table) and mean shell thickness (S2 Table) at each sampling depth interval. This is particularly true for *T. quinqueloba* in the shallowest depth interval 0–50 m where the CT numbers of individual specimens ~~were~~ are evenly distributed from 539 to 826, and the mean shell thickness ranges~~d~~ from 2.02 to 3.25 µm. Furthermore, in the 0–50 m depth interval the average CT numbers for *N. pachyderma* and *L. helicina* ranges from 592 to 857, and 637 to 751, respectively. The shell thickness of *N. pachyderma* and *L. helicina* at the 0–50 m depth interval ranged from 1.94 to 5.28 µm, and 1.98 to 2.75 µm, respectively.

3.3 Planktonic Foraminifera

3.3.1 Planktonic Foraminifera from the water column

Both *N. pachyderma* and *T. quinqueloba* show a statistically significant positive correlation between individual shell weight, CT number, mean shell thickness and area density with water depth (S4–S5 Table). Cytoplasm-bearing specimens of both species ~~were~~ are found in each sampling depth interval and constitute 80–100 % of XMCT scanned shells from the top 150 m (S7 Table). Below 150 m the percentage of live specimens decreases to 75 % and 78.6 % for *N. pachyderma* in the 150–200 m and 200–300 m depth interval, respectively (S7 Table). For *T. quinqueloba* there is a greater decrease in the percentage of live specimens below 150 m, with 14.3 % and 23.5 % containing a cytoplasm in the 150–200 m and 200–300 m depth interval, respectively (S7 Table). For both *T. quinqueloba* and *N. pachyderma* there is increasing formation of a layer of crust on the outer shell with depth. The texture of the shells in the shallowest samples are smooth without any calcite crust. Thereafter ridges appear that become increasingly "rough" with depth and increase in CT number (Figs 3A and 4A).

Both species undergo gradual shell thickening with depth. At 0–50 m water depth the average shell thickness of *N. pachyderma* and *T. quinqueloba* is 2.5±0.8 µm (n = 15) and 2±0.5 µm (n = 28),

respectively. *Neogloboquadrina pachyderma* reaches peak thickness at 200–300 m, where the average shell thickness is 4.3±0.7 μm (n = 29). *Turborotalita quinqueloba* reaches peak thickness at 150–200 m, where the average shell thickness is 3.5±0.7 μm (n = 13). In the 200–300 m depth interval the shell of *T. quinqueloba* has decreased to 3.1±0.8 μm (n = 24). Collectively, the shell walls of *N. pachyderma* and *T. quinqueloba* thicken by 40.8 % and 35.1 %, respectively, from their thinnest at the 0–50 m sampling interval to their peak shell thickness.

The mean shell thickness shows a strong correlation with the CT number (Fig 5; S4–S5 Table). The mean shell thickness of individual *T. quinqueloba* and *N. pachyderma* have an exponential relationship with their respective CT numbers (Figs 5A–5B). The exponential curve for *N. pachyderma* is steeper than the curve for *T. quinqueloba*. Furthermore, *N. pachyderma* (n = 120) tend to be larger, denser, and thicker than *T. quinqueloba* (n = 115), based on mean CT numbers and calcite volume (S1–S2 Table).

Fig 5. Shell thickness versus shell density. Mean shell thickness of A) *Neogloboquadrina pachyderma* and B) *Turborotalita quinqueloba* plotted versus mean shell density in the form of a CT number, fitted with an exponential model. Shells from water column samples are represented by circles, while crosses represent shells from surface sediments. Exponential model is only fitted to shells from water column. Arrow in B) is pointing to an outlier.

3.3.2 Planktonic Foraminifera from the surface sediments

In the top 1 cm of the sediments, both *N. pachyderma* and *T. quinqueloba* are found in a wide range of dissolution states. Some of the planktonic foraminiferal specimens found in the surface sediments have similar shell densities as those found in the overlying water column (Figs 6A and 6C; Figs 7A and 7C), while other specimens have undergone dissolution (Figs 6D and 6E; Figs 7E and 7F). Out of all of the *N. pachyderma* shells found in the surface sediments, there is a high proportion of low-density shells (9 out of 12, 75%), i.e. shells which can be regarded as outliers in the thickness versus density plot (Fig 5A). In contrast, low-density *T. quinqueloba* shells are in the minority (7 out of 18, 39%) (Fig 5B). The surface texture of *N. pachyderma* and *T. quinqueloba* vary in terms of CT number (Figs 6 and 7). In *T. quinqueloba*, the loss of the base features of the prominent spines is evident as the CT number reduces

from 817 to 555, and the surface texture takes on a smoother appearance (Figs 6B and 6F). The surface texture of *N. pachyderma* appears to be mostly unaffected by post-depositional dissolution (Figs 7B and 7G). In the low-density shells, the calcite ridges are more prominent, giving it a more rugose texture overall (Fig 7G). In *N. pachyderma* we see a two-layered dissolution pattern (Fig 7F). There is a clear divide between the less dense (CT number ~ 400) inner calcite, and the denser outer crust (CT number ~ 650) (Fig. 7F). Shells of both species from the surface sediments that have undergone post-depositional dissolution plot to the left of the exponential trendline (Fig 5). The external shell walls of the dissolved specimens remain at a similar thickness to those with a high--density shell (Figs 5–7). Dissolution primarily aeffects the CT number (Fig 5).

Fig 6. *Turborotalita quinqueloba* from surface sediments. Cross-sections of *Turborotalita quinqueloba* specimens (A,C,D,E) from surface sediment sample (0–1 cm), including surface texture of a B) high-density (n = 11) and F) low-density specimen (n = 7). Scale bars measure 100 μm.

Fig 7. *Neogloboquadrina pachyderma* from surface sediments. Cross-sections of *Neogloboquadrina pachyderma* specimens (A,C,D,E,F) from surface sediment sample (0–1 cm), including surface texture of a B) high-density (n = 3) and G) low-density specimen (n = 9). F) Close-up of shell wall cross-section. Scale bars measure 100 μm.

3.4 *Limacina helicina*

In *L. helicina* we see the same trend in the shell density with water depth as we do with the PF (Fig 2). *Limacina helicina* show a statistically significant positive correlation between shell diameter, CT number, and mean shell thickness with water depth (S6 Table). On average, the shell density of *L. helicina* increases with depth (Fig 8A). The mean density given by the CT number starts at a minimum, at 670, in the shallowest sampling interval (0–50 m) (Fig 8A). There is a steady increase until the deepest sampling interval where the mean CT number is 819 (Fig 8A). In contrast to the PF in the crater area, *L. helicina* generally increase in shell diameter with depth (Fig 8A; S6 Table). In the 0–50 m depth interval, the shells have the narrowest size range (131–457 μm), and an average size of 274 μm. The

150–200 m water depth interval has the largest range of shell sizes, 124–1190 µm (Fig 8A). The largest shells, on average, are found in the 200–300 m water depth interval and are 511 µm (Fig 8A). The number of whorls varied between 0.6 and 3.6 and is strongly correlated to the shell diameter ($p < 0.001$).

Fig 8. *Limacina helicina* from water column. A) *Limacina helicina* shell diameter (n = 175) and density (n = 25) (given by CT number) with depth. B) Generalized shell size with depth plotted against aragonite saturation. C) Cross-sections of *L. helicina* specimens from 0–50 m (2 whorls), and 150–200 m (2.75 whorls) water depth interval~~, including shell thickness measurements on individual whorls~~. Grey boxes are shown as close-ups in ~~f~~E. ~~D) Boxplot of *L. helicina* individual whorl shell thickness (n = 23). E~~D) Boxplot of Mann-Whitney *U* test on top shell thickness of *L. helicina* as a function of whorl number. ~~F~~E) Top of *L. helicina* specimens shown in C, schematic of shell thickness measurements performed on all shells. Scale bars measure 100 µm.

The way that *L. helicina* is distributed~~ion~~ in the water column means that shell density has an inverse relationship with Ω_{Ar} ($R^2 = 0.54$, $p < 0.001$, Figs 8A–8B). The mean shell thickness also increases with depth, starting at 2.2 µm at 0–50 m water depth, to 2.8 µm at 200–300 m water depth. ~~The whorls get increasingly thicker which each revolution (Figs 8C–8D). Measurements of the base of individual whorls show a mean thickness of 3.4±1 µm in whorl 1, 6.1±2.4 µm in whorl 2, 11.2±2.6 µm in whorl 3, and 13.4±2.4 µm in whorl 4 (Fig 8C).~~ As the number of whorls increase~~s~~, the shell apex ~~also gets~~ thicken~~sr~~. The sum of four measurements done on the central-top part of the shell show that shells with 2.5 to 3.5 whorls is 25.9±3.1 µm, while shells with 1.5 to 2.25 whorls has a sum of 19.4±2 µm (Fig 8F).

4. Discussion

4.1 Distribution of PF, life cycles and shell density

Calcified shells are thought to have evolved as a mean for protection, and is widely found throughout the animal phyla [57]. Calcification intensity, the term often used to refer to shell density is believed to be primarily controlled by ambient seawater $\left[CO_3^{2-}\right]$ [38,58], and hence Ω, which is largely dictated by

absolute $[CO_3^{2-}]$. In addition, the shell size of planktonic foraminifera ~~l shell size~~ appears to be controlled by temperature and food availability [36,38,59]. *Globigerina bulloides* when growing in favourable conditions, but with low Ω_{Ca} (~1.5), were found to grow large in size, with low density tests characterised by large and porous crystalline structures, suggesting that PF in some cases may prioritize shell size over shell density [36]. Furthermore, shell thickening by encrustation during ontogeny and/or gametogenic calcification is poorly understood and exhibit inter-species variation [60,61]. Encrustation of *N. pachyderma* in polar waters occurs at 50–200 m, and an increase in secondary calcification of *N. pachyderma* has been shown to occur with depth [62]. The degree of encrustation in *N. pachyderma* is highly variable, it can amount to 50–70% of the total shell weight, and there is no consensus on which factors initiates the crust formation [62–64].

Planktonic foraminifera do not perform diel vertical migration [65], but it is hypothesized that they descend into deeper waters as they mature, and reproduce at certain water depths (see e.g. [66–68]). However, it is unclear how PF shell density changes with increasing water depth.

4.1.1 Comparison of *N. pachyderma* and *T. quinqueloba* in the water column and their preservation patterns

The dominant living planktonic foraminiferal species in the polar region are *N. pachyderma* and *T. quinqueloba* [69–73], which is reflected in our sampling area [30]. The differences in the shell density depth profile between *N. pachyderma* and *T. quinqueloba* can be explained in part by the differences in depth habitat and depth of reproduction [74,75]. Another factor, which may affect their calcification is that *T. quinqueloba* is a spinose species, while *N. pachyderma* is not. *Turborotalita quinqueloba* calcify within 25–75 m water depth, while *N. pachyderma* calcify within the much wider range of 25–280 m [74,75]. *Neogloboquadrina pachyderma* continue to calcify and apparently grow denser as they migrate to deeper depths throughout their lifecycle (Fig 4), an observation consistent with previous studies [62,76]. Not all *N. pachyderma* shells develop a secondary crust with depth, and these thin non-encrusted shells can be found throughout the water column [62,77]. In the North Pacific, shell parameters of *G.*

bulloides such as the area density and outermost chamber wall thickness increase~~s~~ 20 % from the 0–50 m to the 100–150 m water depth interval [36]. We find similar results in the northern Barents Sea; the area density of *T. quinqueloba* increase~~sd~~ by 50.1 % from the 0–50 m to the 100–150 m water depth interval, while the mean area density of *N. pachyderma* increase~~sd~~ by 29.5 %. Furthermore, the CT number~~s~~ of *N. pachyderma* and *T. quinqueloba* increase~~s~~ by 10.2 % and 20.3 %, respectively, from the 0–50 m to the 150–200 m water depth interval. By the deepest sampling interval, 200–300 m, the CT number of *N. pachyderma* has increased by a further 6.6 % (n = 32), resulting in a total increase in CT number by 15.8 %. Below the 150–200 m water depth interval (n = 38), *T. quinqueloba* decrease in density by 3.4%. The shallower and narrower depth habitat in the water column of *T. quinqueloba* compared to *N. pachyderma* is reflected in the faster rate of both increasing shell density and shell thickening per meter. However, we find thin low-density shells and thick high-density shells of both species in the entire water column (Fig 2). If we use thick high-density shells as a proxy for reproduction, then reproduction occurs in the entire water column. Cytoplasm-bearing specimens are also present in the entire water column (S7 Table), although in lower abundance in the deepest sampling intervals, especially *T. quinqueloba*. The increasing density curve with water depth may partly be the result of the higher presence of dead shells that have already released gametes.

The decrease in the CT number of *T. quinqueloba* from the 150–200 m depth interval to the 200–300 m depth interval likely reflects the dissolution of their internal shell walls (S1 Fig). This internal dissolution may be due to gamete formation and release (Fig 3D), which has been documented to occur in certain PF species [61]. Early culture studies on PF also showed that dissolution starts in the internal shell walls [78,79]. In preparation for the release of gametes, PF increase the Ω_{Ca} of the microenvironment adjacent to their shell [80]. Some foraminifera may do so by discharging alkaline seawater vacuoles, which would result in the internal environment of the foraminifera to become less basic [81]. Another explanation for the internal dissolution is the oxidation of internal organic matter, documented in the pteropod species *Limacina retroversa* and ~~*Limacina*~~ *L. helicina antarctica* [82]. However, this is less likely in PF shells, because they are made of calcite, which is more robust than aragonite and the proportion of soft tissue to shell size is significantly smaller than in pteropods [83]. The Ω_{Ca} is supersaturated throughout the

438 water column (Ω_{Ca} = 2.4–4), yet there are no known Ω_{Ca} thresholds for PF. The presence of *T.*
439 *quinqueloba* shells in the deepest sampling interval may also reflect a relic population. The internally
440 dissolved shells may have a slower sinking rate than the specimens without dissolved internal walls,
441 making them more likely to be sampled.

442 At our study site, PF shell density is strongly related to shell volume (S4–5 Table). In general, the larger
443 the shell volume, the more dense it is. However, the increase in CT number with depth after size-
444 normalization is still significant ($p < 0.01$). This means that the increase in shell density with depth is
445 not a function of shell volume.

446 Our results highlight the importance of comparing PF in the same life stage, because the shell thickness
447 and density gradually increases as they mature. The same size is not enough to eliminate ontogenetic
448 effects (Figs 3 and 4), therefore it is also advisable to compare shells from the same sampling depth. In
449 a study showing shell thinning in PF due to OA by comparing pre-industrial and modern shells, sampling
450 depth may not have been the same [37]. A discrepancy in sampling depth may mean that the results
451 simply show natural variation in shell thickness with depth.

452 The PF sampled from the water column in our study area did not show any signs of dissolution, both in
453 the outer and inner shell wall (Figs 5A and 5B). The only exceptions are some specimens of *T.*
454 *quinqueloba* found below 150 m water depth (Fig S2). There is a clear depth zonation in individual
455 abundance [30], and shell density in both species. The increase in shell density with depth is in
456 agreement with observations in the North Pacific [36], and is believed to be driven by ontogeny.

457 ### 4.1.2 Comparison *N. pachyderma* and *T. quinqueloba* from the sediment
458 ### and species-specific dissolution

459 The sedimentation rate in the northern Barents Sea ranges from 0.5–1.3 mm/yr [84], meaning that it
460 takes anywhere from 8 to 20 years to accumulate 1 cm of sediment. The top 1 cm of sediments will
461 therefore host PF that have settled at different times and thus can show a variable degree of dissolution
462 (Figs 6 and 7). When PF from sediment samples are used in geochemical studies, it is often stated that

the samples do not show any evidence of dissolution. The surface texture of *T. quinqueloba*, and especially that of *N. pachyderma* undergo only slight changes in their external appearance as they dissolve. The subtle dissolution in the surface texture may go undetected under a light microscope if all chambers are intact, which was the case for the samples used in this study. The post-depositional dissolution found in some of the specimens (Figs 6D–6E and Figs 7D–7F) is likely to alter the original chemical composition of their tests, mainly the Mg/Ca ratio, and the oxygen and carbon isotopic composition [85,86]. The higher percentage of low-density *N. pachyderma* shells (75%) compared to *T. quinqeloba* (39%) suggests that fewer low-density *T. quinqeuloba* shells remain intact in the surface sediments, which may lead to an underrepresentation of *T. quinqueloba* in the sediment records. Selective dissolution of *T. quinqueloba* is also likely because of the extensive internal dissolution in the low-density shells (Figs 6D and 6E), which could lead to a collapse of the entire shell resulting in fragmentation.

The inter-species differences in the manifestation of post-depositional dissolution is thought to be primarily due to the magnesium content in the calcite structure [87], thus also suggesting that the calcification process is species-specific. *Neogloboquadrina pachyderma* consistently rank as one of the planktonic foraminiferal species most resistant to dissolution, regardless of the region they are found, while *T. quinqueloba* has a low resistance to dissolution [87,88]. The exponential curve for *N. pachyderma* shell thickness versus CT number (Fig 5A) is steeper than that of *T. quinqueloba* (Fig 5B). The steeper *N. pachyderma* curve suggests that they calcify more than *T. quinqueloba*, leading to a thicker crust. The ability to build a thicker and denser crust may have a number of different explanations. Firstly, there could be a difference in lifecycle length between *N. pachyderma* and *T. quinqueloba*. *Neogloboquadrina pachyderma* may have a longer lifecycle than *T. quinqueloba* meaning that they could calcify over a longer period of time and build thicker and denser shells. Individuals of *N. pachyderma* have been kept alive in culture for up to 200 days [89,90]. The tendency of *N. pachyderma* to build thicker and denser shells may be due to a naturally higher calcification rate, rather than a longer lifecycle compared to *T. quinqueloba*. The two species may also have very different calcification

strategies because, unlike *N. pachyderma*, *T. quinqueloba* builds numerous spines on most of its chambers at the expense of chamber walls resulting in thinner shells.

The two-layered dissolution pattern seen in *N. pachyderma* highlights their higher degree of resistance to dissolution (Fig 7F). A similar pattern was also found in *G. bulloides* [91]. The denser outer calcite of *G. bulloides* was resistant to dissolution and remained well preserved in water undersaturated with respect to calcite, while the Mg-rich inner calcite dissolved [91]. This mechanism of selective dissolution likely skews the sediment record to favor species with a dense outer calcite layer. Following dissolution in the surface sediments, the thickness of the shell walls remains intact while the whole shell gets a more porous crystalline structure, resulting in a lower mean CT number (Figs 6 and 7). In our study, the dissolved shells from the surface sediments plotted to the left of the trend line showcase~~s~~ this phenomenon (Figs 5A–5B), suggesting that the comparison between CT number and shell thickness can be used as a tool to identify shells which have undergone either post-depositional dissolution or calcified in low Ω_{Ca} waters [92]. However, outliers may occur if specimens have an unusual morphology. A *T. quinqueloba* with an abnormally large and ~~low-density~~low-density final chamber plotted significantly to the left of the other shells from the water column (Fig 5B). Large, yet low-~~-~~density shells may be found when PF calcify in low Ω_{Ca} waters, and shift their ecological strategy to favor shell size over shell density [36], although, *T. quinqueloba* has been shown to present a large phenotypic variation related to changes in sea surface temperature [93].

4.2 *Limacina helicina*

4.2.1 Distribution in the water column and shell density

In contrast to PF, *L. helicina* do perform diel vertical migrations. Mature individuals diurnally migrate in the upper 200 m of the water column, while veligers and juveniles migrate in the top 50 m [94]. Like PF, it is also not known how the shell density of *L. helicina* changes with depth and increasing number of whorls. There is a skewness towards numerous small individuals at the surface, which is in agreement with previous findings in the polar region [95]. Because they migrate vertically, *L. helicina* showed less

of a vertical zonation in shell density through the water column (S8 – 10 Tables). The statistical significance in the increase in shell density with depth is driven by the low-density, smaller specimens in the 0–50 m depth interval (S10 Table). This is an observation consistent with their distribution in the water column [94]. The dominance of small individuals at the surface is likely because they have not developed their swimming wings and must therefore stay in the food-rich layer for growth. Once they have developed their wings they are able to migrate deeper in order to avoid predators, and this predation risk is likely what controls the vertical distribution of *Limacina helicina* [96].

4.2.2 Dissolution of *L. helicina*, ontogeny, and future outlook

The connection between low Ω_{Ar} and shell damage in *L. helicina* has been confirmed by observations from marine environments with large natural gradients in the carbonate chemistry [97]. However, recent studies on the periostracum of *L. helicina* suggests that they may not be as sensitive to OA as previously claimed [98,99]. Further, an increased food supply may reduce or even negate the effects of living in low-Ω waters [100,101]. In the Arctic, *L. helicina* juveniles may experience waters with lowest [CO_3^{2-}] and Ω_{Ar} during fall and winter, and it is unclear whether they calcify during this time or await elevated saturation states at the onset of CO_2 uptake by phytoplankton production in spring [18]. Seasonal decline in carbonate parameters was found to coincide with a higher proportion of pteropod shell dissolution in the North Sea [100]. *Limacina helicina* shell dissolution has been recorded at a Ω_{Ar} of 1.4 [97], and greatly reduced calcification at Ω_{Ar}<1.2 [101]. An Ω_{Ar} of 1.4 is close to the values we observe at the bottom waters in our study area. Moreover, our saturation states are based on a summer situation when the surface water has higher saturation states than what we would expect in fall and winter.

~~The increase in whorl thickness in their inner spiral is likely to be a structural necessity rather than related to the Ω_{Ar} in the depth interval in which they live (Figs 8C and 8D). However, a comparative study with *L. helicina* shells from regions with a different carbonate chemistry and seasonal fluctuations is needed to confirm that thickening of each consecutive whorl is always present.~~ The increase in the thickness of their shell apex with growth could mean that they are more resistant to dissolution if the Ω_{Ar} at out study site decreases in fall and winter (Figs ~~8E~~ 8D and 8E~~F~~), and their depth habitat deepens

Formatted: Font color: Red

with growth. In the surface water (0–50 m) during the summer, the Ω_{Ar} conditions are favourable (Fig 8B), allowing the small, low-density individuals to prioritize the growth of their muscles. Their thin and delicate shells during this stage of their life cycle will be less compromised with the higher Ω_{Ar}. It is possible that the thickening of the shell apex with increasing whorl number could be linked to re-directing the energy to calcification after finalizing the development of their soft body. It has been demonstrated that *L. helicina* can add new shell material after damage [98], and as long as the Ω_{Ar} is $\geq$1.2 ongoing thickening can occur over the entire shell, including the protoconch [101]. The repair mechanism of *L. helicina* and ongoing thickening means that they can choose specific areas of their shell to thicken after the initial calcification as part of a resilience strategy to environmental stress. Instances of over-calcification as a reaction to low Ω values have been found in barnacles [102] and coccolithophores [103,104], further suggesting that some calcifiers can re-direct energy for calcification when their shells are vulnerable.

Longer term studies using the techniques described here could shed light on the natural variability in the shell properties of *L. helicina* throughout their life cycle. Topics which could be addressed are to what extent calcification intensity varies with Ω_{Ar} and nutrients, and if specimens living in low Ω_{Ar} environments have adapted by building of thicker and denser shells. One could also investigate if there are geographical variations in whorl thickness depending on seasonality and chemical environment. Furthermore, with the ongoing climate change, water temperatures in the Barents Sea have increased [4] and are projected to continue to increase globally [105]. Synergistic effects of OA and warming have been demonstrated to be especially lethal for juvenile *L. helicina* [106,107], highlighting the need for a better understanding of the *L. helicina* calcification strategy.

5. Conclusions

The application of the XMCT scanning technique on the extant planktonic calcifying foraminiferal (PF) species *Neogloboquadrina pachyderma* and *Turborotalita quinqueloba* and the pteropod species

Limacina helicina retrieved from stratified plankton net samples from the northern Barents Sea ~~have~~, provided us with a unique dataset to better understand the shell density distribution with depth and ontogeny of these species at high Arctic latitudes. We found that both PF and *L. helicina* increase in shell density with depth, however there were inter-species differences in the PF due to depth habitat and reproduction. *Neogloboquadrina pachyderma* tends to be both thicker and denser than *T. quinqueloba*, and continues to increase in density until the deepest sampling interval 200–300 m. *Turborotalita quinqueloba* decrease in shell density below the depth interval 150–200 m, this loss may be due to internal dissolution associated with gamete release or bacterial degradation of the cytoplasm. Our results highlight the importance of sampling at the same water depth interval when comparing PF calcification intensity. In the surface sediments (0–1 cm) the shell preservation state was highly variable in both planktonic foraminiferal species with little alteration of the surface shell texture. In the surface sediments, *N. pachyderma* appeared more resilient towards post-depositional dissolution. In this area from the Barents Sea, the PF did not suffer from dissolution effects. Dissolution occurred after death and after settling on the sea floor. We observed that *L. helicina* thickens their shell apex as the number of whorls increase. There was a weaker zonation in shell density through the water column compared to PF, which is probably due to vertical migration. We recommend longer-~~-~~term studies on planktonic calcifiers using the XMCT scanning ~~techinique~~technique. Longer studies in different carbonate chemistry environments would provide even greater insight on the natural variability in shell density. This knowledge is important in order to use PF and *L. helicina* as biological indicators for ocean acidification and to predict future developments in food webs. It is also important in the use of PF as paleo-proxies.

Acknowledgements

We thank the captain and crew of the R/V *Helmer Hanssen*, without whom this work would not have been possible. We thank Dr. Arunima Sen for help with statistical analysis. We are very grateful to Dr. Brett Metcalfe and two A~~an a~~nonymous reviewers ~~-~~for their comments that greatly helped us improve the manuscript. The study was supported by the Centre for Arctic Gas Hydrate, Environment and

591 Climate (CAGE).

592 Author Contributions

593 **Conceptualization:** Siri Ofstad.

594 **Data Curation:** Siri Ofstad.

595 **Formal analysis:** Siri Ofstad, Katsunori Kimoto.

596 **Funding acquisition:** Tine L. Rasmussen, Katsunori Kimoto, Melissa Chierici, Agneta Fransson.

597 **Investigation:** Siri Ofstad, Katarzyna Zamelczyk, Katsunori Kimoto.

598 **Resources:** Katsunori Kimoto, Melissa Chierici, Agneta Fransson, Tine L. Rasmussen.

599 **Supervision:** Katarzyna Zamelczyk, Tine L. Rasmussen.

600 **Validation:** Katarzyna Zamelczyk, Katsunori Kimoto, Melissa Chierici, Agneta Fransson, Tine L.
601 Rasmussen.

602 **Visualization:** Siri Ofstad.

603 **Writing – original draft:** Siri Ofstad.

604 **Writing – review & editing:** Siri Ofstad, Katarzyna Zamelczyk, Katsunori Kimoto, Melissa Chierici,
605 Agneta Fransson, Tine L. Rasmussen.

606

607 Financial Disclosure Statement

608 This work was funded by the Research Council of Norway through its Centres of Excellence scheme
609 (grant number 223259). The XMCT analysis was funded by Japan Agency for Marine-Earth Science
610 and Technology Grants-In-Aid for Scientific Research (KAKENHI) Grant Numbers 15H05712 and

16H04961. The water chemistry sampling and analysis was funded by the Flagship research program "Ocean Acidification and effects in northern waters" within the FRAM- High North Research Centre for Climate and the Environment. The funders had no role in study design, data collection and analysis, decision to publish, or preparation of the manuscript. The publication charges for this article have been funded by a grant from the publication fund of UiT - The Arctic University of Norway.

Data Set

The CTD and carbonate chemistry data from the crater area in June 2016 is available at Norwegian Marine Data Center (https://doi.org/10.21335/NMDC- 225800978). All other data is available in the supporting information file (S1-10 Table, S1-3 Dataset).

References

1. Årthun M, Eldevik T, Smedsrud LH, Skagseth Ø, Ingvaldsen RB. Quantifying the Influence of Atlantic Heat on Barents Sea Ice Variability and Retreat. J Clim. 2012;25(13): 4736–4743. doi:10.1175/JCLI-D-11-00466.1

2. Smedsrud LH, Esau I, Ingvaldsen RB, Eldevik T, Haugan PM, Li C, et al. The role of the Barents Sea in the Arctic climate system. 2013;5(2012): 415–449. doi:10.1002/rog.20017.1.INTRODUCTION

3. Loeng H. Features of the physical oceanographic conditions of the Barents Sea. Polar Res. 1991;10(1): 5–18. doi:10.1111/j.1751-8369.1991.tb00630.x

4. Lind S, Ingvaldsen RB, Furevik T. Arctic warming hotspot in the northern Barents Sea linked to declining sea-ice import. Nat Clim Chang. 2018;8(7): 634–639. doi:10.1038/s41558-018-0205-y

5. Skagseth Ø, Furevik T, Ingvaldsen R, Loeng H, Mork KA, Orvik KA, et al. Volume and Heat Transports to the Arctic Ocean Via the Norwegian and Barents Seas. In: Dickson RR, Meincke J, Rhines P, editors. Arctic-Subarctic Ocean Fluxes: Defining the Role of the Northern Seas in Climate. Dordrecht: Springer Netherlands; 2008. pp. 45–64. doi:10.1007/978-1-4020-6774-7_3

6. Oziel L, Sirven J, Gascard JC. The Barents Sea frontal zones and water masses variability (1980-2011). Ocean Sci. 2016;12(1): 169–184. doi:10.5194/os-12-169-2016

7. Wassmann P, Kosobokova KN, Slagstad D, Drinkwater KF, Hopcroft RR, Moore SE, et al. The contiguous domains of Arctic Ocean advection: Trails of life and death. Prog Oceanogr. 2015;139: 42–65. doi:10.1016/j.pocean.2015.06.011

8. Dalpadado P, Ingvaldsen RB, Stige LC, Bogstad B, Knutsen T, Ottersen G, et al. Climate effects on Barents Sea ecosystem dynamics. ICES J Mar Sci. 2012;69(7): 1303–1316. doi:10.1093/icesjms/fss063

Formatted: Norwegian (Bokmål)

Formatted: Norwegian (Bokmål)

Formatted: Norwegian (Bokmål)

9. Neukermans G, Oziel L, Babin M. Increased intrusion of warming Atlantic water leads to rapid expansion of temperate phytoplankton in the Arctic. Glob Chang Biol. 2018;24(6): 2545–2553. doi:10.1111/gcb.14075

10. Fossheim M, Primicerio R, Johannesen E, Ingvaldsen RB, Aschan MM, Dolgov A V. Recent warming leads to a rapid borealization of fish communities in the Arctic. Nat Clim Chang. 2015;5(7): 673–677. doi:10.1038/nclimate2647

11. Bjørklund KR, Kruglikova SB, Anderson OR. Modern incursions of tropical Radiolaria into the Arctic Ocean. J Micropalaeontology. 2012;31(2): 139–158. doi:10.1144/0262-821X11-030

12. Fransson A, Chierici M, Anderson LG, Bussmann I, Kattner G, Peter Jones E, et al. The importance of shelf processes for the modification of chemical constituents in the waters of the Eurasian Arctic Ocean: Implication for carbon fluxes. Cont Shelf Res. 2001;21(3): 225–242. doi:10.1016/S0278-4343(00)00088-1

13. Bates NR, Mathis JT. The Arctic Ocean marine carbon cycle: evaluation of air-sea CO2 exchanges, ocean acidification impacts and potential feedbacks. Biogeosciences. 2009;6(11): 2433–2459. doi:10.5194/bg-6-2433-2009

14. Skogen MD, Olsen A, Børsheim KY, Sandø AB, Skjelvan I. Modelling ocean acidification in the Nordic and Barents Seas in present and future climate. J Mar Syst. 2014;131: 10–20. doi:10.1016/j.jmarsys.2013.10.005

15. Omar A, Johannessen T, Kaltin S, Olsen A. Anthropogenic increase of oceanic pCO2 in the Barents Sea surface water. J Geophys Res Ocean. 2003;108(C12): 1–8. doi:10.1029/2002JC001628

16. Evans W, Mathis JT, Cross JN. Calcium carbonate corrosivity in an Alaskan inland sea. Biogeosciences. 2014;11: 365–379. doi:10.5194/bg-11-365-2014

17. Fransson A, Chierici M, Nomura D, Granskog MA, Kristiansen S, Martma T, et al. Effect of glacial drainage water on the CO2 system and ocean acidification state in an Arctic tidewater-glacier fjord during two contrasting years. J Geophys Res Ocean. 2015;120. doi:10.1002/2014JC010320

18. Fransson A, Chierici M, Hop H, Findlay HS, Kristiansen S, Wold A. Late winter-to-summer change in ocean acidification state in Kongsfjorden, with implications for calcifying organisms. Polar Biol. 2016;39(10): 1841–1857. doi:10.1007/s00300-016-1955-5

19. Piquet AMT, Van De Poll WH, Visser RJW, Wiencke C, Bolhuis H, Buma AGJ. Springtime phytoplankton dynamics in Arctic Krossfjorden and Kongsfjorden (Spitsbergen) as a function of glacier proximity. Biogeosciences. 2014;11(8): 2263–2279. doi:10.5194/bg-11-2263-2014

20. Fabry VJ, Seibel BA, Feely RA, Orr JC. Impacts of ocean acidification on marine fauna and ecosystem processes. ICES J Mar Sci. 2008;65(3): 414–432. doi:10.1093/icesjms/fsn048

21. Larson RJ, Harbison GR. Source and Fate of Lipids in Polar Gelatinous Zooplankton. Arctic. 1989;42(4): 339–346. doi:10.14430/arctic1675

22. Hunt BPV, Pakhomov EA, Hosie GW, Siegel V, Ward P, Bernard K. Pteropods in Southern Ocean ecosystems. Prog Oceanogr. 2008;78(3): 193–221. doi:10.1016/j.pocean.2008.06.001

23. Weslawski JM, Hacquebord L, Stempniewicz L, Malinga M. Greenland whales and walruses in the Svalbard food web before and after exploitation. Oceanologia. 2000;42(1): 37–56.

685 24. Willette TM, Cooney RT. Ecological processes influencing mortality of juvenile pink salmon
686 (Oncorhynchus gorbuscha) in Prince William Sound, Alaska. Fish Oceanogr. 2001;10: 14–41.
687 doi:10.1046/j.1054-6006.2001.00043.x

688 25. Bathmann U V., Noji TT, von Bodungen B. Sedimentation of pteropods in the Norwegian Sea
689 in autumn. Deep Res. 1991;38(10): 1341–1360. doi:10.1016/0198- 0149(91)90031- A

690 26. Schiebel R. Planktic foraminiferal sedimentation and the marine calcite budget. Global
691 Biogeochem Cycles. 2002;16(4): 1–21. doi:10.1029/2001GB001459

692 27. Meilland J, Schiebel R, Lo Monaco C, Sanchez S, Howa H. Abundances and test weights of
693 living planktic foraminifers across the Southwest Indian Ocean: Implications for carbon fluxes.
694 Deep Res Part I Oceanogr Res Pap. 2018;131(March 2017): 27–40.
695 doi:10.1016/j.dsr.2017.11.004

696 28. Meilland J, Fabri-Ruiz S, Koubbi P, Monaco C Lo, Cotte C, Hosie GW, et al. Planktonic
697 foraminiferal biogeography in the Indian sector of the Southern Ocean: Contribution from CPR
698 data. Deep Res Part I Oceanogr Res Pap. 2016;110: 75–89. doi:10.1016/j.dsr.2015.12.014

699 29. Manno C, Accornero A, Umani SF. Importance of the contribution of Limacina helicina faecal
700 pellets to the carbon pump in Terra Nova Bay (Antarctica). J Plankton Res. 2010;32(2): 145–
701 152. doi:10.1093/plankt/fbp108

702 30. Ofstad S, Meilland J, Zamelczyk K, Chierici M. Development, Productivity, and Seasonality of
703 Living Planktonic Foraminiferal Faunas and Limacina helicina in an Area of Intense Methane
704 Seepage in the Barents Sea. J Geophys Res Biogeosciences. 2020;125(2): 1–24.
705 doi:10.1029/2019JG005387

706 31. Meilland J, Howa H, Hulot V, Demangel I, Salaün J, Garlan T. Population dynamics of modern
707 planktonic foraminifera in the western Barents Sea. Biogeosciences. 2020;17(6): 1437–1450.

708 32. Kacprzak P, Panasiuk A, Wawrzynek J, Weydmann A. Distribution and abundance of
709 pteropods in the western Barents Sea. Oceanol Hydrobiol Stud. 2017;46(4): 393–404.
710 doi:10.1515/ohs-2017-0039

711 33. Howes EL, Eagle RA, Gattuso JP, Bijma J. Comparison of Mediterranean pteropod shell
712 biometrics and ultrastructure from historical (1910 and 1921) and present day (2012) samples
713 provides baseline for monitoring effects of global change. PLoS One. 2017;12(1): 1–23.
714 doi:10.1371/journal.pone.0167891

715 34. Oakes RL, Sessa JA. Assessing annual variability in the shell thickness of the pteropod
716 Heliconoides inflatus in the Cariaco Basin using micro-CT scanning. 2019(October).

717 35. Beer CJ, Schiebel R, Wilson PA. Testing planktic foraminiferal shell weight as a surface water
718 [CO2-3] proxy using plankton net samples. Geology. 2010;38(2): 103–106.
719 doi:10.1130/G30150.1

720 36. Iwasaki S, Kimoto K, Sasaki O, Kano H, Uchida H. Sensitivity of planktic foraminiferal test
721 bulk density to ocean acidification. 2019;(June): 1–9. doi:10.1038/s41598-019-46041-x

722 37. Fox L, Stukins S, Hill T, Miller CG. Quantifying the Effect of Anthropogenic Climate Change
723 on Calcifying Plankton. Sci Rep. 2020;10(1620): 1–9. doi:10.1038/s41598-020-58501-w

724 38. Osborne EB, Thunell RC, Marshall BJ, Holm JA, Tapa EJ, Benitez-Nelson C, et al.
725 Calcification of the planktonic foraminifera Globigerina bulloides and carbonate ion
726 concentration: Results from the Santa Barbara Basin. Paleoceanography. 2016;31(8): 1083–

1102. doi:10.1002/2016PA002933

39. Marshall BJ, Thunell RC, Henehan MJ, Astor Y, Wejnert KE. Planktonic foraminiferal area density as a proxy for carbonate ion concentration: A calibration study using the Cariaco Basin ocean time series. Paleoceanography. 2013;28(2): 363–376. doi:10.1002/palo.20034

40. de Moel H, Ganssen GM, Peeters FJC, Jung SJA, Kroon D, Brummer GJA, et al. Planktic foraminiferal shell thinning in the Arabian Sea due to anthropogenic ocean acidification? Biogeosciences. 2009;6(9): 1917–1925. doi:10.5194/bg-6-1917-2009

41. Barker S, Elderfield H. Foraminiferal Calcification Response to Glacial-Interglacial Changes in Atmospheric CO2. Science (80-). 2002;297(5582): 833–836. doi:10.1126/science.1072815

42. Todd C. Planktic foraminiferal test size and weight response to the late Pliocene environment Planktic Foraminiferal Test Size and Weight Response to the Late Pliocene Environment. Paleoceanogr Paleoclimatology. 2020;35(1): e2019PA003738. doi:10.1029/2019PA003738

43. Naik SS, Naidu PD, Govil P, Godad S. Relationship between weights of planktonic foraminifer shell and surface water CO3= concentration during the Holocene and Last Glacial Period. Mar Geol. 2010;275(1–4): 278–282. doi:10.1016/j.margeo.2010.05.004

44. Gonzalez-Mora B, Sierro FJ, Flores JA. Controls of shell calcification in planktonic foraminifers. Quat Sci Rev. 2008;27: 956–961. doi:10.1016/j.quascirev.2008.01.008

45. Andreassen K, Hubbard A, Winsborrow MCM, Patton H, Vadakkepuliyambatta S, Plaza-Faverola A, et al. Massive blow-out craters formed by hydrate-controlled methane expulsion from the Arctic seafloor. Science (80-). 2017;356(6341): 948–953. doi:10.1126/science.aal4500

46. Jakobsson M, Mayer L, Coakley B, Dowdeswell JA, Forbes S, Fridman B, et al. The International Bathymetric Chart of the Arctic Ocean (IBCAO) Version 3.0. Geophys Res Lett. 2012;39(12). doi:10.1029/2012GL052219

47. Lalli CM, Wells FE. Reproduction in the genus Limacina (Opisthobranchia Thecosomata). J Zool. 1978;186(1): 95–108. doi:10.1111/j.1469-7998.1978.tb03359.x

48. Janssen AW. Holoplanktonic Mollusca (Gastropoda: Pterotracheoidea, Janthinoidea, Thecosomata and Gymnosomata) from the Pliocene of Pangasinan (Luzon, Philippines). Scr Geol. 2007;135: 29–177.

49. RStudio Team. RStudio: Integrated Development for R. RStudio, Inc. Boston, MA; 2015. Available: http://www.rstudio.com/

50. Pierrot DE, Wallace DWR. MS Excel program developed for CO2 system calculations. Oak Ridge, Tenn.: ORNL/CDIAC-105, Carbon Dioxide Inf. Anal. Cent., Oak Ridge Natl. Lab., U.S. Dep. of Energy; 2006.

51. Lewis E, Wallace DWR. CO2SYS-Program developed for CO2 system calculations, ORNL/CDIAC-105. Oak Ridge, Tenn.: Carbon Dioxide Inf. Anal. Cent., Oak Ridge Natl. Lab.; 1998. doi:10.2172/639712

52. Dickson AG. Thermodynamics of the dissociation of boric acid in synthetic seawater from 273.15 to 318.15 K. Deep Sea Res Part A Oceanogr Res Pap. 1990;37(5): 755–766. doi:10.1016/0198-0149(90)90004-F

53. Mehrbach C, Culberson CH, Hawley JE, Pytkowicx RM. Measurement of the Apparent

Formatted: Norwegian (Bokmål)

Dissociation Constants of Carbonic Acid in Seawater At Atmospheric Pressure. Limnol Oceanogr. 1973;18(6): 897–907. doi:10.4319/lo.1973.18.6.0897

54. Dickson A, Millero F. A Comparison of the Equilibrium Constants for the Dissociation of Carbonic Acid in Seawater Media. Deep Sea Research Part A. Oceanographic Research Papers. 1987. doi:10.1016/0198-0149(87)90021-5

55. Dickson A, Millero F. A Comparison of the Equilibrium Constants for the Dissociation of Carbonic Acid in Seawater Media. Deep Sea Research Part A. Oceanographic Research Papers. 1987. doi:10.1016/0198-0149(87)90021-5

56. Cottier F, Tverberg V, Inall M, Svendsen H, Nilsen F, Griffiths C. Water mass modification in an Arctic fjord through cross-shelf exchange: The seasonal hydrography of Kongsfjorden, Svalbard. J Geophys Res Ocean. 2005;110(12): 1–18. doi:10.1029/2004JC002757

57. Bengtson S. The advent of skeletons. Early life on earth. New York, NY: Nobel symposium No. 84. Columbia University Press; 1994. pp. 412–425.

58. Weinkauf MFG, Moller T, Koch MC, Kucera M. Calcification intensity in planktonic foraminifera reflects ambient conditions irrespective of environmental stress. Biogeosciences. 2013;10(10): 6639–6655. doi:10.5194/bg-10-6639-2013

59. Manno C, Morata N, Bellerby R. Effect of ocean acidification and temperature increase on the planktonic foraminifer Neogloboquadrina pachyderma (sinistral). Polar Biol. 2012;35(9): 1311–1319. doi:10.1007/s00300-012-1174-7

60. Steinhardt J, Nooijer LJ De, Brummer GJ, Reichart G. Profiling planktonic foraminiferal crust formation. Geochemistry Geophys Geosystems. 2015;18(1–2): 1541–1576. doi:10.1002/2014GC005684.Key

61. Caron DA, Anderson OR, Lindsey JL, Faber WW, Lin EE. Effects of Gametogenesis on Test Structure and Dissolution of Some Spinose Planktonic Foraminifera and Implications for Test Preservation. Mar Micropaleontol. 1990;16(1–2): 93–116. doi:10.1016/0377-8398(90)90031-G

62. Kohfeld KE, Fairbanks RG, Smith SL, Walsh ID. Neogloboquadrina pachyderma (sinistral coiling) as paleoceanographic tracers in polar oceans: Evidence from Northeast Water Polynya plankton tows, sediment traps, and surface sediments. Paleoceanography. 1996;11(6): 679–699. doi:10.1029/96PA02617

63. Arikawa R. Distribution and Taxonomy of Globigerina pachyderma (Ehrenberg) off the Sanriku Coast, Northeast Honshu, Japan. Tohoku Univ Sci Rep Ser Geol. 1983;53: 103–157.

64. Stangeew E. Distribution and Isotopic Composition of Living Planktonic Foraminifera N. pachyderma (sinistral) and T. quinqueloba in the High Latitude North Atlantic. Christian-Albrechts-Universität, Kiel. 2001. Available: https://macau.uni-kiel.de/rsc/thumbnail/diss_mods_00000464.png

65. Meilland J, Siccha M, Weinkauf MFG, Jonkers L, Morard R. Highly replicated sampling reveals no species-specific vertical habitats in diurnal vertical migration but stable planktonic foraminifera. J Plankton Res. 2019;41(2): 127–141. doi:10.1093/zoolinnean/zly093

66. Bijma J, Erez J, Hemleben C. Lunar and semi-lunar reproductive cycles in some spinose planktonic foraminifers. J Foraminifer Res. 1990;20(2): 117–127. doi:10.2113/gsjfr.20.2.117

67. Hemleben C, Spindler M, Anderson OR. Modern Planktonic Foraminifera. 1st ed. Springer-Verlag New York; 1989. doi:10.1007/978-1-4612-3544-6

Formatted: Norwegian (Bokmål)

68. Schiebel R, Bijma J, Hemleben C. Population dynamics of the planktic foraminifer Globigerina bulloides from the eastern North Atlantic. Deep Res Part I Oceanogr Res Pap. 1997;44(9–10): 1701–1713. doi:10.1016/S0967-0637(97)00036-8

69. Carstens J, Hebbeln D, Wefer G. Distribution of planktic foraminifera at the ice margin in the Arctic (Fram Strait). Mar Micropaleontol. 1997;29(3–4): 257–269. doi:10.1016/S0377-8398(96)00014-X

70. Eynaud F. Planktonic foraminifera in the arctic: Potentials and issues regarding modern and quaternary populations. IOP Conf Ser Earth Environ Sci. 2011;14(1). doi:10.1088/1755-1315/14/1/012005

71. Jensen S. Planktische Foraminiferen im Europäischen Nordmeer: Verbreitung und Vertikalfluß sowie ihre Entwicklung während der letzten 15000 Jahre. Berichte Sonderforschungsbereich 313, Univ Kiel. 1998;75(75): 1–105.

72. Pados T, Spielhagen RF. Species distribution and depth habitat of recent planktic foraminifera in Fram Strait, Arctic Ocean. Polar Res. 2014;33(1): 22483. doi:10.3402/polar.v33.22483

73. Volkmann R. Planktic Foraminifers in the Outer Laptev Sea and the Fram Strait-Modern Distribution and Ecology. J Foraminifer Res. 2000;30(3): 157–176. doi:10.2113/0300157

74. Simstich J, Sarnthein M, Erlenkeuser H. Paired δ18O signals of Neogloboquadrina pachyderma (s) and Turborotalita quinqueloba show thermal stratification structure in Nordic Seas. Mar Micropaleontol. 2003;48(1–2): 107–125. doi:10.1016/S0377-8398(02)00165-2

75. Greco M, Jonkers L, Kretschmer K, Bijma J, Kucera M. Variable habitat depth of the planktonic foraminifera Neogloboquadrina pachyderma in the northern high latitudes explained by sea-ice and chlorophyll concentration. Biogeosciences. 2019;16(17): 3425–3437. doi:10.5194/bg-16-3425-2019

76. Carstens J, Wefer G. Recent distribution of planktonic foraminifera in the Nansen Basin, Arctic Ocean. Deep Res. 1992;39.

77. Kozdon R, Ushikubo T, Kita NT, Spicuzza M, Valley JW. Intratest oxygen isotope variability in the planktonic foraminifer N . pachyderma: Real vs . apparent vital effects by ion microprobe. Chem Geol. 2009;258(3–4): 327–337. doi:10.1016/j.chemgeo.2008.10.032

78. Brown SJ, Elderfield H. Variations in Mg/Ca and Sr/Ca ratios of planktonic foraminifera caused by postdepositional dissolution: Evidence of shallow Mg-dependent dissolution. Paleoceanography. 1996;11(5): 543–551. doi:10.1029/96PA01491

79. Hecht AD, Eslinger E V, Garmon LB. Experimental studies on the dissolution of planktonic foraminifera. In: Sliter W V, Bé AWH, Berger WH, editors. Dissolution of Deep-sea Carbonates. Cushman Foundation for Foraminiferal Research; 1975. pp. 59–69.

80. Hamilton CP, Spero HJ, Bijma J, Lea DW. Geochemical investigation of gametogenic calcite addition in the planktonic foraminifera Orbulina universa. Mar Micropaleontol. 2008;68(3–4): 256–267. doi:10.1016/j.marmicro.2008.04.003

81. Erez J. The Source of Ions for Biomineralization in Foraminifera and Their Implications for Paleoceanographic Proxies. Rev Mineral Geochemistry. 2003;54(1): 115–149. doi:10.2113/0540115

82. Oakes RL, Peck VL, Manno C, Bralower TJ. Degradation of Internal Organic Matter is the Main Control on Pteropod Shell Dissolution After Death. Global Biogeochem Cycles.

2019;33(6): 749–760. doi:10.1029/2019GB006223

83. Watanabe E, Onodera J, Harada N, Honda MC, Kimoto K, Kikuchi T, et al. Enhanced role of eddies in the Arctic marine biological pump. Nat Commun. 2014;5(1): 3950. doi:10.1038/ncomms4950

84. Zaborska A, Carroll J, Papucci C, Torricelli L, Carroll ML, Walkusz-Miotk J, et al. Recent sediment accumulation rates for the Western margin of the Barents Sea. Deep Res II. 2008;55(20–11): 2352–2360. doi:10.1016/j.dsr2.2008.05.026

85. Wu G, Berger WH. Planktonic foraminifera: Differential dissolution and the Quaternary stable isotope Record in the west equatorial Pacific. Paleoceanography. 1989;4(2): 181–198. doi:10.1029/PA004i002p00181

86. Nürnberg D. Magnesium in tests of Neogloboquadrina pachyderma sinistral from high northern and southern latitudes. J Foraminifer Res. 1995;25(4): 350–368. doi:10.2113/gsjfr.25.4.350

87. Petro SM, Pivel MAG, Coimbra JC. Foraminiferal solubility rankings: A contribution to the search for consensus. J Foraminifer Res. 2018;48(4): 301–313. doi:10.2113/gsjfr.48.4.301

88. Malmgren BA. Ranking of dissolution susceptibility of planktonic foraminifera at high latitudes of the South Atlantic Ocean. Mar Micropaleontol. 1983;8(3): 183–191. doi:10.1016/0377-8398(83)90023-3

89. Spindler M. On the salinity tolerance of the planktonic foraminifera Neogloboquadrina pachyderma from Antarctic sea ice. Proc NIPR Symp Polar Biol. 1996;9: 85–91.

90. Kimoto K. Planktic Foraminifera. In: Ohtsuka S, Suzaki T, Horiguchi T, Suzuki N, Not F, editors. Marine protists: diversity and dynamics. Tokyo: Springer Japan; 2015. pp. 129–178. doi:10.1007/978-4-431-55130-0

91. Iwasaki S, Kimoto K, Sasaki O, Kano H, Honda MC, Okazaki Y. Observation of the dissolution process of Globigerina bulloides tests (planktic foraminifera) by X-ray microcomputed tomography. Paleoceanography. 2015;30(4): 317–331. doi:10.1002/2014PA002639

92. Johnstone HJH, Schulz M, Barker S, Elderfield H. Inside story: An X-ray computed tomography method for assessing dissolution in the tests of planktonic foraminifera. Mar Micropaleontol. 2010;77(1–2): 58–70. doi:10.1016/j.marmicro.2010.07.004

93. Kroon D, Wouters P, Moodley L, Ganssen G, Troelstra SR. Phenotypic variation of Turborotalita quinqueloba (Natland) tests in living populations and in the Pleistocene of an eastern Mediterranean piston core. In: Brummer GJA, Kroon D, editors. Planktonic Foraminifers as Tracers of Ocean-Climate History. Amsterdam: Free Univ. Press; 1988. pp. 131–143.

94. Falk-Petersen S, Leu E, Berge J, Kwasniewski S, Røstad A, Keskinen E, et al. Vertical migration in high Arctic waters during autumn 2004. Deep Res II. 2008;55: 2275–2284. doi:10.1016/j.dsr2.2008.05.010

95. Kobayashi HA. Growth Cycle and Related Vertical Distribution of the Thecosomatous Pteropod Spiratella (" Limacina ") helicina in the Central Arctic Ocean. Mar Biol. 1974;26: 295–301. doi:10.1007/BF00391513

96. Lampert W. The Adaptive Significance of Diel Vertical Migration of Zooplankton. Funct Ecol. 1989;3(1): 21–27. doi:10.2307/2389671

97. Bednaršek N, Ohman MD. Changes in pteropod distributions and shell dissolution across a frontal system in the California Current System. Mar Ecol Prog Ser. 2015;523: 93–103. doi:10.3354/meps11199

98. Peck VL, Oakes RL, Harper EM, Manno C, Tarling GA. Pteropods counter mechanical damage and dissolution through extensive shell repair. Nat Commun. 2018;9(1): 264. doi:10.1038/s41467-017-02692-w

99. Peck VL, Tarling GA, Manno C, Harper EM, Tynan E. Outer organic layer and internal repair mechanism protects pteropod Limacina helicina from ocean acidification. Deep Res Part II Top Stud Oceanogr. 2016;127: 41–52. doi:10.1016/j.dsr2.2015.12.005

100. León P, Bednaršek N, Walsham P, Cook K, Hartman SE, Wall-Palmer D, et al. Relationship between shell integrity of pelagic gastropods and carbonate chemistry parameters at a Scottish Coastal Observatory monitoring site. ICES J Mar Sci. 2020;77(1): 436–450. doi:10.1093/icesjms/fsz178

101. Bednaršek N, Feely RA, Tolimieri N, Hermann AJ, Siedlecki SA, Waldbusser GG, et al. Exposure history determines pteropod vulnerability to ocean acidification along the US West Coast article. Sci Rep. 2017;7(1): 1–12. doi:10.1038/s41598-017-03934-z

102. McDonald MR, McClintock JB, Amsler CD, Rittschof D, Angus RA, Orihuela B, et al. Effects of ocean acidification over the life history of the barnacle Amphibalanus amphitrite. Mar Ecol Prog Ser. 2009;385: 179–187. doi:10.3354/meps08099

103. Smith HEK, Tyrrell T, Charalampopoulou A, Dumousseaud C, Legge OJ. Predominance of heavily calcified coccolithophores at low CaCO3 saturation during winter in the Bay of Biscay. Proc Natl Acad Sci. 2012;109(23): 8845–8849. doi:10.1073/pnas.1117508109

104. Rigual-Hernán AS, Trull TW, Flores JA, No SD, Eriksen R. Full annual monitoring of Subantarctic Emiliania huxleyi populations reveals highly calcified conditions. Sci Rep. 2020;10: 2594. doi:10.1038/s41598-020-59375-8

105. IPCC. Climate Change 2013: The Physical Science Basis. Contribution of Working Group I to the Fifth Assessment Report of the Intergovernmental Panel on Climate Change. Stocker TF, Qin D, Plattner G-K, Tignor M, Allen SK, Boschung J, et al., editors. Cambridge University Press. Cambridge, United Kingdom and New York, NY, USA: Cambridge University Press; 2013. doi:10.1017/CBO9781107415324

106. Lischka S, Riebesell U. Synergistic effects of ocean acidification and warming on overwintering pteropods in the Arctic. Glob Chang Biol. 2012;18(12): 3517–3528. doi:10.1111/gcb.12020

107. Lischka S, Büdenbender J, Boxhammer T, Riebesell U. Impact of ocean acidification and elevated temperatures on early juveniles of the polar shelled pteropod Limacina helicina: Mortality, shell degradation, and shell growth. Biogeosciences. 2011;8(4): 919–932. doi:10.5194/bg-8-919-2011

108. Janssen AW. Holoplanktonic Mollusca (Gastropoda: Pterotracheoidea, Janthinoidea, Thecosomata and Gymnosomata) from the Pliocene of Pangasinan (Luzon, Philippines). Scr Geol. 2007;(135): 29–177.

Supporting Information

Fig S1. Temperature and salinity profile at study area.

Formatted: Norwegian (Bokmål)

Fig S2. Cross-sections of *Turborotalita quinqueloba* found in the 200–300 m water depth interval.

Scale bars measure 100 µm.

Fig S3. Annotated *Limacina helicina* to demonstrate measurement of physical parameters. More details on whorl counting method can be found in Janssen [48]. Wall thickness measurements were done along a cross-section (blue), and diameter measured along white stippled line. ~~Yellow stars~~Black circles show location of shell thickness measurements. The shell in the figure has 3.5 whorls.

Table S1. Plankton tow sampling depth for planktonic foraminifera, ambient seawater characteristics and calcite volume at the crater area in June 2016.

Table S2. CT Number and shell thickness of *Neogloboquadrina pachyderma*, *Turborotalita quinqueloba* and *Limacina helicina* at each depth interval.

Table S3. Plankton tow sampling depth for *Limacina helicina*, ambient seawater characteristics and calcite volume at the crater area in June 2016.

Table S4. Linear regression analysis of *Neogloboquadrina pachyderma* shell properties and environment.

Table S5. Linear regression analysis of *Turborotalita quinqueloba* shell properties and environment.

Table S6. Linear regression analysis of *Limacina helicina* shell properties and environment.

Table S7. Percentage of *Neogloboquadrina pachyderma* and *Turborotalita quinqueloba* shells containing cytoplasm.

Table S8. *Neogloboquadrina pachyderma* significance test (p-value) in CT number between depth intervals.

Table S9. *Turborotalita quinqueloba* significance test (p-value) in CT number between depth intervals.

Table S10. *Limacina helicina* significance test (p-value) in CT number between depth intervals.

S1 Dataset. Raw X-ray microcomputed tomography (XMCT) data of planktonic foraminifera *Neogloboquadrina pachyderma* and *Turborotalita quinqueloba* from the surface sediments.

S2 Dataset. Raw X-ray microcomputed tomography (XMCT) data of *Limacina helicina* from plankton tows, including whorl count ~~, whorl thickness~~ and shell apex thickness.

S3 Dataset. Raw X-ray microcomputed tomography (XMCT) data of planktonic foraminifera *Neogloboquadrina pachyderma* and *Turborotalita quinqueloba* from plankton tows.

Formatted: Norwegian (Bokmål)

Formatted: Font: Italic

Formatted: Font: Italic

Formatted: Font: Italic

Formatted: Font: Italic

Formatted: Font: Italic

Formatted: Font: Italic

Formatted: Font: Italic

Formatted: Font: Italic

Formatted: Font: Italic

Formatted: Font: Italic

Formatted: Font: Italic

Formatted: Font: Italic

Formatted: Font: Italic

Formatted: Font: Italic

Formatted: Font: Italic